FFAR4 REGULATES CARDIAC OXYLIPIN BALANCE TO PROMOTE INFLAMMATION RESOLUTION IN HFPEF SECONDARY TO METABOLIC SYNDROME

A Dissertation
SUBMITTED TO THE FACULTY OF
UNIVERSITY OF MINNESOTA
BY

Naixin Zhang

IN PARTIAL FULFILLMENT OF THE
REQUIRMENTS FOR THE DEGREE OF
DOCTOR OF PHILOSOPHY

Advisor: Dr. Timothy D. O'Connell
Co-advisor: Dr. Catherine M. Kotz

April 2023

ACKNOWLEDGEMENT

I would like to express my gratitude to all individuals who have helped me along this journey. First and foremost, I would like to thank my advisor, Dr. Timothy O'Connell. Tim, thank you for always being supportive and generous with your time, whether it was for practice sessions, one-on-one meetings, or draft revisions. Your work ethic and scientific rigor has inspired me a lot. I'm proud to be part of O'Connell lab and feel lucky to be pursuing my Ph.D. under your guidance. I also wanted to thank my co-advisor, Dr. Catherine Kotz. Cathy, thank you for your valuable advice on model development and phenotypic characterization, and for generously letting me use the bench space.

A special thanks goes to all the former and current members in O'Connell lab for your support, especially the ladies. Chastity, thanks for your years of effort in keeping the lab well-organized and for teaching me all the techniques when I first started in the lab. Sara, your optimism and positive attitude towards science and life always lift my spirits. Katie, thanks for being super supportive and caring not only for my research project, but also for some of the challenging life circumstances I faced.

I'm also grateful for having an incredible thesis committee consisting of Dr. Douglas Mashek, Dr. Catherine Kotz, Dr. Hai-bin Ruan, and Dr. Timothy O'Connell. Your insightful feedback and suggestions after every stage of committee meeting helped me explore more possibilities in my research and tell a comprehensive story.

Additionally, I would like to thank my lovely friends who have been there for me through thick and thin. Chenxu, Wenqiu, Zijian, and Zengtao, I'm fortunate to have you being my neighbors and friends that share unforgettable memories with me during the pandemic. Those dinners, hiking, and travels give me mental breaks from the research and allow me to explore life outside of the lab. A special thanks to Ruixuan, who has always been by my side, patiently listening to my frustrations and failures and providing me with full support and comfort. I could not be as mentally strong without your encouragement. And I want to thank my cat, Shizi, for keeping me company and making my life so much more fun.

Finally, I want to express my deepest appreciation to my amazing parents, Wei Huang and Mingxue Zhang. Thank you for being open-minded and understanding. Your unconditional love and support have made me become a confident person and enabled me to study abroad carefree. You are my biggest advocates in my life, and I love you so much.

ABSTRACT

Heart failure with preserved ejection fraction (HFpEF) is a complex clinical syndrome, but a predominant subset of HFpEF patients has metabolic syndrome (MetS). Mechanistically, systemic, non-resolving inflammation associated with MetS might drive HFpEF remodeling. Free fatty acid receptor 4 (FFAR4) is a GPCR for long-chain fatty acids that attenuates metabolic dysfunction and resolves inflammation. Therefore, we hypothesized that FFAR4 would attenuate remodeling in HFpEF secondary to MetS (HFpEF-MetS). To test this hypothesis, mice with systemic deletion of FFAR4 (FFAR4KO) were fed a high-fat/high-sucrose diet with L-NAME in their water to induce HFpEF-MetS. In male FFAR4KO mice, this HFpEF-MetS diet induced similar metabolic deficits, but worsened diastolic function and microvascular rarefaction relative to wild-type (WT) mice. Conversely, in female FFAR4KO mice, the diet produced greater obesity but no worsened ventricular remodeling relative to WT mice. In FFAR4KO males, MetS altered the balance of inflammatory oxylipins systemically in HDL and in the heart, decreasing the eicosapentaenoic acid-derived, pro-resolving oxylipin 18-hydroxyeicosapentaenoic acid (18-HEPE), while increasing the arachadonic acid-derived, proinflammatory oxylipin 12-hydroxyeicosatetraenoic acid (12-HETE). This increased 12-HETE/18-HEPE ratio reflected a more proinflammatory state both systemically and in the heart in male FFAR4KO mice, and was associated with increased macrophage numbers in the heart, which in turn correlated with worsened ventricular remodeling. In summary, our data suggest that FFAR4 controls the proinflammatory/pro-resolving oxylipin balance systemically and in the heart to resolve inflammation and attenuate HFpEF remodeling.

TABLE OF CONTENTS

LIST OF TABLES

CHAPTER 2: Loss of FFAR4 had no effect on the development of MetS but produced a more severe HFpEF-like phenotype in a model of cardiometabolic disease in male mice.

CHAPTER 3: Loss of FFAR4 increased weight gain and obesity but did not affect cardiac dysfunction in a model of cardiometabolic disease in female mice.

LIST OF FIGURES

CHAPTER 2: Loss of FFAR4 had no effect on the development of MetS but produced a more severe HFpEF-like phenotype in a model of cardiometabolic disease in male mice.

CHAPTER 3: Loss of FFAR4 increased weight gain and obesity but did not affect cardiac dysfunction in a model of cardiometabolic disease in female mice.

CHAPTER 4: Loss of FFAR4 promoted systematic pro-inflammatory state by regulating oxylipin synthesis

CHAPTER 1: Introduction

1.1 Free fatty acid receptors: GPCRs for endogenous free fatty acids

Free fatty acids (FFAs) are not only essential dietary nutrients, stored in triglycerides as an energy source and found as structural components of lipid bilayers, but can also serve as activators of G-protein coupled receptor (GPR) signaling to regulate physiologic function in many systems [1, 2]. Within the last 17 years, a family of class A or rhodopsin-like G-protein coupled receptors (GPCRs), the free fatty acid receptors (FFAR), have been identified as receptors for endogenous free fatty acids [1, 2]. There are currently 4 known receptors in the family: FFAR1 (GPR40), FFAR2 (GPR43), FFAR3 (GPR41), and FFAR4 (GPR120). FFAR1-3 are related and share significant homology in gene sequences and location on chromosome 19 in the human genome, whereas FFAR4 is distinct from the other three and is located on chromosome 10 [3]. Despite only 10% amino acid sequence homology, both FFAR1 and FFAR4 are receptors for medium- (MCFAs, 6-12 carbons) and long-chain FAs (LCFAs, >12 carbons), whereas FFAR2 and FFAR3 are receptors for short-chain FAs (SCFAs,< 6 carbons) [1, 2, 4].

1.1.1 Free fatty acid receptor 4 (FFAR4)

In mice, FFAR4 is expressed in several cells/tissues including intestinal I, K, and L enteroendocrine cells, pancreas, brain, lung, immune cells, and taste buds [1,

2]. More importantly, FFAR4 is expressed in tissues with direct relevance to cardiometabolic disease including, rodent and human heart, with expression in both cardiac myocytes and fibroblasts[5, 6], macrophages [5-8] , and both white and brown adipocytes [9-11].

In humans, there are two isoforms of FFAR4: FFAR4S (361 amino acids) and FFARL (377 amino acids), differing by a 16 amino acids insertion in the third intracellular loop of FFAR4L [12]. However, FFAR4L is expressed only in humans, all other species express only one isoform homologous to the FFAR4S. Interestingly, FFAR4L has a low level of basal phosphorylation [13], and signals only through activation of βArrestin2 mediated pathways [14]. However, FFAR4L expression is rather limited [14], and its physiologic relevance has been questions [15, 16].

The endogenous ligands for FFAR4 include medium and long-chain saturated, monounsaturated, and polyunsaturated fatty acids (SFAs, MUFAs, PUFAs). Previous studies indicate that SFAs are partial agonists, whereas MUFAs and PUFAs are full agonists.[8] [13]. This has implications for FFAR4 signaling in cardiometabolic disease, which is associated with increased dietary SFAs intake [17]. In this case, increased dietary SFAs might function as neutral antagonists to attenuate FFAR4 signaling. In addition, there are several synthetic FFAR4 agonists, including TUG-891 [18], cpdA [7], GW9508 [8] and compound 34 [19], that have been shown to attenuate metabolic dysfunction in mouse models of obesity/type 2 diabetes.

FFAR4 is a Gαq-coupled receptor that activates both Gαq- and βArrestin2 (βArr2)-mediated signaling pathways [8, 14, 20], although FFAR4 also activates Gi-mediated signaling pathways in pancreatic δ-cells [21]. FFAR4 signaling through

Gαq/11 activates phospholipase Cβ (PLCβ) to promote hydrolysis of phosphatidylinositol-4,5-bisphosphate (PIP_2), producing inositol 1,4,5-trisphosphate (IP_3) and diacylglycerol (DAG), leading to release of Ca^{2+} from IP_3 -sensitive intracellular stores and activation of PKC [22]. Alternatively, FFAR4 can recruit βarr2, which acts as a scaffold to recruit and activate different protein kinases. Interestingly, Oh *et al.* suggested that activation of proximal FFAR4 signaling pathways might be cell-specific [8]. In RAW 264.7 macrophages, FFAR4 activation leads to association with βarr2, which prevents TAB1/TAK1 interaction, inhibiting NFkB signaling, to attenuate inflammation, whereas in 3T3-L1 adipocytes, FFAR4 signals through Gαq to stimulate GLUT4 membrane translocation and glucose uptake. In addition, synthetic biased ligands for FFAR4 were discovered to activate βarrestin-2 signaling [2] [23], suggesting whether FFAR4 signals through Gαq or βarr2 is not only cell-dependent but can also be ligand-dependent.

1.1.2 FFAR4-cPLA2α signaling pathway

Downstream of proximal activation of Gαq and βarr2, FFAR4 activates cytosolic phospholipase A2α (cPLA2α). cPLA2α is a member of the Group IV family of phospholipase A2 enzymes. Once activated, cPLA2α cleaves PUFAs, traditionally thought to be the ω6-PUFA arachidonic acid (AA), from the sn2-acyl bond in membrane phospholipids [24]. cPLA2α is activated by increased calcium and phosphorylation at several sites, with phosphorylation at Ser505 by MAPK considered most important [25]. Despite the past focus on cPLA2α cleavage of AA,

cPLA2α does not specifically cleave AA, but will cleave whichever PUFA is at the Sn-2 position in membrane phospholipids, including ω3-PUFAs [24]. Once released from phospholipids, ω6-PUFAs like AA or linoleic acid (LA), but also ω3-PUFAs including eicosapentaenoic acid (EPA) and docosahexaenoic acid (DHA) can be further metabolized intracellularly by lipoxygenases (LOX), cyclooxygenases (COX), and $CYP_{hydroxylases}$ and $CYP_{epoxygenases}$ to produce oxylipins, which are simply biologically active oxygenated fatty acids. Oxylipins, including for example, leukotrienes and prostaglandins, signaling through GPRs to mediate several pro- or anti-inflammatory responses, or promote resolution of inflammation [26]. In macrophages for instance, FFAR4-mediated activation of cPLA2α-COX2 signaling and production of oxylipins can attenuate pro-inflammatory signaling [27-29].

Recently we found that in cardiac myocytes cultured from WT but not FFAR4KO mice, the FFAR4 agonist TUG-891 specifically increased production of the EPA-derived oxylipin 18-hydroxyeicosapentaenoic acid (18-HEPE) [6]. More importantly, TUG-891 and 18-HEPE attenuated cardiac myocyte death induced by oxidative stress in wild-type cardiac myocytes, and 18-HEPE rescued cell death in FFAR4KO cardiac myocytes [6]. Macrophages also produce pro-resolving oxylipins to attenuate immune response in response to pressure overload heart failure (transverse aortic constriction, TAC). In fat-1 transgenic mice which have elevated endogenous levels of ω3-PUFAs, 18-HEPE was selectively increased in the bone marrow-derived cells, which attenuate IL-6 production, macrophage-mediated proinflammatory activation of cardiac fibroblast, and pathologic remodeling post-TAC

[30]. Furthermore, in vivo administration of 18-HEPE also attenuated cardiac fibrosis, inflammation, and ventricular remodeling post-TAC. In addition, EPA-supplementation increased 18-HEPE levels and attenuated atherosclerosis in mice [31].

No receptor has been identified for 18-HEPE that might explain these cardioprotective effects, however, 18-HEPE is the precursor for E-series resolvins (RvE), which signal through the GPR ChemR23 [32, 33]. E-resolvins, together with D-resolvins, lipoxins, protectins and maresins, are classified as specialized pro-resolving mediators (SPMs), which as the name implies, resolve inflammation to restore the tissue homeostasis [34] . In the heart, RvE1 attenuates ischemic injury both *ex vivo* [35] and *in vivo*. [36]. Collectively, these studies suggest that 18-HEPE has cardioprotective effects, but whether this is a direct effect of 18-HEPE, or if these protective effects are mediated through RvE1 is not clear, nor has it been demonstrated that ChemR23 is expressed in cardiac myocytes.

The receptor for E-resolvins, ChemR23, is expressed in macrophages [37], smooth muscle cells [31], endothelial cells [38], and adipocytes [39]. However, ChemR23 expression in cardiac myocyte has not been demonstrated, although based the ability of 18-HEPE to prevent cardiac myocytes cell death [6] and RvE1 infusion to attenuate post-infarction remodeling [40], it is likely that ChemR23 might also be expressed in cardiac myocytes. ChemR23 is a dual ligand receptor, and in addition to binding E-series resolvins [32, 33], ChemR23 binds chemerin, a macrophage chemoattractant [41]. In macrophages, ChemR23 expression is restricted to naïve and M1-like macrophages, which respond to chemerin produced in

inflamed tissue to recruit macrophages, while RvE1 promotes repolarization of M1-like macrophages towards a more resolving M2-like phenotype [42]. Further, the balance between the two ChemR23 ligands, chemerin and RvE1, might dictate functional outcomes [43].

1.2 FFAR4 physiology

FFAR4 is expressed in several cells or tissues involved in the regulation of metabolic homeostasis and inflammation including adipocytes and macrophages. Importantly, FFAR4 is also expressed in the heart, in both cardiac myocytes and fibroblasts, and my current results indicated that FFAR4 attenuates cardiometabolic disease.

1.2.1 Obesity/Diabetes

In the gut, FFAR4 is expressed in intestinal enteroendocrine L cells in mice [20] and activation of FFAR4 stimulates GLP-1 release *in vitro* and *in vivo* and increases circulating insulin. Additionally, activation of FFAR4 in enteroendocrine I cells induces secretion of cholecystokinin (CCK) [44], while activation of FFAR4 in enteroendocrine K cells induces the release of gastric inhibitory polypeptide (GIP) [45].

In the pancreas, FFAR4 expression and function is not settled. FFAR4 in α-cells regulates glucagon secretion [46], while FFAR4 in β-cells regulates insulin secretion, possibly through regulation of PDX1 [47-50]. However, others report that FFAR4 is not expressed in pancreatic β-cells [9]. Furthermore, FFAR4 in δ-cells can

inhibit glucose-induced somatostatin secretion somatostatin secretion [21, 51], and FFAR4 in PP-cells regulates pancreatic peptide secretion [52].

Amongst the FFAR family, only FFAR4 is expressed in adipose tissue, and in both mice and humans, FFAR4 expression was detected only in mature adipocytes and macrophages [8], but not in preadipocytes [9]. Adipose expression of FFAR4 is increased by dietary intervention with a high-fat diet (HFD) in mice, and in obese humans [10]. In mice, systemic deletion of FFAR4 (FFA4 KO mice) worsens metabolic disease. Previous reports indicate that in response to HFD, male FFAR4 KO mice develop insulin resistance, glucose intolerance, adipocyte dysfunction, and fatty liver, but with little or no effect on weight gain in males, although females were not tested [8, 10, 53, 54]. However, others have demonstrated no effect on weight gain or metabolic function in response to HFD in FFAR4 KO mice [55]. Conversely, in primary adipocytes and NIH 3T3-L1 adipocytes, cpdA, a synthetic FFAR4 agonist, stimulated glucose transport via GfLUT4[8], and in mice, cpdA attenuated adipose tissue macrophage infiltration and down-regulated inflammatory gene expression [7]. Furthermore, activation of FFAR4 with synthetic ligands has also been consistently shown to improve insulin sensitivity and glucose tolerance [7, 19], promote lipid oxidation and brown adipose tissue thermogenesis [56, 57], and reduce food intake and weight gain [58] in mouse models of diet-induced obesity and sleep apnea.

There is also a discrepancy of the role of FFAR4 in obesity in human studies. One natural non-synonymous mutation at codon 270 of FFAR4 (R270H, minor allele frequency,~ 3%) inhibited the FFAR4 signaling pathway and increased the risk of obesity in the European (French and German) population [10]. On the contrary,

another study indicated that the R270H variant was not associated with an increased risk of obesity nor increased fasting plasma glucose levels in a Danish population [55].

FFAR4 also has a significant role in adipocyte differentiation. During adipocyte differentiation, the expression of FFAR4 is upregulated at the transcriptional level both *in vivo* in adipose tissue of mice on a HFD and *in vitro* in cultured 3T3-L1 cells [10]. Furthermore, knocking down FFAR4 dramatically inhibited adipocyte differentiation, suggesting FFAR4 can play a role in regulating adipogenesis [9]. In ciliated preadipocytes, activation of FFAR4 by DHA enhanced adipogenesis, which provides a possible explanation of the anti-diabetic effect of FFAR4: activation of FFAR4 increases the adipocyte numbers with lower fat content in each adipocyte, thus maintaining the homeostasis of the healthy fat tissue [59].

1.2.2 Inflammation

FFAR4 is expressed in bone marrow-derived macrophages (BMDM), primary intraperitoneal macrophages, murine RAW 246.7 cells, and human THP-1 cells [8, 60], suggesting a role in regulating systemic inflammation. The expression of FFAR4 is increased in proinflammatory M1-like macrophages [61]. Activation of FFAR4 by the synthetic ligand GW9508 suppressed LPS-induced inflammatory response in RAW246.7 cells [8]. Specifically, GW9508 mediated activation of FFAR4 recruited βArr2 and promoted the interaction between βArr2 and TAB-1, blocking TAB-1/TAK-1 interaction, thereby attenuating downstream activation of MKK4 and IKKβ, and inhibiting pro-inflammatory signaling through NFkB and JNK. This also suggested

that the anti-inflammatory effects of FFAR4 were exclusively dependent on βArr2 mediated signaling [61]. Similar results were observed in human epithelial cell line EA.hy926, where FFAR4 activation inhibited TAK1/TAB1 interaction, attenuating ERK-dependent NFkB activation and Egr-1 and ICAM-1 expression [62]. In addition, ω3-PUFAs mediated activation of FFAR4 inhibited the expression of proinflammatory genes, including IL-6, TNFα, MCP-1, IL-1β, iNOS, and CD-11c, but promoted the expression of anti-inflammatory genes, indicating that FFAR4 induced switching from M1 to M2 polarization [8]. Additionally, ω3-PUFA mediated activation of FFAR1 and FFAR4 suppressed NLRP3 inflammasome activation both *in vitro* in human THP-1 cells and *in vivo* in HFD-induced obesity [63].

In adipose, FFAR4 decreased inflammatory macrophage infiltration induced by HFD[8]). FFAR4 could also reduce chemokine secretion and block of chemotaxis *in vitro* and *in vivo* [7, 8]. In human adipocytes, expression of FFAR4 was downregulated due to macrophage secretions, which may amplify the inflammatory response in adipose tissue seen in obesity [64].

In the liver, FFAR4 was shown to be exclusively expressed in macrophage-like Kupffer cells [65]. In Kupffer cells FFAR4 attenuated NFkB/JNK mediated hepatic inflammatory response induced by ischemia-reperfusion injury, along with macrophage polarization shift from M1 to M2 in the liver. On the contrary, a human study focusing on children with NAFLD showed that FFAR4 was expressed in hepatocytes, hepatic progenitor cells in addition to liver macrophages [66]. Activation of FFAR4 with long-term DHA supplementation improved NAFLD scores, increased FFAR4 expression in hepatocytes, reduced the number of inflammatory

macrophages, and suppressed phosphorylated NFkB expression, which correlated with the downregulation of proinflammatory cytokines.

1.2.3 Lung disease

FFAR4 is abundantly expressed in murine lungs, and more specifically, in the Clara cells located at the surface epithelium of small airways [67]. Therefore, reasonable hypotheses of FFAR4 function include the production and secretion of surfactant in Clara cells in the lung. Recently, FFAR4 expression was confirmed in the club (Clara) cells and ω3-PUFA mediated activation of FFAR4 in club cells was found to promote proliferation and migration of club cells, resulting in accelerated recovery from naphthalene-induced airway injury [68]. Additionally, FFAR4 expression was identified in airway smooth muscles (ASM), as well as the epithelium of mid and lower airways. In ASM, activation of FFAR4 with the synthetic ligand TUG-891 decreased airway hyper-responsiveness and reduced inflammatory response in various pre-established inflammatory lung disease models [69]. Alternatively, FFAR4 can also mediate bronchodilation indirectly by releasing prostaglandin E2 (PGE2), which acts on EP2 prostanoid receptors. Moreover, the expression and functionality of FFAR4 found in human ASMs and human bronchial epithelial cells (HBECs) indicate the therapeutic potential of FFAR4 for treating inflammatory airway diseases [69]. A study focusing on patients with allergic rhinitis (AR) revealed a significantly lower ratio of pro-resolving mediator RvE1 to proinflammatory LTB4 in AR patients than healthy controls, despite the absolute high levels of both molecules in serum [70]. Considering that the FFAR4-cPLA2 signaling pathway is involved in oxylipins

production (which include RvE1 and LTB4) [6], disruption of FFAR4-cPLA2 regulation in oxylipin production may contribute to the defective resolution in airway and progression of chronic inflammation in AR patients.

1.2.4 Cancer

In cancer, FFAR4 was initially considered a tumor-promoting receptor for its role in inducing angiogenesis and migration in colorectal carcinoma [71], and other studies have suggested that FFAR4 is involved in tumorigenesis, migration, and metastasis [72]. However, FFAR4 inhibits lysophosphatidic acid (LPA)- and epidermal growth factor(EGF)-induced proliferation and migration in prostate cancer cell lines DU145 and PC-3 [73] by inhibiting the phosphorylation of ERK, FAK, and P70S6K, and expression of the matricellular protein CCN1. In addition, ω3-PUFAs and FFAR4 seem to have similar inhibitory effects in breast cancer cell lines [74]. In obese mice, ω3-PUFAa inhibit mammary tumor growth independent of expression of FFAR4 [75], which could be achieved via direct induction of apoptotic pathways. Alternatively, in mammary tumors, the mixed FFAR1/4 agonist GW9508, the FFAR4 agonist TUG-891, and the endogenous FFAR1/4 ligand EPA all inhibited LPA- and EGF- stimulated proliferation, ERK activation, and Akt activation in a dose-dependent manner, suggesting both FFAR1 and FFAR4 suppress breast cancer cell proliferation [73]. In summary, FFAR4 has various (even opposite) effects on different cancer types and models, and therefore further investigation is still needed to address the role of FFAR4 in cancer.

1.2.5 Cardiovascular disease

FFAR4 has a significant cardioprotective role in atherosclerosis and cardiovascular disease. In the vasculature, FFAR4 is expressed in perivascular cells including adipocytes, and macrophages, with much lower expression in vascular smooth muscle cells but not in platelets. In a model of femoral arterial thrombosis following induced by $FeCl_3$, loss of FFAR4 in fat-1 transgenic mice (FFAR4KO crossed to fat-1 Tg mice), which endogenously synthesize high levels of ω3-PUFAs (EPA and DHA), worsened femoral arterial thrombosis following acute $FeCl_3$ injury. Moreover, vascular inflammation and neointimal hyperplasia induced by long-term $FeCl_3$ injury were markedly worsened by loss of FFAR4, including decreased luminal diameter and reduced blood flow. Furthermore, infiltrating macrophages in the vasculature and peri-vasculature were also increased, suggesting loss of FFAR4 worsens the inflammatory responses in vascular remodeling, indicating FFAR4 attenuates inflammation to reduce vascular injury. In atherosclerosis, TUG-891 administration in ApoE-knockout mice effectively reduced atherosclerotic plaque size and necrotic cores in the plaque lesions via FFAR4 [76]. In addition, activation of FFAR4 decreased total macrophage numbers whereas increased the population of smooth muscle cells in the lesions. Moreover, FFAR4 activation decreased M1-like macrophages but increased M2-like macrophages in the plaques, indicating a polarization shift towards M2 phenotype, which might contribute to the inhibition of atherosclerosis. In the human aortic endothelial cells (HAECs) treated with oxidized low-density lipoprotein (ox-LDL), FFAR4 agonism prevented oxidative stress and inflammation by inhibiting ROS production and proinflammatory cytokine expression

[77]. In addition, FFAR4 suppressed monocyte attachment to endothelial cells by inhibiting VCAM-1 and E-selectin expression. FFAR4 was also shown to play a beneficial role in the attenuation of abdominal aortic aneurysms (AAAs), in which the abdominal aorta is expanded, leading to rupture and a high mortality rate [78]. EPA and GW9508 could both effectively attenuate the progression of AAAs via FFAR4, by reducing phosphorylation of TAK1 and JNK, as well as expression of Mmp-9.

In the heart, recent work from our lab indicates that FFAR4 protects the heart by reducing oxidative stress and induces the production of pro-resolving oxylipin. In mice with whole body knockout of FFAR4 (FFAR4KO), our lab demonstrated pathologic pressure overload (transverse aortic constriction, TAC) increased hypertrophy and further decreased systolic and diastolic function, but surprisingly had no effect on fibrosis in FFAR4KO mice relative to WT mice [6]. Despite previous work from our lab suggesting that FFAR4 inhibits TGFβ1-mediated pro-fibrotic signaling in cardiac fibroblasts *in vitro* [5], the failure to observe worsening fibrosis post-TAC *in vivo*, suggests the worsened outcome in FFAR4KO mice could be attributed to the lack of FFAR4 in the cardiac myocytes. Transcriptome analysis of myocytes isolated from FFAR4KO hearts highlighted specific transcriptional deficits of genes associated with cell death and inflammation [6]. Specifically, genes involved in cPLA2 signaling, oxylipin synthesis, and reduction of oxidative stress were increased in myocytes from WT mice, but not in those from FFAR4KO mice. As a result, the production of EPA-derived, anti-inflammatory oxylipin 18-HEPE was abolished in the FFAR4KO heart, suggesting a systemic proinflammatory state. *In vitro* evidence also supported the cardioprotective effect of FFAR4 by preventing oxidative stress in cultured cardiac

myocytes following oxidative stress [6]. Taken together, there is an emerging interest in studying the cardioprotective role of FFAR4 on cardiovascular diseases, which potentially serves as the mechanistic basis of the beneficial role of omega-3 PUFAs in cardiovascular disease.

1.3 Heart failure

Heart failure (HF) is a complex clinical syndrome defined by the inability of the ventricle to adequately eject or fill with blood to meet the body's requirements [79]. Patients with HF present with multiple symptoms including dyspnea upon exertion (exercise intolerance), fatigue, peripheral edema, and tachycardia, which are often attributed to structural or functional changes in the heart, a process known as remodeling [80]. While HF is classically associated with systolic dysfunction, diastolic dysfunction, or both, structural deficits in the endocardium or epicardium, or even abnormalities in cardiac conduction can also contribute to heart failure [80].

Clinically, HF is classified by symptomatic severity. Based on the New York Heart Association (NYHA) functional classification: Class I includes patients who have no limitation of physical activity and ordinary physical activity does not cause fatigue, breathlessness, or palpitations; Class II includes patients who have a slight limitation of physical activity. They are comfortable at rest but ordinary physical activity causes fatigue, breathlessness, or palpitations; Class III includes patients who have marked limitations of physical activity. They are comfortable at rest but less than ordinary physical activity causes fatigue, breathlessness, or palpitations; Class IV includes patients who are unable to carry on any physical activity without

discomfort. Symptoms can be presented at rest and discomfort is increased if physical activity is undertaken [80]. The American Heart Association has a similar classification system [79].

HF is one of the leading causes of morbidity and mortality globally. There are approximately 26 million adults living with HF worldwide, making it a growing public health concern [81]. Specifically in developed countries, the incidence of HF is increasing rapidly with aging populations. In the United States, HF prevalence is estimated at 6.2 million people based on the data from 2013-2016, more than 80% of which are 65 years of age or older [81, 82]. More importantly, 5 year HF survival is less than 50%, exceeding the mortality rate of most cancers [83].

1.3.1 HFpEF vs HFrEF

Classically, HF is associated with left ventricular (LV) systolic dysfunction and ventricular dilation. However, in the last 20 years, a distinct HF phenotype has been recognized, one in which patients present with the signs and symptoms of heart failure, but seemingly normal LV systolic function. Current clinical practices classify HF based on the measurement of left ventricular ejection fraction (LVEF), and HF can be classified into three categories based on recent guidelines [80]:

1. Heart failure with reduced ejection fraction (HFrEF), with LVEF ≤40%.
2. Heart failure with mildly reduced ejection fraction (HFmrEF), with LVEF between 41%-49%.
3. Heart failure with preserved ejection fraction (HFpEF), with LVEF≥50%.

This classification is clinically important because different types of HF may share

similar symptoms but with distinct etiology. Therefore, personalized treatments or interventions are required.

Analyses of the Framingham Heart Study and the Cardiovascular Health Study indicate that the incidence of HFrEF is decreasing, while the incidence of HFpEF is increasing over the past two decades [84], such that both the incidence and prevalence of HFpEF now exceed HFrEF. Of note, HF prevalence increases with age, and in the populations over 70 years old, prevalence can be as high as 10%. While the overall incidence and prevalence of HF is similar between men and women [84], women have a higher prevalence of HFpEF than men, especially in older patients [80]. Mortality of overall HF is nearly 66% within 5 years after initial diagnosis, with similar mortality rates between HFrEF and HFpEF. Interestingly, there are more cardiovascular disease (CVD) deaths in HFrEF but more non-CVD deaths in HFpEF [84].

Over the last 30 years, multiple clinical trials have led to a defined drug regimen for HFrEF patients, including, angiotensin-converting enzyme inhibitors (ACE-I), angiotensin receptor blockers, diuretics, β-adrenergic receptor antagonists (β-blockers), neprilysin inhibitor (including the newer class of angiotensin receptor-neprilysin inhibitor (ARNI)), and mineralocorticoid receptor antagonists (MRA) improve survival and reduce symptoms by inhibiting overactivation of the renin-angiotensin-aldosterone (RAAS) and sympathetic nervous systems [85]. Conversely, conventional therapies for HFrEF have shown no efficacy to reduce mortality in HFpEF [86]. However, recent trials have indicated that sodium-glucose transporter 2 inhibitors (SGLT2i) reduce HF hospitalizations in two trials (empagliflozin,

EMPORER-Preserve [87], and dapagliflozin, DELIVERY [88]) However, this beneficial effect is did not extend to reducing all-cause mortality. Current clinical recommendations for HFpEF management involve controlling hypertension and alleviating symptoms of congestion [79]. It is also recommended to identify and provide treatments for risk factors, etiology, and comorbidities associated with HFpEF [80].

1.3.2 Pathophysiology of HFpEF

HFpEF etiology is distinct HFrEF and is much more phenotypically heterogeneous than HFrEF, potentially explaining the failure of conventional HFrEF pharmacologic therapies in the context of HFpEF. HFpEF patients tend to be older, female [86], and more likely to have atrial fibrillation, chronic kidney disease, and other non-CVD comorbidities such as obesity, diabetes, and hypertension [89].

Clinically, a prospective analysis of 397 patients with HFpEF classified three distinct phenotypes of HFpEF based on clinical characteristics, cardiac function, and invasive hemodynamics [90]. It was reported that three phenogroups were significantly different from each other, with distinct phenotypes: Group 1 was the youngest, with the least cardiac remodeling and lowest BNP levels; Group 2 had the highest prevalence in comorbidities of MetS including hypertension, obesity, and diabetes, and has highest LV relaxation; Group 3 was the oldest and has the most severe cardiac remodeling and worst RV function with the highest association with chronic kidney disease [90]. Adverse outcomes analysis also suggested a step-wise

increase in the risk of adverse events from the lowest (group 1) to the highest (group 3).

Mechanistically, a new paradigm was proposed to help understand the progression of HFpEF [91, 92]. In HFpEF, low-grade systemic inflammation occurs following comorbidities associated with MetS and/or chronic kidney diseases. This inflammation is proposed to target coronary microvascular endothelial cells inducing production of reactive oxygen species (ROS), leading to reduced NO bioactivity and lower soluble guanylate cyclase (sGC) activity in neighboring cardiac myocytes, which increases passive stiffness and hypertrophy. On the other hand, in response to systemic inflammation, endothelial expression of adhesion molecules attracts leukocytes to infiltrate through endothelium and secret transforming growth factor β (TGF- β). As a result, fibroblasts are converted into myofibroblasts, and increase the production of collagen, thus inducing interstitial fibrosis. Inflamed endothelial cells may also undergo cell death which ultimately promotes microvascular rarefaction (MVR). This hypothetical model for explaining the development of HFpEF fits nicely into the clinical observation of patients with HFpEF, in which ventricular remodeling is defined by cardiac hypertrophy, myocardial fibrosis, and MVR [93].

1.3.3 Comorbidities associated with HFpEF

HF is often associated with one or more comorbid conditions. For HFpEF patients, It is common for HFpEF patients to have multiple, severe comorbidities [86], and on average, most HFpEF patients suffer with at least one comorbidity, but almost 50% have five or more major comorbidities.

Hypertension is the most prevalent comorbidity for HFpEF and is found in 80% or more of patients with HFpEF [91]. In hypertension, myocardial pressure overload and systemic inflammation may be the driving force of myocardial remodeling and dysfunction [94].

Obesity is a well-known risk factor for HF and not only increases the risk myocardial infarction which drives systolic dysfunction but also increases the risk of HFpEF which is independent of ischemic injury [95]. Pathophysiologic mechanisms by which obesity contributes to the progression of HFpEF include: 1) Obese people experience sodium retention, which increases circulating volume to trigger hypertension; and 2) Obesity induces chronic inflammation in the adipose tissue which subsequently becomes systemic, adversely affecting vasculature and visceral organs [95].

Type 2 Diabetes (T2D), commonly observed secondary to obesity, is also associated with HFpEF and LV remodeling [96]. Although diabetes is not an independent risk factor of HFpEF with adjustment of other risk factors, it is still prevalent with 20-40% of HFpEF patients having diabetes [86]. A report from Irbesartan in Heart Failure With Preserved Ejection Fraction(I-Preserve Trial) suggested HFpEF patients with diabetes were more signs of congestion, worse quality of life, higher NT pro-BNP levels, and a poorer prognosis with greater structural and functional abnormalities [97]. Furthermore, SGLT1i are used to treat T2D and have been shown to reduce hospitalizations in HFpEF patients, suggesting that attenuating T2D might improve HFpEF outcomes.

Atrial fibrillation (AF) is also common in HFpEF [86, 98]. The prevalence varies from 15% to 41%, depending on study design and diagnostic method [99]. A community-based study reported two thirds of HFpEF patients developed AF before or after the diagnosis [100].

1.4 Overarching hypothesis and aims

The beneficial effects of FFAR4 on metabolism and inflammation, the high incidence of MetS in a subset of HFpEF patients, and the cardioprotective effects of FFAR4 form the premise of our central hypothesis that in the heart, FFAR4 functions as a cardioprotective nutrient sensor for medium and long-chain fatty acids, to protect the heart from pathologic stress.

Here, we tested the specific hypothesis that FFAR4 would attenuate HFpEF secondary to MetS. Using mice with systemic deletion of FFAR4 (FFAR4KO mice), we examined FFAR4 mediated cardioprotection in the context of HFpEF-MetS from three different aspects: 1) We determined the requirement for FFAR4 to attenuate metabolic disease and pathologic cardiac remodeling in response to dietary challenge with a diet designed to induce MetS (HFpEF-MetS diet) , 2) We evaluated FFAR4-specific sex-based differences in metabolic function and cardiac remodeling in response to the HFpEF-MetS diet, and 3) We examined the signaling mechanism underlying FFAR4-mediated cardioprotection in the context of HFpEF-MetS.

My first aim is designed to test the hypothesis that FFAR4 is required to attenuate metabolic disease and cardiac pathologic remodeling in a mouse model of HFpEF-MetS. In support of the hypothesis, previous work in our lab has indicated

that FFAR4 is required for an adaptive response to transverse aortic constriction (TAC) with worse remodeling observed in FFAR4KO mice post-TAC. In humans, we found that *FFAR4* R270H was associated with left ventricular hypertrophy and dilation in a cohort of 7,140 genotyped subjects who had a clinically indicated echocardiography exam [6].To study the effect of FFAR4 in HFpEF-MetS, we employed a model of HFpEF by feeding mice with a high-fat/high-sucrose western diet with L-NAME in the drinking water to induce HFpEF secondary to MetS. Using EchoMRI to measure body composition, a tail-cuff system to monitor blood pressure, as well as measuring glucose tolerance and plasma lipids, we found that HFpEF-MetS diet induced similar degree of metabolic dysfunction in both male WT and FFAR4KO mice. Furthermore, using echocardiography and assessing cardiac morphology, we found that, as expected, the HFpEF-MetS diet induced a HFpEF-like phenotype in WT mice. More importantly, we found that the HFpEF-MetS worsened cardiac pathology in FFAR4KO mice, evidenced by worse diastolic dysfunction and more microvascular rarefaction. Thus, our data support the hypothesis that FFAR4 protects the heart by mitigating pathologic remodeling in HFpEF-MetS. This is the first report to study FFAR4 mediated cardioprotection in the context of HFpEF-MetS.

My second aim is designed to test the hypothesis that males are more dependent on FFAR4 mediated cardioprotection than females. We previously demonstrated that unlike males, TAC-induced remodeling was not worsened in female FFAR4KO mice [6]. Similarly, we found that in a large clinical cohort, the FFAR4 R270H inactivating polymorphism was associated with hypertrophy and ventricular dilation in males but not females, extending the sex-based difference

observed in mice to humans [6]. To test the hypothesis, we employed the same animal model of HFpEF-MetS to compare outcomes between female WT and FFAR4KO mice. Our results indicate that the HFpEF-MetS diet induced greater weight gain and more obesity, but no worsening of the HFpEF-like phenotype in female mice. This is the first report describing sex-based difference in cardioprotection of FFAR4 as well as the metabolic regulation of FFAR4 in the context of HFpEF-MetS.

My third aim is designed to test the hypothesis that FFAR4 promotes production of the EPA-derived, pro-resolving, cardioprotective oxylipin 18-HEPE to attenuate/resolve inflammation and attenuate remodeling in HFpEF-MetS. Recently, we demonstrated that FFAR4 mediated cardioprotection requires activation of cPLA2α signaling and production of 18-HEPE [6]. To test the hypothesis, we measured high-density lipoprotein (HDL) oxylipin profiles as an indication of systemic cPLA2α activity in response to HFpEF-MetS. Interestingly, we found that in HDL, 18-HEPE levels were decreased slightly as baseline in male FFAR4KO mice, and that the HFpEF-MetS diet promoted even further reduction in 18-HEPE in male FFAR4KO mice. Surprisingly, we found that in HDL, the pro-inflammatory oxylipin 12-HETE was increased at baseline in male FFAR4KO mice, and that the HFpEF-MetS diet induced an even further increase in 12-HETE in male FFAR4KO mice. As such, the HFpEF-MetS diet produced a very large increase in the 12-HETE/18-HEPE ratio in HDL in male FFAR4KO mice, suggesting a systemic pro-inflammatory state. Interestingly, the increased in the 12-HETE/18-HEPE ratio in HDL induced by the HFpEF-MetS diet was not observed in females. Additionally, we measure cardiac

oxylipin levels in male mice, and found similar results, with the striking exception that the 12-HETE/18-HEPE ratio was increased even at baseline. Interestingly, this proinflammatory state characterized by the increased 12-HETE/18-HEPE ratio correlated with increased number of macrophages in the heart and worsened cardiac outcome in FFAR4KO males. We are the first to explore the underlying mechanism of FFAR4-mediated cardioprotection by linking cardiac phenotypes with an altered oxylipin balance in the context of HFpEF-MetS.

CHAPTER 2: Loss of FFAR4 had no effect on the development of MetS but produced a more severe HFpEF-like phenotype in a model of cardiometabolic disease in male mice.

Naixin Zhang, Katherine A. Murphy, Dylan J. Gyberg, Michael J. Zhang, Jackie A. Stevens, Chastity L. Healy, DeWayne Townsend and Timothy D. O'Connell

Department of Integrative Biology and Physiology, University of Minnesota, Minneapolis, MN 55455 USA

2.1 Summary

Heart failure with preserved ejection fraction (HFpEF) is a complex clinical syndrome in which patients show symptoms of heart failure but with preserved ejection fraction (LVEF>=50%). HFpEF accounts for more than 50% of the HF population, and its incidence is still increasing. Unfortunately, conventional therapies that work for HFrEF failed to show efficacy in HFpEF. HFpEF etiology is complex and heterogeneous, with patients showing significant phenotypic variation [90]. Generally, patients tend to be older, female, and a predominant subset has comorbidities associated with MetS (MetS) [91, 92, 101]. Previously, our lab suggested free fatty acid receptor 4 (FFAR4) is cardioprotective in the context of pressure overload-induced heart failure. However, the role of FFAR4 in HFpEF is still unknown. Here, we developed a model of HFpEF secondary to MetS to model the comorbidities

observed in HFpEF patients. To induce MetS, mice were fed a high-sucrose high-fat (42% of fat and 30% of sucrose) Western diet with L-NAME in the drinking water (abbreviated to the HFpEF-MetS diet). In male WT mice, the HFpEF-MetS diet induced MetS, but surprisingly, metabolic dysfunction was not worsened by loss of FFAR4 (FFAR4KO mice). Furthermore, the HFpEF-MetS diet induced significant diastolic dysfunction and fibrosis in male WT mice. However, the HFpEF-MetS diet exacerbated the HFpEF-like phenotype in male FFAR4KO mice, with further worsening diastolic dysfunction and more microvascular rarefaction.

2.2 Introduction

Of the roughly 6 million total cases of HF in the US, the prevalence of HFpEF now exceeds 50% [86, 91], and despite the recent success of empagliflozin in EMPEROR-Preserved [87], therapeutic options for HFpEF remain limited. HFpEF etiology is complex and heterogeneous, and patients tend to be older, female, and demonstrate significant phenotypic variation [86, 91]. Clinically, attempts have been made to subdivide HFpEF patients based on etiology, and this has identified a predominant subset of HFpEF patients with comorbidities associated with MetS [90, 92, 101].

Free fatty acid receptor 4 (FFAR4) is a G-protein coupled receptor (GPCR) for endogenous medium- and long-chain saturated, monounsaturated, and polyunsaturated fatty acids (SFA, MUFA, PUFA) [13]. This includes, but is not limited to, the cardioprotective w3-PUFAs, eicosapentaenoic acid (EPA) and docosahexaenoic acid (DHA) [15]. FFAR4 is expressed in several tissues with similar

expression patterns in mouse and human [20], and high levels of expression in lung, brain, and GI-tract, but lower levels in other tissues including pancreas, small intestine, adipose, taste buds, muscle, heart, liver, and macrophages [20, 44, 102]. Historically, FFAR4 is proposed to attenuate metabolic dysfunction and resolve inflammation in a variety of settings. In adipose tissue, activation of FFAR4 with synthetic ligands including compound A, TUG-891, or compound 34 generally improves metabolic dysfunction and insulin resistance [7, 19, 57]. In macrophages, FFAR4 activation inhibits NFκB signaling and subsequent production of the inflammatory cytokines IL-6 and TNFα, rendering these macrophages less inflammatory and attenuating adipocyte dysfunction in obesity [7, 8].

Although we previously detected FFAR4 expression in both cardiac myocytes and fibroblasts [5], little was known about the physiologic function of FFAR4 in the heart until we recently demonstrated that FFAR4 is cardioprotective in a model of pathologic pressure overload (TAC). Although we found that mice with systemic deletion of FFAR4 (FFAR4KO) had no obvious phenotype at baseline, loss of FFAR4 amplified TAC-induced hypertrophy without excessive fibrosis and worsened TAC-induced systolic and diastolic dysfunction in males, but not females [6]. In adult cardiac myocytes, we observed that FFAR4-cPLA2α signaling specifically and uniquely induced the production of the EPA-derived, cardioprotective, pro-resolving oxylipin 18-hydroxyeicosapentaenoic acid (18-HEPE), which attenuated cardiac myocyte death induced by oxidative stress [6]. In humans, we found that *FFAR4* R270H was associated with left ventricular hypertrophy and dilation in a cohort of 7,140 genotyped subjects who had a clinically indicated echocardiogram [6].

The high incidence of MetS in HFpEF patients [90], the beneficial effects of FFAR4 on metabolism and inflammation [7, 8, 10] and the recently described cardioprotective effects of FFAR4 [6] led us to hypothesize that the loss of FFAR4 would worsen ventricular remodeling in a mouse model of HFpEF secondary to MetS (HFpEF-MetS).

2.3 Methods

Mice

FFAR4KO mice that were generated from cryopreserved sperm from C57Bl/6N-FFAR4tm1(KOMP)Vlcg (Design ID: 15078; Project ID: VG15078) purchased from The Mutant Mouse Resource and Research Centers (MMRRC), UC-Davis (Davis, CA, USA). All mice are backcrossed into the C57Bl/6J strain as previously described [6].

At 8 weeks of age, male WT and FFAR4KO mice were randomized to be fed a control diet or a diet designed to induce heart failure preserved ejection fraction secondary to MetS (HFpEF-MetS) for 20 weeks. Mice were maintained on a 12-hour light/dark cycle at 25°C with ad libitum access to food and water. For all experimental analyses, data collection was done with the investigator blinded to genotype and treatment.

The HFpEF-MetS diet was designed to induce MetS: obesity, hypertension, Type 2 diabetes, increased levels of plasma triglycerides (TG), and decreased levels of plasma high-density lipoprotein (HDL). As such, exclusion criteria included failure to induce obesity (adiposity index (AI) < 0.25) and/or hypertension (systolic blood

pressure < 120 mmHg) after 20 weeks on the HFpEF-MetS diet. Of the 36 WT and 48 FFAR4KO male mice randomized to the HFpEF-MetS diet, 3 WT and 5 FFAR4KO males were excluded based on these exclusion criteria.

Diet

The control diet consisted of the combination of an 11% fat and 11% sucrose chow (DYET #104607, Dyets Inc., Bethlehem, PA, Diet composition: Table 1A). The HFpEF-MetS diet consisted of the combination of a 42% fat and 30% sucrose chow (DYET #104608, Dyets Inc, Diet composition: Table 1B) and L-nitroarginine methyl ester (L-NAME, 1 mg/ml, Cat #N5751, Sigma Chemical, St Louis, MO) in the drinking water.

Body weight and body composition

Body weights were obtained weekly for all mice for 20 weeks. To measure body composition, EchoMRI scans (EchoMRI, Houston, TX, USA) were performed on all mice after 20 weeks on diet to record fat mass, lean mass, and free water. The adiposity index (AI) was calculated by the equation: AI = fat mass/lean mass.

Blood pressure

Blood pressure (BP), including mean arterial pressure (MAP), systolic pressure (SP), and diastolic pressure (DP), was measured in all mice after 20 weeks using the CODA non-invasive tail-cuff blood pressure system (Kent Scientific, Torrington, CT, USA). The procedure involved 2 days of acclimation, followed by measurements of blood pressure on 2 subsequent days to determine the average BP. For acclimation, mice were placed in cylindrical restrainers for 15 minutes each day prior to the test. Prior to measurements of BP, the Occlusion (O)-cuff and

Volume/Pressure Recording (VPR)-cuff were tested for patency, per manufacturer's instructions. For measurements of BP, mice were placed into cylindrical restrainers, with the tail left outside to attach the O-cuff and VPR cuff, and placed on a warming plate to acclimate and allow the tail temperature to reach 35°C. Once at temperature, the O-cuff was placed at the base of the tail followed by the VPR-cuff. Tail temperature was closely monitored throughout the experiment and maintained between 35-36°C. During each session, 25 blood pressure measurement cycles were recorded, with the first 3 or 4 cycles considered acclimation cycles.

Intraperitoneal glucose tolerance test

Blood glucose was sequentially measured at 0, 1, 15, 30, 60, and 120 min following an intraperitoneal glucose challenge in all mice after 20 weeks. Briefly, after an overnight fast (14 h), fasting glucose level was measured from tail blood using Quintet AC® Blood Glucose Monitor (McKesson, Irving, TX, USA). Mice were then injected i.p. with D-glucose at 2g/kg fasted body weight (#D16-500, Fisher Scientific, Waltham, MA, USA) and glucose was again measured from tail blood at the indicated time points.

Triglyceride (TG) and high-density lipoprotein (HDL) levels

Blood was collected from the retro-orbital plexus into EDTA tubes from all mice after 20 weeks as previously described [6], Total HDL and TG were measured by colorimetric assays. HDL was measured using an HDL-Cholesterol E kit (Wako Laboratory Chemicals; Richmond, VA) and TG was measured using an Infinity reagent colorimetric kit (Thermo Fisher Scientific; Waltham, MA).

Cardiac function

Cardiac function was measured by echocardiography in all mice after 20 weeks using the Vevo 2100 system (FujiFilm VisualSonics Inc. Toronto, ON, Canada) with a MS400 transducer. For all measurements, mice were anesthetized with isoflurane, gently restrained in the supine position on the prewarmed monitoring pad, and echocardiographic images were captured as mice recovered from anesthesia to achieve a target heart rate (HR) of 450 – 500 bpm. Isoflurane was maintained at 2-5% and adjusted accordingly in order to maintain a heart rate of 400-500 bpm. Parasternal long axis M-mode images of the left ventricle were captured to measure left ventricular parameters including: left ventricular posterior wall thicknesses (LVPW;s: systolic left ventricular posterior wall; LVPW;d: diastolic left ventricular posterior wall), left ventricular internal diameters (LVID;s: systolic left ventricular internal diameter; LVID;d: diastolic left ventricular internal diameter), left ventricular volumes (ESV: end systolic volume, ((7.0/(2.4 + LVID;s))*LVID;s3); EDV: end diastolic volume, ((7.0/(2.4 + LVID;d))*LVID;d3)), fractional shortening (FS: 100*((LVID;d – LVID;s)/LVID;d)), ejection fraction (EF: 100*((EDV – ESV)/EDV)), stroke volume (SV: EDV – ESV), and cardiac output (CO: SV*HR).Pulsed-wave Doppler images of the apical four-chamber view and Tissue Doppler images at the level of mitral valve were captured to measure diastolic function, including peak velocity of mitral flow from left ventricular relaxation in early diastole (E wave), peak velocity of mitral flow from left ventricular relaxation in late diastole (A wave), and peak early diastolic mitral annular velocity (e’). Parasternal short axis Pulse-wave Doppler images were captured at the level of aortic valve to measure parameters of pulmonary artery flow including pulmonary acceleration time (PAT) and pulmonary

ejection time (PET).

Strain Analysis

Global longitudinal strain (GLS) and reverse longitudinal peak strain rate were measured using the speckle-tracking based imaging analysis in the VisualSonics Vevo LAB software version 5.5.0 (Toronto, Canada). Briefly, cine loops of the B-mode in parasternal long axis view were captured. Three consecutive cardiac cycles were chosen to manually draw the endocardial wall border and trace the movement of endocardium over time.

Langendorff-perfused Hearts

Following 20 weeks of experimental treatment, mice were injected with 100 U of heparin and a barbiturate overdose. Hearts were rapidly harvested and placed in ice cold Krebs physiological salt solution. The aorta was cannulated and the heart was then perfused with warm oxygenated Krebs solution as previously described (36). A balloon was placed in the left ventricle to monitor ventricular pressures, oxygen probes monitored the oxygen concentrations in the perfusate and effluent, and a Transonic ultrasonic flow probe. The diastolic pressure was set to 10 mmHg and the heart was given a 20-minute equilibration period before the protocol began. After collection of baseline contractile data, the diastolic pressure-volume relationship was determined. This was accomplished by removing volume from the ventricular balloon until the systolic pulse was no longer detected, then 5µl of fluid was added back every minute until the diastolic pressure reached 30 mmHg. After this protocol the diastolic pressure was again set to 10 mmHg and the heart allowed to recover for 10 minutes. After this second equilibration period, 500 nM (-)-isoproterenol (Sigma)

was infused directly into the coronary arteries. Maximum contractile response was measured within 5 minutes of the start of the infusion.

Tissue histology

Ventricular fibrosis and microvascular density were measured in hearts harvested from mice after 20 weeks. Hearts were injected with 200 ml cold PBS with 60 mM KCl to arrest in diastole, excised, weighed, and subsequently perfused with PBS with 60 mM KCl to clear the heart of blood at 4ml/min rate for 4 mins. Atria were trimmed before hearts were flash-frozen in optimal cutting temperature (OCT) embedding medium. 10-micron cryosections at the midventricular level were cut and mounted at -25°C.

Fibrosis

Cryosections were stained in 0.1% solution of Sirius red (direct red 80, Sigma-Aldrich, St Louis, MO) and fast green (Sigma-Aldrich) in 1.2% picric acid (Ricca Chemical Company, Arlington, TX) (20 min, 25°C). To quantify LV fibrotic area, sections were imaged at 10X using a BZ-X800 fluorescent microscope (Keyence, Itasca, IL, USA). Using NIH FIJI software, the color balance of all images was corrected before quantification. Using the color threshold function, picrosirius red positively stained area (fibrotic area) and whole ventricle area (right and left) were defined and fibrotic area/ventricular area was calculated.

Microvascular (Capillary) Density

Cryosections were stained with isolectin GS-IB4 (Alexa Fluor™ 594 conjugated; Thermo fisher # I21413) at 20 µg/ml (2 hr, 25°C). and counterstained with DAPI at 1µg/ml (5 min, 25°C). To quantify capillary density, sections were

imaged at 20X using a Keyence BZ-X800 fluorescent microscope. Using NIH FIJI software, images were converted to 8-bit images, and following application of the threshold function, images were further converted into bi-color mode. Subsequently, 7-9 regions of interests (ROIs) in a section with a total area between 400000-600000 mm2 near the endocardium were randomly selected for analysis. To quantify capillary density, we used an automated quantification algorithm for particle counting (stained capillary endothelium) in which we considered that the diameter of a capillary to be larger than 3 mm, and thus we set the particle size threshold to greater than 7.1 mm2. Using this algorithm, average capillary density of the total area was calculated in two representative sections from each heart.

Hydroxyproline content

A hydroxyproline assay kit (Sigma, Burlington, MA, USA #MAK008) was used to quantify total collagen content in the heart. After 20 weeks, hearts were harvested and a portion of the ventricle, ~20 mg, was frozen and homogenized in ultra-pure water. The ventricular tissue was hydrolyzed in 12M HCl, and after 3 h at 120°C in pressure-tight capped vials, samples were centrifuged at 10000x g for 3 minutes at room temperature. Subsequently, 10 ml (HFpEF samples) or 40 ml (control samples) of supernatant was transferred to the 96-well plate and dried out overnight at 60°C. After drying, the Chloramine T/Oxidation Buffer Mixture provided with the hydroxyproline kit was added to both the sample and standard curve wells and incubated at room temperature. After 5 minutes, diluted DMAB reagent provided with the kit was added to all wells and incubated at 60°C for 90 mins. Finally, absorbance was read at 560nm using a Synergy H1 plate reader (Agilent Technologies, Santa

Clara, CA, USA). Hydroxyproline content was calculated using the standard curve and was normalized to tissue weight.

Statistical analysis

Cardiac phenotyping was analyzed using two-way ANOVA with a Tukey's post-test using Prism 9.0 (GraphPad Software Inc, San Diego, CA). Statistical significance was set at 0.05; Tukey's test was used to test for specified post-hoc differences using JMP version 13.2.1.

2.4 Results

To test the hypothesis that the loss of FFAR4 would worsen HFpEF-MetS, we developed a dietary intervention designed to induce HFpEF secondary to MetS, by adapting the recently described 2-hit model [103]. Mice were fed a high-fat/high-sucrose diet (42% fat/30% sucrose, less fat and more sucrose than [103] with L-NAME (1 mg/ml in the drinking water) designed to induce MetS (HFpEF-MetS diet). Specifically, at 8 weeks of age, male WT and FFAR4KO mice were randomized to the control diet (Cont diet: standard low fat diet, no L-NAME) or the high-fat/high-sucrose/L-NAME diet (HFpEF-MetS diet) (Diet composition: Tables 1A and 1B, Summary data: Table 2). After 20 weeks, we assessed metabolic parameters including weight gain, adiposity, arterial pressure, glucose tolerance, plasma triglycerides, and plasma HDL, as well as parameters of cardiac remodeling including cardiac function and cardiac histology.

The HFpEF-MetS diet induced a similar level of obesity in male WT and FFAR4KO mice

The HFpEF-MetS diet induced similar and significant weight gains in male WT and FFAR4KO mice (Figure 1A). In both WT and FFAR4KO mice, these weight gains were due to significant increases in fat mass (Figure 1B), while lean mass remained unchanged (Figure 1C), resulting in significant increases in the adiposity index (AI, Figure 1D), indicating male WT and FFAR4KO mice developed similar levels of obesity.

The HFpEF-MetS diet induced a similar level of mild hypertension in male WT and FFAR4KO mice

Mean arterial pressure (MAP) measured by tail cuff in male WT and FFAR4KO mice fed with the control diet were the same and were within a normal range (Figure 2A). As expected, the HFpEF-MetS diet (due to L-NAME) induced mild hypertension in both male WT and FFAR4KO male mice (Figure 2A). Similar trends were observed in systolic blood pressure (SBP) and diastolic blood pressure (DBP) (Figure 2B,C), suggesting male WT and FFAR4KO mice developed similar levels of hypertension.

The HFpEF-MetS diet induced a similar level of glucose intolerance in male WT and FFAR4KO mice

The HFpEF-MetS diet induced a similar degree of glucose intolerance following glucose challenge in male WT and FFAR4KO male mice, which is supported by similar blood glucose AUC (Figure 3B).

The HFpEF-MetS diet increased TG and HDL levels more in male FFAR4KO mice relative to male WT mice

Plasma was collected and isolated from male WT and FFAR4KO mice to analyze for triglyceride (TG) and high-density lipoprotein (HDL) levels. Both TG

(Figure 3C) and HDL (Figure 3D) levels were elevated by HFpEF-MetS diet in WT male mice. Interestingly, HFpEF-MetS induced greater increases in TG and HDL levels in male FFAR4KO mice relative to WT mice.

The HFpEF-MetS diet worsened diastolic dysfunction in male FFAR4KO mice relative to male WT mice.

Systolic and diastolic function were assessed by echocardiography (Figure 4A-B,Table 3). In WT male mice, as expected, the HFpEF-MetS died significantly increased both E/e' and E/A ratios, indicating of diastolic dysfunction (Figure 4C-D, green symbols). More importantly, in male FFAR4KO mice, the HFpEF-MetS diet significantly worsened diastolic dysfunction relative to male WT mice, evidenced by higher E/e' and E/A ratios (Figure 4C-D, closed green symbols vs closed blue symbols). As expected, ejection fraction was preserved regardless of diet or genotype (Figure 4E).

The HFpEF-MetS diet did not induce cardiac hypertrophy but induced a trend towards pulmonary hypertension in male FFAR4KO mice

Surprisingly, the HFpEF-MetS diet did not induce significant cardiac hypertrophy, and no significant differences were observed in heart weights across all four groups (Figure 5A), with the exception of a slight increase in posterior wall thickness at diastole (LVPW,d) in HFpEF-MetS diet-fed groups (Figure 5B). In this model, we would expect that increased afterload secondary to hypertension would induce hypertrophy, but again, we observed only a mild-hypertensive response of ~25 mmHg, which might explain the lack of significant hypertrophy. Interestingly, pulmonary acceleration time (PAT) normalized with heart rate is significantly

shortened only in FFAR4KO mice fed with HFpEF-MetS diet (Figure 5C,open blue symbols vs close blue symbols), suggesting a trend of pulmonary hypertension in response to MetS, which would imply left atrial dysfunction, a common finding in HFpEF patients.

The HFpEF-MetS diet produced a similar level of cardiac fibrosis but more severe microvascular rarefaction in male FFAR4KO mice

Total cardiac collagen content was measured by quantifying hydroxyproline content. The HFpEF-MetS diet significantly increased collagen levels to a similar degree in both male WT and FFAR4KO mice (Figure 6A). Interestingly, hydroxyproline content was directly correlated with diastolic function (E/e' ratio) (Figure 6B). Interestingly, there was no detectable change in interstitial fibrosis measured by picrosirius red staining, which stains primarily fibrillar collagens I and III, in either male WT or FFAR4KO mice (Figure 6C-D). However, a failure to observe interstitial fibrosis with picrosirius red staining was also noted in a mouse model of chronic kidney disease-induced HFpEF, although a further proteomic analysis revealed profound changes in the extracellular matrix, including many non-fibrillar collagens (38).

The HFpEF-MetS diet reduced capillary density in male FFAR4KO mice relative to FFAR4KO mice on the control diet (Figure E-F). Capillary density was also inversely correlated with diastolic function (E/A ratio) across all groups (Figure 6G).

The HFpEF-MetS diet worsened ventricular strain in male FFAR4KO mice

To gain further insight into the effects of the HFpEF-MetS diet on cardiac function, we used echocardiographic strain analysis to assess the effects the diet on

systolic and diastolic function in male WT and FFAR4KO mice. Interestingly, the HFpEF-MetS diet decreased global longitudinal strain in male FFAR4KO mice (GLS, Figure 7A), indicating systolic dysfunction in male FFAR4KO mice in response to MetS. Furthermore, the HFpEF-MetS diet reduced the reverse longitudinal peak strain rate (RLPSR) in male FFAR4KO mice (Figure 7B), a measure of ventricular wall velocity during diastole, confirming worsened diastolic function in these mice [104, 105][106]).

The HFpEF-MetS diet had no effect on isometric force generation in the heart, but increased oxygen extraction but lowered cardiac efficiency in male FFAR4KO mice

To eliminate the confounding effects of vascular loading and neuronal influences on cardiac function, we evaluated cardiac function in male mice using isolated Langendorff-perfused hearts. Surprisingly, in isolated hearts, isometric measures of systolic (dP/dT max) and diastolic function (dP/dT min) were not altered by the HFpEF-MetS diet or loss of FFAR4 (Figure 8A-B). Further, there were no significant differences in diastolic pressure-volume relationships between male WT and FFAR4KO hearts, a measure of the passive properties of the ventricle across several beats.

Interestingly, the HFpEF-MetS diet increased oxygen extraction from the coronary arteries but reduced cardiac efficiency in male FFAR4KO hearts (Figure C-D). Finally, while the baseline maximal isometric rate of pressure increase was the same across all groups, the HFpEF-diet attenuated the response to the b-adrenergic receptor agonist isoproterenol (Figure 8E), indicating that loss of FFAR4 in male mice

attenuates maximal systolic function.

2.5 Discussion

To test our hypothesis that loss of FFAR4 would worsen HFpEF, we developed a dietary intervention designed to induce HFpEF secondary to MetS, by adapting the recently described 2-hit model [103]. Mice were fed a high-fat/high-sucrose diet (42% fat/30% sucrose, less fat and more sucrose than [103]) with L-NAME (1 mg/ml in the drinking water) designed to induce MetS (Summary data: Table 2). As we hypothesized, HFpEF-MetS diet developed MetS, including obesity, hypertension, and pre-diabetic condition in both WT and FFAR4KO mice. Surprisingly, no difference in metabolic status was observed between WT and FFAR4KO mice with HFpEF-MetS diet, suggesting that mice responded to HFpEF-MetS diet equally in developing MetS, regardless of the absence of FFAR4. In other words, FFAR4 does not have an effect on the development of MetS. Our results are consistent with the some of the previous findings that FFAR4 has no effect on metabolic function in response to HFD [55].

Previous studies in mice [103, 107] and humans [90] have demonstrated a link between MetS and HFpEF. After 20 weeks, we measured cardiac function by echocardiography in both male WT and FFAR4KO mice to determine if MetS induced HFpEF in WT mice and if loss of FFAR4 worsened cardiac function secondary to MetS. As we hypothesized, mice fed with HFpEF-MetS diet developed a HFpEF-like syndrome (signs of diastolic dysfunction with preserved ejection fraction) secondary to MetS. More importantly, FFAR4KO mice exhibited more severe diastolic

dysfunction than WT mice in response to MetS. These data suggest that FFAR4 attenuated diastolic dysfunction in a mouse model of HFpEF secondary to MetS, which further supports our previous results that FFAR4 is cardioprotective in a model of pressure overload [6].

The development of HFpEF is often characterized by cardiac hypertrophy, interstitial fibrosis, and microvascular rarefaction (MVR). Here we evaluated hypertrophy by measuring heart weight and posterior wall thickness at diastole (LVPW,d). Surprisingly, no hypertrophy is developed in any group, likely due to the failure to develop significant hypertension as noted. In addition, while the HFpEF-diet induced fibrosis, there was no difference between WT and FFAR4KO mice. Capillary density was significantly reduced in FFAR4KO mice in response to MetS but not in WT mice, suggesting that the loss of FFAR4 worsened MVR. Both fibrosis and capillary density were correlated with diastolic function, which strengthens the reliability of our results.

Clinically, pulmonary hypertension is normally associated with and is secondary to HFpEF. It is characterized by the shortening of pulmonary artery acceleration time (PAT) measured by echocardiography [108]. Here, we observed shortened PAT in FFAR4KO mice in response to MetS but not in WT mice, suggesting that pulmonary hypertension is trending because of the loss of FFAR4.

Using strain analysis, mechanical changes in WT and FFAR4KO hearts in response to MetS were examined. Surprisingly, systolic dysfunction characterized by reduced GLS was observed in FFAR4KO mice in response to MetS. Although EF was unchanged in either male WT or FFAR4KO mice fed the HFpEF-MetS diet, it is

important to note that EF does not reflect myocardial contractility and is load-dependent [109, 110]. In addition, worsened diastolic dysfunction characterized by decreased RLPSR was observed in FFAR4KO mice, which was in alignment with the results assessing conventional cardiac parameters (E/A ratio, E/e' ratio).

Unexpectedly, there was no difference in systolic function or diastolic function in isolated hearts between WT and FFAR4KO mice, which suggests that the worsened diastolic dysfunction observed in male FFAR4 KO hearts is only evident in hearts with dynamic changes in volume that occur in vivo. Furthermore, the absence of increased passive stiffness in isolated hearts of FFAR4KO mice implies that a reduction in the rate of cellular re-lengthening drives the worsened diastolic dysfunction in male FFAR4KO hearts, which is consistent with the decrease in reverse longitudinal peak strain rate observed in these mice. The discrepancy between oxygen consumption and cardiac efficiency indicated that loss of FFAR4 affects cardiac oxygen delivery and the ability of the heart to convert oxygen into mechanical function and is likely the result of microvascular rarefaction.

In conclusion, we have identified a novel cardioprotective role for FFAR4 in the context of HFpEF secondary to MetS, suggesting a potentially new therapeutic target for the management of cardiometabolic disease. In response to a dietary challenge designed to induce MetS, modified from the original 2-hit HFpEF model proposed by Schiattarella *et al.* [102], we found that systemic deletion of FFAR4 surprisingly did not affect development of MetS, but significantly worsened ventricular remodeling in male mice.

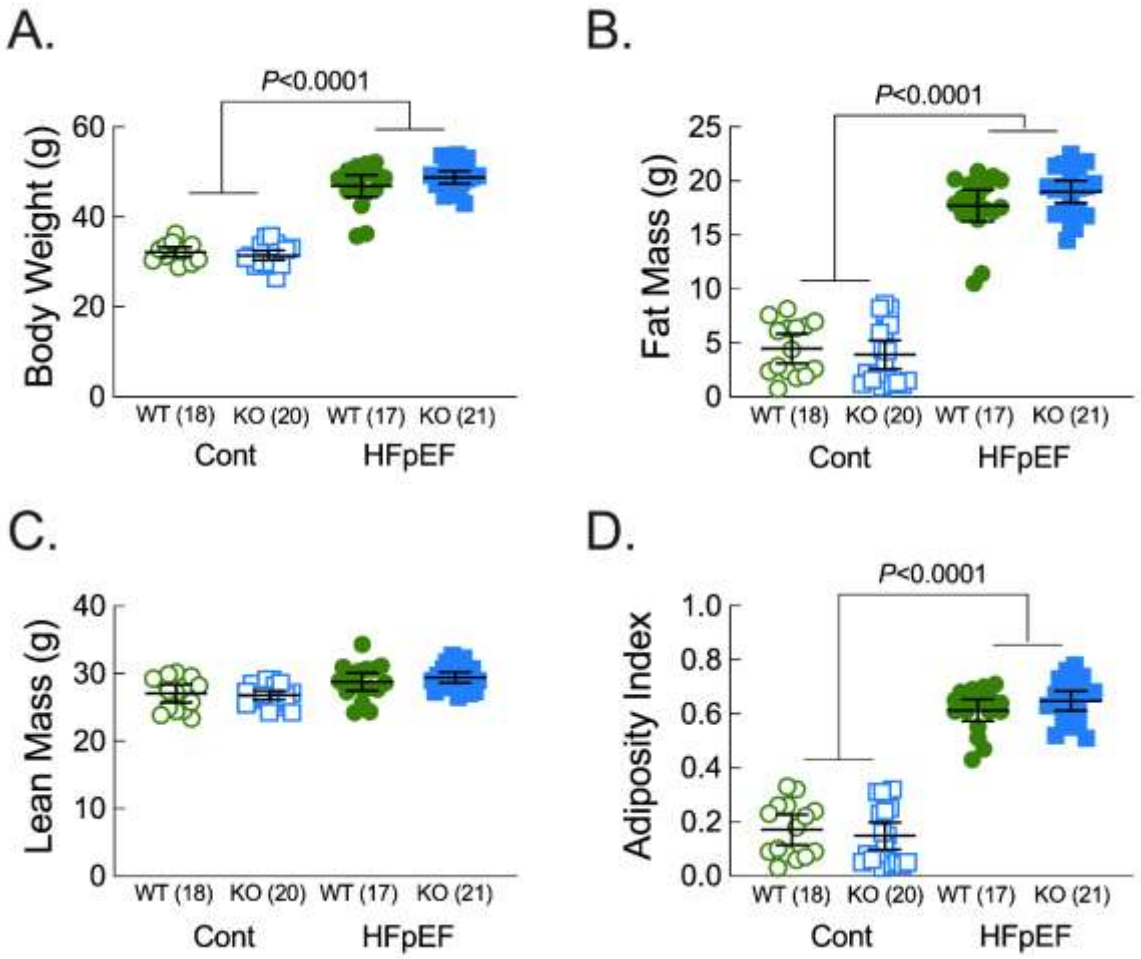

Figure 1. HFpEF-MetS diet induced a similar level of obesity in WT and FFAR4KO mice.

Male wild-type (WT, green) and FFAR4KO (KO, blue) mice were fed a control diet (Cont., open symbols) or the combination of a high-fat (42%)/high-sucrose (30%) diet and L-NAME (1 mg/ml) in the drinking water (HFpEF, closed symbols) for 20 wks. After 20 weeks, **A**. Body weight was recorded, and body composition, including: **B**. Fat Mass and **C**. Lean Mass were determined by EchoMRI; and **D**. Adiposity Index (fat mass/lean mass) was calculated. Data (**A-D**) are presented as Mean ± 95% CI and were analyzed by two-way ANOVA with Tukey's multiple comparison test.

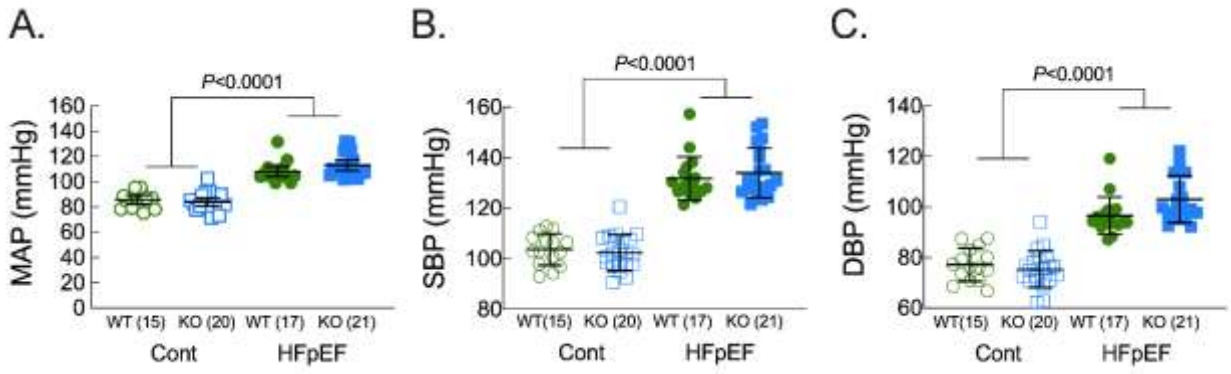

Figure 2. HFpEF-MetS diet induced a similar level of mild hypertension in WT and FFAR4KO mice.
Male wild-type (WT, green) and FFAR4KO (KO, blue) mice were fed a control diet (Cont., open symbols) or the combination of a high-fat (42%)/high-sucrose (30%) diet and L-NAME (1 mg/ml) in the drinking water (HFpEF, closed symbols) for 20 wks. After 20 weeks, **A.** Mean Arterial Pressure (MAP), **B.** Systolic Blood Pressure (SBP), and **C.** Diastolic Blood Pressure (DBP) was measured by tail-cuff**.** Data (**A-C**) are presented as Mean ± 95% CI and were analyzed by two-way ANOVA with Tukey's multiple comparison test.

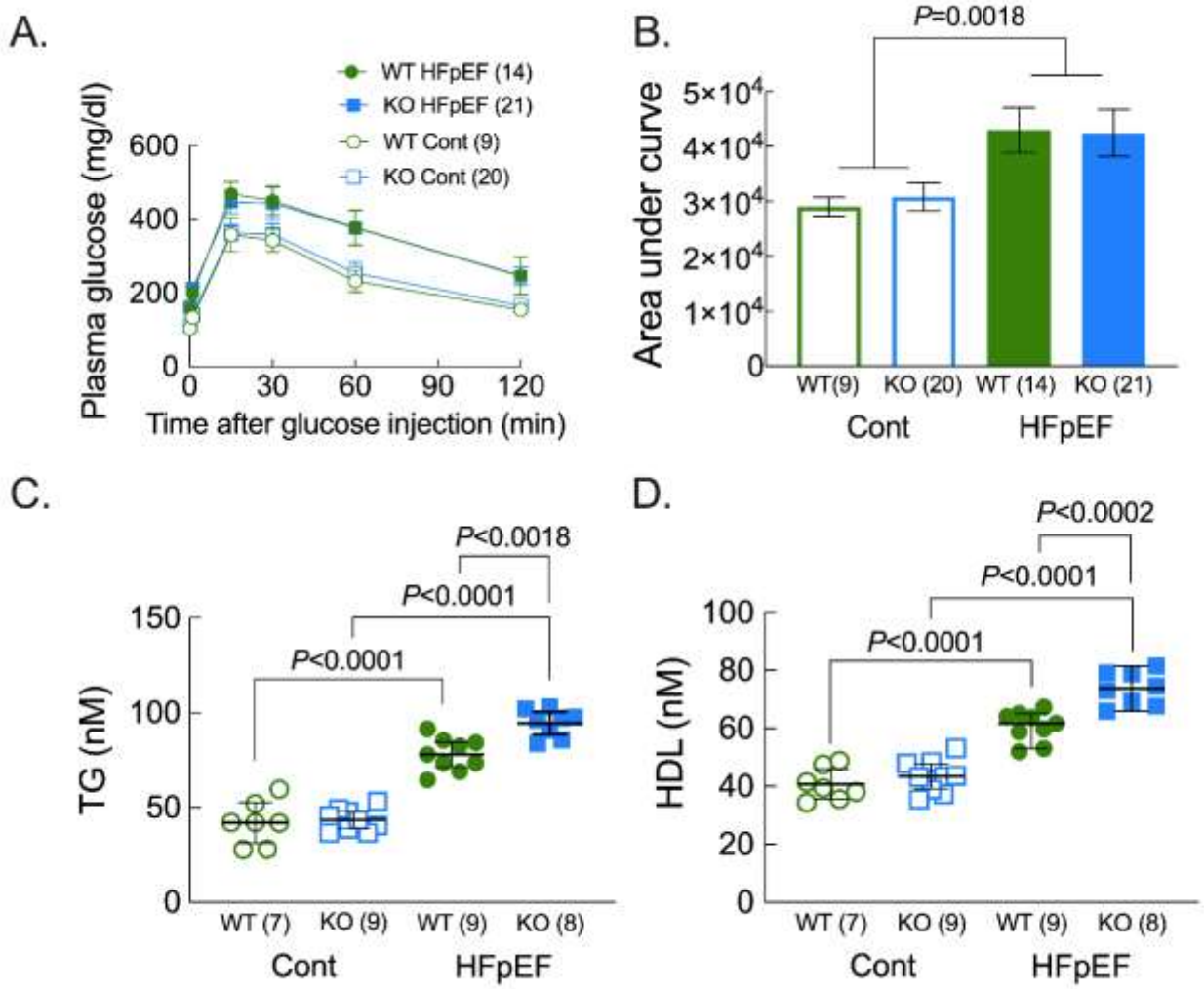

Figure 3. HFpEF-MetS diet induced a similar level of glucose intolerance in both genotypes but with an increased TG and HDL in FFAR4KO mice
Male wild-type (WT, green) and FFAR4KO (KO, blue) mice were fed a control diet (Cont., open symbols) or the combination of a high-fat (42%)/high-sucrose (30%) diet and L-NAME (1 mg/ml) in the drinking water (HFpEF, closed symbols) for 20 wks. After 20 weeks, **A.** Intraperitoneal glucose tolerance test (IPGTT). **B.** Area under the curve of the IPGTT. **C.** Triglyceride levels and **D.** High density lipoprotein- cholesterol levels were measured from plasma. Data (**A-D**) are presented as Mean ± 95% CI and were analyzed by two-way ANOVA with Tukey's multiple comparison test.

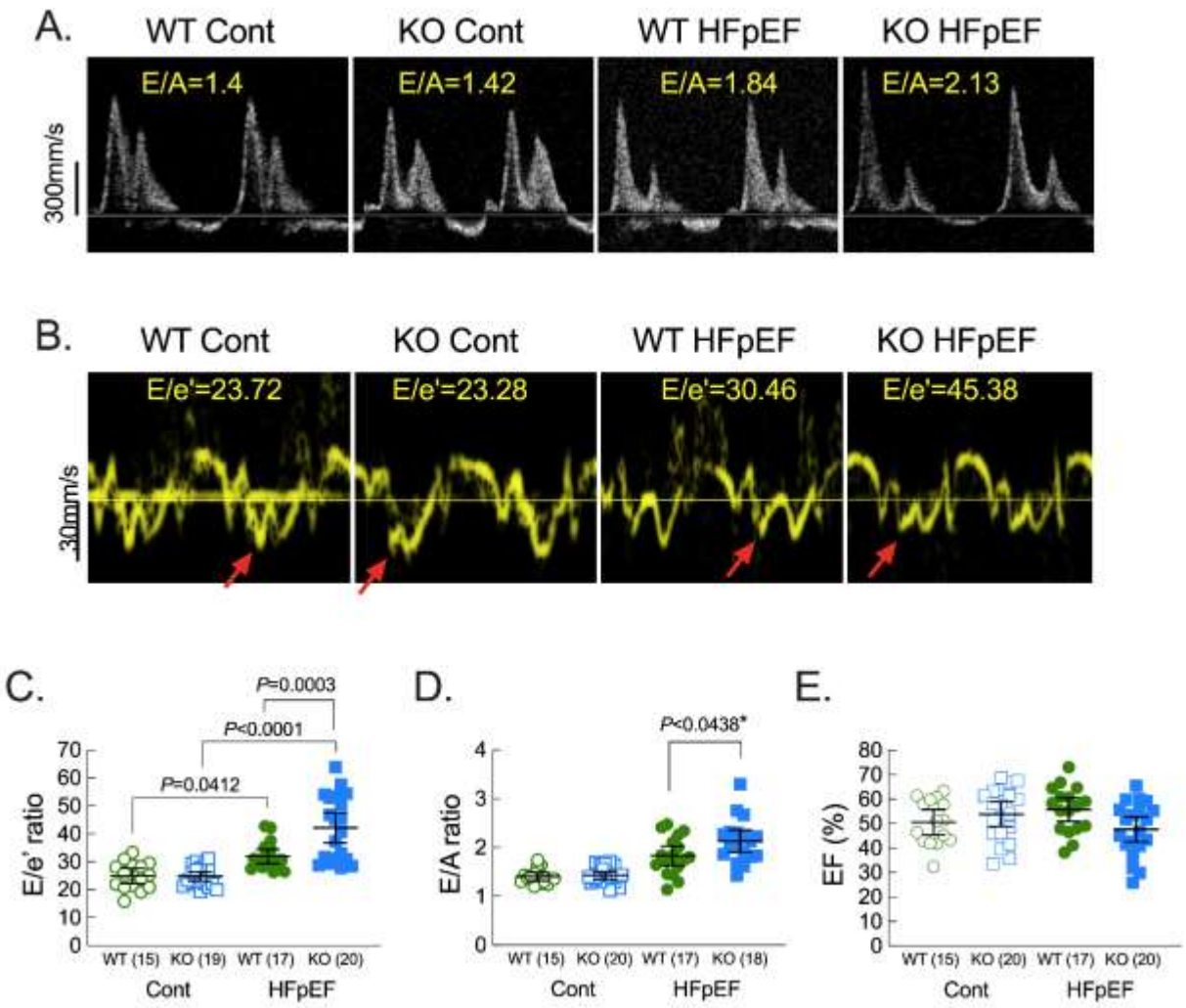

Figure 4. HFpEF-MetS diet resulted in a worsened diastolic dysfunction in FFAR4KO mice than in WT mice, but with a preserved ejection fraction

Cardiac function was measured by echocardiography in male wild-type (WT, green) and FFAR4KO (KO, blue) mice after 20 weeks on the control diet (Cont., open symbols) or HFpEF-MetS diet (HFpEF, closed symbols). **A.** Representative images of Pulse Wave doppler tracings from male WT and FFAR4KO mice. **B.** Representative images of Tissue doppler tracings from male WT and FFAR4KO mice. E' waves were indicated by red arrows. **C.** E/e' ratio. **D.** E/A ratio. **E.** Ejection fraction (EF,%). Data (**C-E**) are presented as Mean ± 95% CI and were analyzed by two-way ANOVA with Tukey's multiple comparison test.
* Primary interaction: *P*=0.0779, Welch's t-test for WT HFpEF vs FFAR4KO HFpEF, employed due to unequal variance between Control and HFpEF-MetS diet groups: *P*=0.0438.

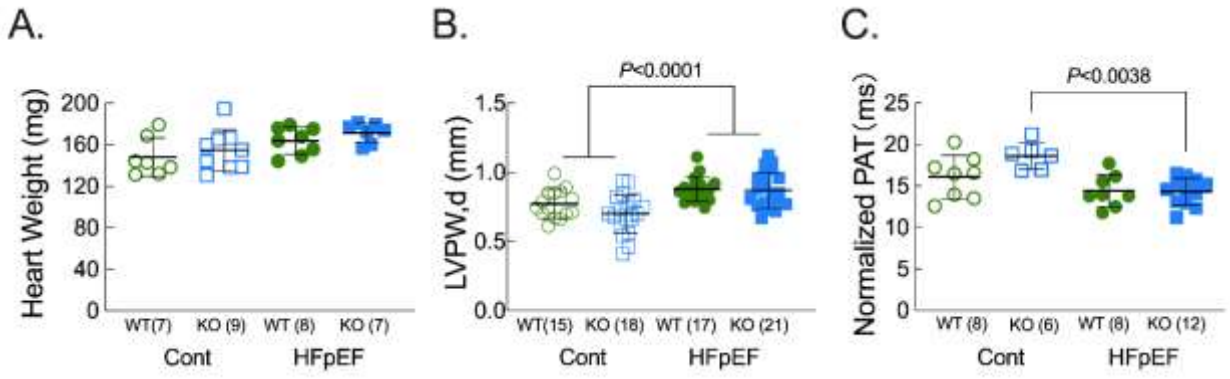

Figure 5. HFpEF-MetS diet did not induce cardiac hypertrophy in any groups but induced a trend of pulmonary hypertension

Morphological changes (**A,B**) and pulmonary function (**C**) were measured by echocardiography in male wild-type (WT, green) and FFAR4KO (KO, blue) mice after 20 weeks on the control diet (Cont., open symbols) or HFpEF-MetS diet (HFpEF, closed symbols). **A.** Heart weights. **B.** Left ventricular posterior wall thickness at diastole (LVPW,d) and **C.** Pulmonary acceleration time normalized with heart rate (Normalized PAT). Data (**A-C**) are presented as Mean ± 95% CI and were analyzed by two-way ANOVA with Tukey's multiple comparison test.

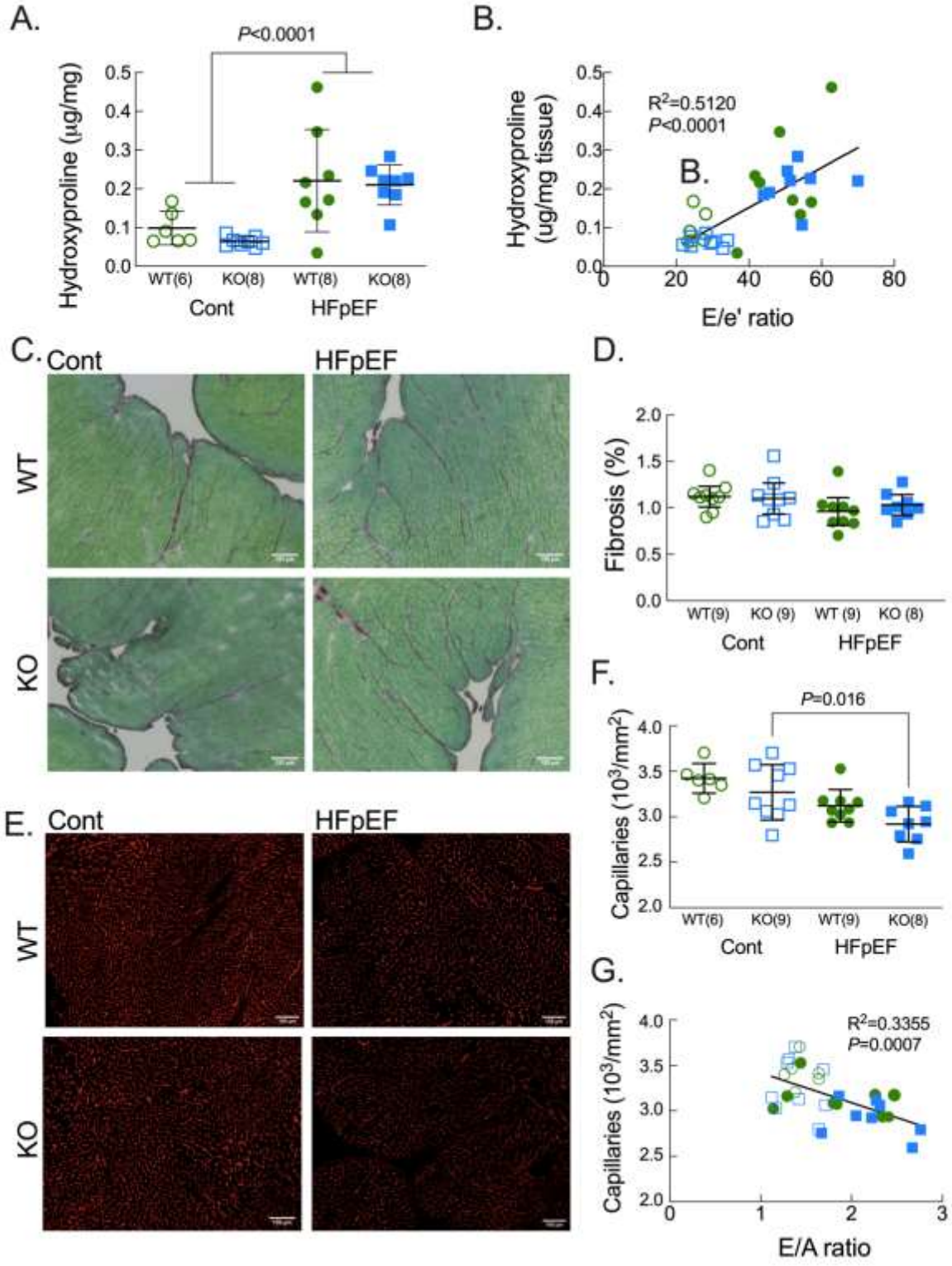
A.
P<0.0001
Hydroxyproline (μg/mg)
0.5
0.4
0.3
0.2
0.1
0.0
WT(6)
KO(8)
WT(8)
KO(8)
Cont
HFpEF
B.
Hydroxyproline (ug/mg tissue)
R2=0.5120
P<0.0001
B.
E/e' ratio
C.
Cont
HFpEF
WT
KO
D.
Fibrosis (%)
2.0
1.5
1.0
0.5
0.0
WT(9)
KO (9)
WT (9)
KO (8)
Cont
HFpEF
E.
Cont
HFpEF
WT
KO
F.
P=0.016
Capillaries (10³/mm²)
4.0
3.5
3.0
2.5
2.0
WT(6)
KO(9)
WT(9)
KO(8)
Cont
HFpEF
G.
Capillaries (10³/mm²)
R2=0.3355
P=0.0007
E/A ratio

Figure 6. FFAR4KO mice developed a similar level of fibrosis but more severe microvascular rarefaction than WT mice in response to MetS

Changes in cardiac structure was measured in male wild-type (WT, green) and FFAR4KO (KO, blue) mice after 20 weeks on the control diet (Cont., open symbols) or HFpEF-MetS diet (HFpEF, closed symbols). **A.** Ventricular fibrosis quantified hydroxyproline content (μg/mg ventricular wet weight). **B.** Relationship between ventricular fibrosis quantified by hydroxyproline content and diastolic function (E/e' ratio) n=30, R^2=0.5120, P<0.0001.**C.** Representative images of ventricular fibrosis quantified from ventricular cross sections from male WT and FFAR4KO mice stained with Sirius red/Fast Green (SR/FG). **D.** Ventricular fibrosis quantified by SR/FG staining. **E.** Representative images of capillaries in LV sections from male WT and FFAR4KO mice stained with isolectin B4 (IB4) (Red). **F.** LV myocardial capillary density quantified by Isolectin-B4. **G.** Relationship between myocardial capillary density and diastolic function (E/A ratio) n=32, R^2=0.3355, P=0.0007. Data (**A-G, excluding C,E**) are presented as Mean ± 95% CI and were analyzed by two-way ANOVA with Tukey's multiple comparison test.

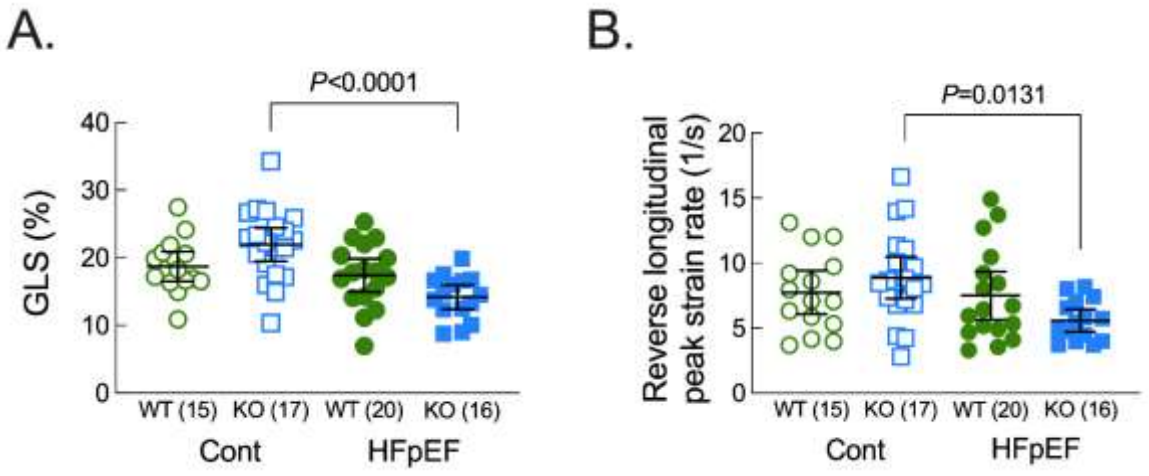

Figure 7. FFAR4KO mice exhibited worse myocardial performance than WT mice in response to MetS by speckle tracking

Cardiac function was measured by echocardiographic strain analysis from male wild-type (WT, green) and FFAR4KO (KO, blue) mice after 20 weeks on the control diet (Cont., open symbols) or HFpEF-MetS diet (HFpEF, closed symbols). **A.** Global longitudinal strain (GLS, %). **B.** Reverse longitudinal peak strain rate (1/s). Data (**A-B**) are presented as Mean ± 95% CI and were analyzed by two-way ANOVA with Tukey's multiple comparison test.

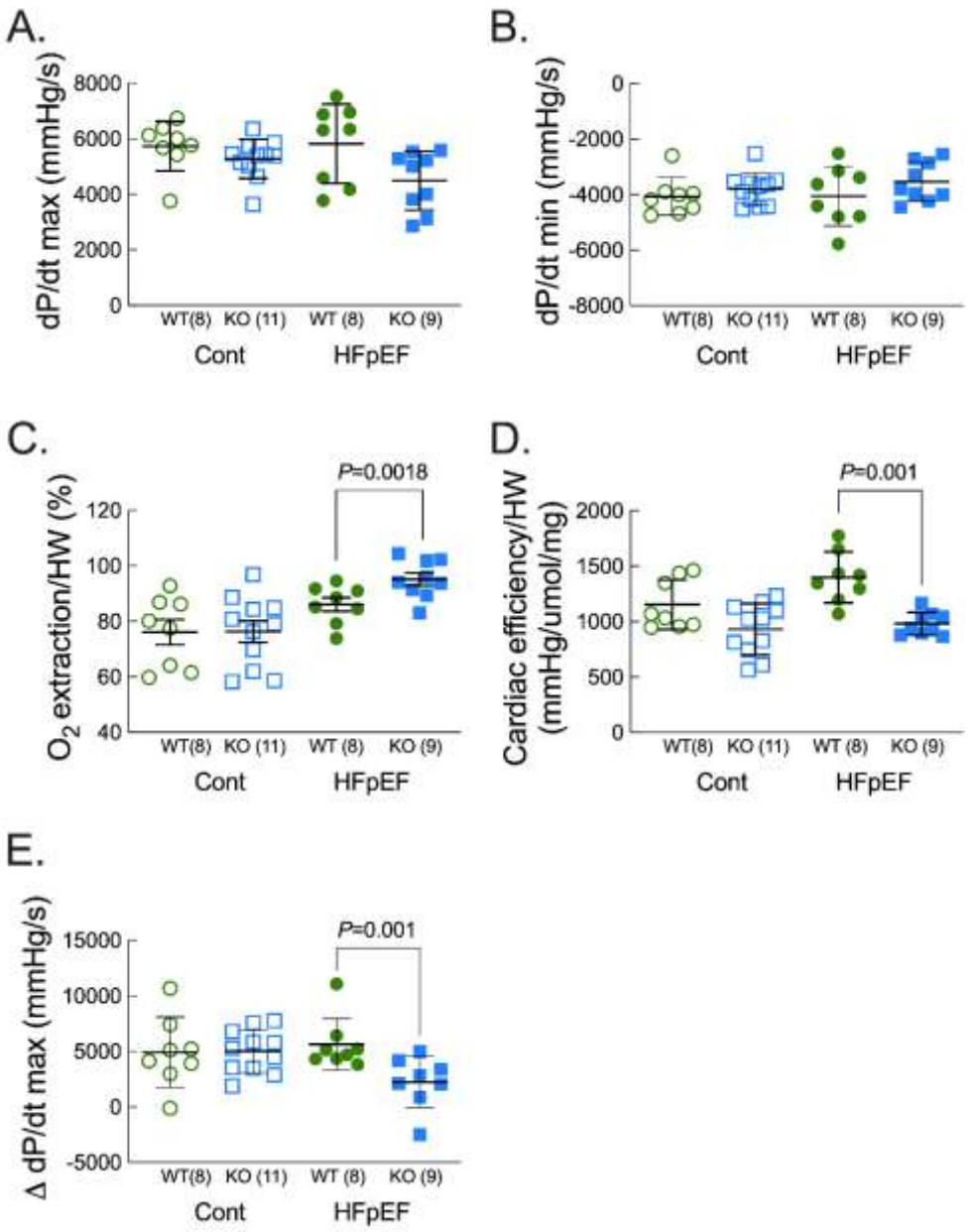

Figure 8. FFAR4KO mice had higher oxygen extraction but lower cardiac efficiency than WT mice in response to MetS by Langendorff

Cardiac function was measured using Langendorff perfused hearts from male wild-type (WT, green) and FFAR4KO (KO, blue) mice after 20 weeks on the control diet (Cont., open symbols) or HFpEF-MetS diet (HFpEF, closed symbols).**A.** dP/dt max. **B.** dP/dt min. **C.** O2 extraction normalized to heart weight (%). **D.** Cardiac efficiency normalized to heart weight (mmHg/μmol/mg). **E.** Change in dP/dt from baseline following isoproterenol administration.

Table 1A: DYETS #104607 Custom Control Diet Composition

Ingredient	kcal/g	g/kg	kcal/kg	%kcal
Casein	3.58	200	716	19.74
L-Cystine	4	3	12	0.33
Sucrose	4	100	400	11.03
Cornstarch	3.6	414.5	1492.2	41.14
Dyetrose	3.8	140	532	14.67
Corn oil	9	25	225	6.20
Lard	9	20	180	4.96
Cellulose	0	50	0	0.00
Mineral Mix #210025	0.88	35	30.8	0.85
Vitamin Mix #310025	3.87	10	38.7	1.07
Choline Bitartrate	0	2.5	0	0.00
Total		**1000**	**3626.7**	**100**

Table 1B: DYETS #104608 Custom High Fat Diet Composition

Ingredient	kcal/g	g/kg	kcal/kg	%kcal
Casein	3.58	200	716	15.56
L-Cystine	4	3	12	0.26
Sucrose	4	350	1400	***30.42***
Cornstarch	3.6	134.5	484.2	10.52
Corn oil	9	25	225	4.89
Lard	9	190	1710	***37.15***
Cellulose	0	50	0	0.00
Mineral Mix #200000	0.47	35	16.45	0.36
Vitamin Mix #310035	3.92	10	39.2	0.85
Calcium Carbonate	0	2.5	0	0.00
Total		**1000**	**4602.85**	**100**

Table 2: Metabolic parameters in male mice after 20 weeks on diet

Metabolic Parameter	**WT Cont (15)**	**KO Cont (20)**	**WT HFpEF (17)**	**KO HFpEF (20)**	**ANOVA** Primary	Diet	Genotype
BW (g)	32.2 (31.1, 33.3)	31.4 (30.4, 32.5)	46.9 (44.4, 49.3)	48.8 (47.4, 50.2)	0.0785	<0.0001	0.4293
Fat mass (g)	4.5 (3.1, 5.8)	3.9 (2.6, 5.2)	17.7 (16.0, 19.0)	19.1 (18.0, 20.0)	0.1199	<0.0001	0.5028
Lean mass (g)	27.0 (25.7, 28.4)	26.8 (26.1, 27.5)	28.8 (27.4, 30.1)	29.4 (28.6, 30.2)	0.3815	<0.0001	0.7032
Adiposity index	0.2 (0.1, 0.2)	0.1 (0.1, 0.2)	0.6 (0.6, 0.7)	0.7 (0.6,0.7)	0.1600	<0.0001	0.7116
Plasma TG (nM)	35.0 (29.6, 40.3)	48.8 (43.7, 54.0)	79.2 (74.1, 84.3)	93.1 (87.9, 98.3)	0.0160	<0.0001	0.0044
Plasma HDL (nM)	41.1 (37.8, 44.4)	44.2 (403., 48.2)	60.6 (57.5, 64.0)	72.3 (68.1, 76.3)	0.0124	<0.0001	0.0004
SBP (mmHg)	103.6 (100.2, 107.1)	102.4 (99.1, 105.7)	131.8 (127.3, 136.2)	134.0 (129.4, 138.6)	0.3741	<0.0001	0.8063
DBP (mmHg)	77.1 (73.5, 80.8)	75.3 (71.9, 78.7)	96.5 (92.7, 100.3)	103.1 (98.7, 107.4)	0.0266	<0.0001	0.2099
MAP (mmHg)	85.6 (82.1, 89.2)	84.0 80.7, 87.3)	107.9 (104.1, 111.8)	113.0 (108.7, 117.4)	0.0716	<0.0001	0.3485

Data are presented as Mean ± standard error for the number of mice indicated in parentheses. TG, triglyceride; HDL, high density lipoprotein; SBP, systolic blood pressure; DBP, diastolic blood pressure; MAP; mean arterial pressure. ANOVA denotes the results of the two-way ANOVA with the *P* values shown for the primary interaction as well as the effects of diet or genotype

Table 3: Cardiac function in male mice after 20 weeks on diet

Cardiac function	**WT Cont (15)**	**KO Cont (20)**	**WT HFpEF (17)**	**KO HFpEF (20)**	**ANOVA** primary	Diet
EF (%)	50.5 (45.4, 55.7)	53.8 (48.8, 58.9)	55.7 (50.8, 60.5)	47.6 (42.5, 52.8)	0.0236	0.8269
SV (μl)	38.3 (35.3, 41.4)	39.9 (34.6, 45.2)	39.5 (35.1, 44.0)	34.5 (30.8, 38.3)	0.1233	0.3181
FS (%)	25.7 (22.5, 28.9)	27.9 (24.7, 31.1)	28.9 (25.8, 32.1)	23.9 (20.9, 27.0)	0.0201	0.8250
EDV (μl)	77.3 (70.3, 84.2)	74.6 (66.6, 82.5)	72.1 (63.8, 80.4)	73.9 (65.9, 81.8)	0.5548	0.4386
ESV (μl)	38.9 (31.7, 46.2)	34.7 (28.9, 40.6)	32.6 (26.0, 39.2)	39.3 (32.3, 46.4)	0.0974	0.7920
CO (ml/min)	17.4 (15.3, 19.4)	18.6 (16.0, 21.2)	16.5 (14.5, 18.4)	15.2 (13.4, 16.9)	0.2158	0.0391
IVS; s (mm)	1.4 (1.3, 1.5)	1.4 (1.3, 1.4)	1.5 (1.5, 1.6)	1.5 (1.4, 1.6)	0.6494	0.0002
IVS; d (mm)	1.0 (0.9, 1.1)	1.0 (0.9, 1.0)	1.1 (1.1, 1.2)	1.1 (1.1, 1.2)	0.4849	<0.0001
LVID; s (mm)	3.1 (2.9, 3.3)	3.0 (2.8, 3.1)	2.9 (2.6, 3.1)	3.1 (2.9, 3.3)	0.0592	0.6635
LVID; d (mm)	4.2 (4.0, 4.3)	4.1 (3.9, 4.3)	4.0 (3.8, 4.2)	4.1 (3.9, 4.2)	0.5636	0.3368
LVPW; s (mm)	1.1 (1.0, 1.2)	1.0 (0.9, 1.1)	1.2 (1.1, 1.3)	1.1 (1.0, 1.2)	0.8638	0.0098
LVPW; d (mm)	0.8 (0.7, 0.8)	0.7 (0.6, 0.8)	0.9 (0.8, 0.9)	0.9 (0.8, 0.9)	0.3836	<0.0001
LV mass corrected (mg)	114.7 (106.8, 122.6)	105.2 (96.0, 114.4)	128.7 (120.1, 137.3)	132.4 (119.9, 144.9)	0.1763	<0.0001
LVRI	34.4 (32.5, 36.3)	32.0 (29.9, 34.1)	39.8 (38.4, 41.3)	40.8 (37.4, 44.2)	0.1568	<0.0001
E/A	1.4 (1.3, 1.5)	1.4 (1.3, 1.5)	1.8 (1.6, 2.0)	2.1 (1.9, 2.4) (18)	0.0779	<0.0001
E (mm/s)	784.2 (740.1, 828.2)	724.6 (695., 753.5)	748.6 (692.1, 805.2)	795.6 (755.9, 835.3)	0.0102	0.3818
A (mm/s)	562.3 (528.3, 596.3)	513.5 (482.9, 544.1)	422.9 (377.0, 468.8)	388.8 (344.1, 433.6) (18)	0.6941	<0.0001
E/e'	24.9 (22.2, 27.6)	24.7 (23.0, 26.5) (19)	31.9 (29.3, 34.4)	42.1 (36.7, 47.6)	0.0036	<0.0001
GLS (%)	-18.7 (-20.9, -16.5)	-22.0 (-24.41, -19.47)	-17.4 (-19.82, -14.93)	-14.2 (-16.0, -12.4)	0.0045	<0.0001
RLPSR (1/s)	7.7 (6.1, 9.4)	8.8 (7.3, 10.5)	7.5 (5.7, 9.4)	5.6 (4.7, 6.4)	0.0463	0.0224
PAT norm. to HR (ms)	16.1 (13.9， 18.2) (8)	18.6 (16.9, 20.3) (6)	14.4 (12.8, 16.0) (8)	14.3 (13.3, 15.4) (12)	0.0717	0.0002
HR (bpm)	450.7 (427.1, 474.3)	466.7 (447.5, 485.8)	417.4 (403.1, 431.8)	439.5 (421.7, 457.3)	0.7359	0.0013

Data are presented as Mean ± standard error for the number of mice indicated in parentheses. HR, heart rate; SV, stroke volume; EF, ejection fraction; FS, fractional shortening; EDV, end diastolic volume; ESV, end systolic volume; CO, cardiac output; IVS;s, interventricular septal thickness at systole; IVS;d, interventricular septal thickness at diastole; LVID;s, left ventricular internal diameter systole; LVID;d, left ventricular internal diameter diastole; LVPW;s, left ventricular posterior wall systole; LVPW;d, left ventricular posterior wall diastole; LVRI, left ventricular remodeling index; E/A, early mitral valve filling velocity/ late mitral valve filling velocity; E, early mitral valve filling velocity ; E/E', early mitral valve filling velocity/early mitral annular tissue velocity; GLS, global longitudinal strain; RLPSR, reverse longitudinal peak strain rare; PAT, pulmonary artery acceleration time normalized to heart rate. ANOVA denotes the results of the two-way ANOVA with the *P* values shown for the primary interaction as well as the effects of diet or genotype

CHAPTER 3: Loss of FFAR4 increased weight gain and obesity but did not affect cardiac dysfunction in a model of cardiometabolic disease in female mice.

Naixin Zhang, Katherine A. Murphy, Chastity L. Healy, and Timothy D. O'Connell

Department of Integrative Biology and Physiology, University of Minnesota, Minneapolis, MN 55455 USA

3.1 Summary

Epidemiological studies have suggested that females are more prone to developing HFpEF than males [111, 112], although the mechanistic basis for these sex-based differences is not entirely clear. In the context of FFAR4, few previous studies have examined sex-based differences. Interestingly, we previously found that following pathologic pressure overload induced by transverse aortic constriction (TAC), pathologic remodeling was worsened in male but not female FFARKO mice [6]. This sex-based difference was confirmed in a large clinical cohort in which the FFAR4 R270H inactivating polymorphism was associated with hypertrophy and ventricular dilation in males but not females [6]. This identifies a significant sex-based difference in FFAR4 mediated cardioprotective signaling in the heart, and to the best of our knowledge, the first finding of its kind. Given that there are sex-based differences in the incidence and prevalence of HFpEF in humans, we examined the sex and FFAR4 in our mouse model of HFpEF. While the HFpEF-MetS diet induced MetS in female WT mice, it was slight less severe than in males, but the degree of diastolic dysfunction was

similar. More importantly, we found that the HFpEF-MetS diet induced greater weight gain and obesity, but no worsening of the HFpEF-like phenotype in female mice.

3.2 Introduction

Epidemiological studies have suggested that females are more prone to developing HFpEF than males [111, 112]. As of 2002, AHA the lifetime risk of developing HF is equivalent between both sexes, but with variations in two distinct HF subtypes. Men are more likely to develop HFrEF, which is driven mostly by coronary disease/myocardial infarction [113]. In contrast, women are 2-fold more likely to develop HFpEF [113, 114]. This is partially due to the difference in cardiac structure between men and women, with which women have higher ejection fraction to start with and tend to develop concentric remodeling [111]. In addition to sex, risk factors for HFpEF include aging, obesity, diabetes, hypertension (MetS). The prevalence of obesity and diabetes is higher in women which might also contribute to the higher incidence of HFpEF in women [115].

Despite the sex-based differences observed in humans with cardiometabolic disease, few studies examined sex-based differences in animal models of HFpEF. A recent paper suggested both male and female feline developed cardiopulmonary dysfunction to pressure overload-induced HFpEF and phenotype in female is less severe [116]. In addition, two studies compared female mice with males in developing HFpEF [117, 118], and the results are mixed. One study reported that remodeling was less severe in female versus male mice with the two-hit HFpEF model (similar to our HFpEF-MetS diet, but with a 60% HFD) [117]. On the contrary, another study suggested

that remodeling was worse in female mice the two-hit HFpEF model [118]. The basis for this discrepancy is unclear.

Prior studies examining the physiologic function of FFAR4 have generally failed to address sex-based differences. However, we recently reported a significant sex-based difference in FFAR4-mediated cardioprotection in response to pathologic pressure overload induced by transverse aortic constriction (TAC). In male FFAR4KO mice, TAC worsened remodeling relative to male WT mice, whereas in female FFAR4KO mice, TAC induced a similar response to female WT mice [6]. Furthermore, in an analysis of a large clinical cohort or patients referred for a medically necessary echocardiogram, we found that the FFAR4 R270H inactivating polymorphism was associated with hypertrophy and ventricular dilation in males but not females [6].

Based on defined sex-based differences in cardiometabolic disease in humans, and our prior findings of a significant sex-based difference in FFAR4-mediated cardioprotection, we hypothesized that the loss of FFAR4 would have no effect on remodeling in response to the HFpEF-MetS diet in female mice.

3.3 Methods

Mice

FFAR4KO mice that were generated from cryopreserved sperm from C57Bl/6N-FFAR4tm1(KOMP)Vlcg (Design ID: 15078; Project ID: VG15078) purchased from The Mutant Mouse Resource and Research Centers (MMRRC), UC-Davis (Davis, CA, USA). All mice are backcrossed into the C57Bl/6J strain as previously described ([6]).

At 8 weeks of age, male WT and FFAR4KO mice were randomized to be fed a

control diet or a diet designed to induce heart failure preserved ejection fraction secondary to MetS (HFpEF-MetS) for 20 weeks. Mice were maintained on a 12-hour light/dark cycle at 25°C with ad libitum access to food and water. For all experimental analyses, data collection was done with the investigator blinded to genotype and treatment.

The HFpEF-MetS diet was designed to induce MetS: obesity, hypertension, Type 2 diabetes, increased levels of plasma triglycerides (TG), and decreased levels of plasma high-density lipoprotein (HDL). As such, exclusion criteria included failure to induce obesity (adiposity index (AI) < 0.25) and/or hypertension (systolic blood pressure < 120 mmHg) after 20 weeks on the HFpEF-MetS diet. Of the 36 WT and 48 FFAR4KO male mice randomized to the HFpEF-MetS diet, 3 WT and 5 FFAR4KO males were excluded based on these exclusion criteria.

Diet

The control diet consisted of the combination of an 11% fat and 11% sucrose chow (DYET #104607, Dyets Inc., Bethlehem, PA). The HFpEF-MetS diet consisted of the combination of a 42% fat and 30% sucrose chow (DYET #104608, Dyets Inc., Bethlehem, PA) and L-nitroarginine methyl ester (L-NAME, 1 mg/ml, Cat #N5751, Sigma Chemical, St Louis, MO) in the drinking water.

Body weight and body composition

Body weights were obtained weekly for all mice for 20 weeks. To measure body composition, EchoMRI scans (EchoMRI, Houston, TX, USA) were performed on all mice after 20 weeks on diet to record fat mass, lean mass, and free water. The adiposity index (AI) was calculated by the equation: AI = fat mass/lean mass.

Blood pressure

Blood pressure (BP), including mean arterial pressure (MAP), systolic pressure (SP), and diastolic pressure (DP), was measured in all mice after 20 weeks using the CODA non-invasive tail-cuff blood pressure system (Kent Scientific, Torrington, CT, USA). The procedure involved 2 days of acclimation, followed by measurements of blood pressure on 2 subsequent days to determine the average BP. For acclimation, mice were placed in cylindrical restrainers for 15 minutes each day prior to the test. Prior to measurements of BP, the Occlusion (O)-cuff and Volume/Pressure Recording (VPR)-cuff were tested for patency, per manufacturer's instructions. For measurements of BP, mice were placed into cylindrical restrainers, with the tail left outside to attach the O-cuff and VPR cuff, and placed on a warming plate to acclimate and allow the tail temperature to reach 35°C. Once at temperature, the O-cuff was placed at the base of the tail followed by the VPR-cuff. Tail temperature was closely monitored throughout the experiment and maintained between 35-36°C. During each session, 25 blood pressure measurement cycles were recorded, with the first 3 or 4 cycles considered acclimation cycles.

Intraperitoneal glucose tolerance test

Blood glucose was sequentially measured at 0, 1, 15, 30, 60, and 120 min following an intraperitoneal glucose challenge in all mice after 20 weeks. Briefly, after an overnight fast (14 h), fasting glucose level was measured from tail blood using Quintet AC® Blood Glucose Monitor (McKesson, Irving, TX, USA). Mice were then injected i.p. with D-glucose at 2g/kg fasted body weight (#D16-500, Fisher Scientific, Waltham, MA, USA) and glucose was again measured from tail blood at the indicated time points.

Triglyceride (TG) and high-density lipoprotein (HDL) levels

Blood was collected from the retro-orbital plexus into EDTA tubes from all mice after 20 weeks as previously described [6], Total HDL and TG were measured by colorimetric assays. HDL was measured using an HDL-Cholesterol E kit (Wako Laboratory Chemicals; Richmond, VA) and TG was measured using an Infinity reagent colorimetric kit (Thermo Fisher Scientific; Waltham, MA)**.**

Cardiac function

Cardiac function was measured by echocardiography in all mice after 20 weeks using the Vevo 2100 system (FujiFilm VisualSonics Inc. Toronto, ON, Canada) with a MS400 transducer. For all measurements, mice were anesthetized with isoflurane, gently restrained in the supine position on the prewarmed monitoring pad, and echocardiographic images were captured as mice recovered from anesthesia to achieve a target heart rate (HR) of 450 – 500 bpm. Isoflurane was maintained at 2-5% and adjusted accordingly in order to maintain a heart rate of 400-500 bpm. Parasternal long axis M-mode images of the left ventricle were captured to measure left ventricular parameters including: left ventricular posterior wall thicknesses (LVPW;s: systolic left ventricular posterior wall; LVPW;d: diastolic left ventricular posterior wall), left ventricular internal diameters (LVID;s: systolic left ventricular internal diameter; LVID;d: diastolic left ventricular internal diameter), left ventricular volumes (ESV: end systolic volume, ((7.0/(2.4 + LVID;s))*LVID;s3); EDV: end diastolic volume, ((7.0/(2.4 + LVID;d))*LVID;d3)), fractional shortening (FS: 100*((LVID;d – LVID;s)/LVID;d)), ejection fraction (EF: 100*((EDV – ESV)/EDV)), stroke volume (SV: EDV – ESV), and cardiac output (CO: SV*HR).Pulsed-wave Doppler images of the apical four-chamber view and

Tissue Doppler images at the level of mitral valve were captured to measure diastolic function, including peak velocity of mitral flow from left ventricular relaxation in early diastole (E wave), peak velocity of mitral flow from left ventricular relaxation in late diastole (A wave), and peak early diastolic mitral annular velocity (e').

Statistical analysis

Cardiac phenotyping was analyzed using two-way ANOVA with a Tukey's post-test using Prism 9.0 (GraphPad Software Inc, San Diego, CA). Statistical significance was set at 0.05; Tukey's test was used to test for specified post-hoc differences using JMP version 13.2.1.

3.4 Results

To test the hypothesis that the loss of FFAR4 would have no effect on remodeling in response to the HFpEF-MetS diet in female mice. Mice were fed the HFpEF-MetS diet designed to induce MetS. Specifically, at 8 weeks of age, female WT and FFAR4KO mice were randomized to the control diet (Cont diet: standard low-fat diet, no L-NAME) or the HFpEF-MetS diet (Diet composition: same as above, Summary data: Table 1). After 20 weeks, we assessed metabolic parameters including weight gain, adiposity, arterial pressure, glucose tolerance, plasma triglycerides, and plasma HDL, as well as cardiac function.

The HFpEF-MetS diet increased obesity in female FFAR4KO mice relative to female WT mice

The HFpEF-MetS diet induced significant weight gain in female WT mice, but surprisingly, weight gain was greater in female FFAR4KO mice (Figure 1A). This

additional weight gain in female FFAR4KO mice was due to a significant increase in fat mass (Figure 1B), while lean mass remained unchanged (Figure 1C), resulting in a significant increase in the adiposity index (Figure 1D), indicating a greater degree of obesity in the female FFAR4KO mice.

The HFpEF-MetS diet induced a similar level of mild hypertension in female WT and FFAR4KO mice

Mean arterial pressure (MAP) measured by tail cuff in female WT and FFAR4KO mice fed with the control diet were the same and were within a normal range (Figure 2A, open symbols). As expected, the HFpEF-MetS diet (due to L-NAME) induced mild hypertension in both female WT and FFAR4KO mice (Figure 2A, closed symbols). Interestingly, MAP trended lower and SBP and DBP were significantly lower in the female FFAR4KO mice (Figures 2A-C, closed orange symbols vs closed purple symbols).

The HFpEF-MetS diet induced a trend towards glucose intolerance in female WT and FFAR4KO mice

The HFpEF-MetS diet induced a non-significant trend towards glucose intolerance following glucose challenge in female WT and FFAR4KO mice (Figure 3A),

The HFpEF-MetS diet induced a similar increase in TG and HDL levels in female WT and FFAR4KO mice

Plasma was collected and isolated from female WT and FFAR4KO mice to analyze for triglyceride (TG) and high-density lipoprotein (HDL) levels. Both TG (Figure 3C) and HDL (Figure 3D) levels were elevated to a similar degree in female WT and FFAR4KO mice by the HFpEF-MetS diet.

The HFpEF-MetS diet induced a similar level of diastolic dysfunction in female WT and FFAR4KO mice

Systolic and diastolic function were assessed by echocardiography. In female WT mice, the HFpEF-MetS diet induced significant diastolic dysfunction evidenced by increased E/e' and E/A ratios (Figures 4A-B, orange symbols, Summary data: Table 2) with preserved EF (Figure 4C, orange symbols). However, despite the increased obesity observed in the female FFAR4KO mice, the HFpEF-MetS diet did not result in any further worsening of diastolic function relative to female WT mice, and EF was preserved (Figures 4C, closed orange versus closed purple symbols).

3.5 Discussion

Here, we found that contrary to males, loss of FFAR4 induced greater weight gain, but no worsening of cardiac remodeling in response to the HFpEF-MetS diet. In female WT mice, the HFpEF-Mets diet induced MetS including obesity, mild hypertension, and increased TG and HDL level, which triggered the progression of diastolic dysfunction, similar to males. However, in female FFAR4KO mice, the HFpEF-Mets diet induced a greater accumulation of fat, but surprisingly, this did not translate to worsened cardiac outcomes. If anything, female FFAR4KO hearts showed a trend towards less diastolic dysfunction.

Although there is some controversy, most studies suggest that the loss of FFAR4 worsens metabolic outcomes, but with little effect on weight gain in mice challenged with HFD [7, 8, 10, 53, 54]. Interestingly, none of these prior studies examined females. Here, we specifically assessed cardiometabolic disease, by including a hypertensive

challenge with the HFD, while none of these prior studies measured cardiac outcomes. Nonetheless, our results indicate that loss of FFAR4 induced 15% more weight gain over 20 weeks in female mice, which is the first report indicating that loss of FFAR4 induces significant and prolonged weight gain, and suggests FFAR4 in females might attenuate weight gain. This finding might inform previous studies in which the examination of the FFAR4 R270H polymorphism and obesity in humans has produced conflicting results [10, 55]. Additionally, in the context of human disease, HFpEF patients tend to be older and female [86], a population in which all HF is more prevalent [84]. In our HFpEF-MetS model, female WT mice developed slightly less diastolic dysfunction, similar to previous reports suggesting female mice are protected from HFpEF [117], a seeming discrepancy with humans. Further, despite the increased weight gain, female FFAR4KO mice showed no worsening of diastolic dysfunction relative to female WT mice. One possible explanation for the sex-based difference between humans and mice is that this might simply reflect a higher survival rate of human females with cardiovascular disease who become more susceptible to HFpEF with age.

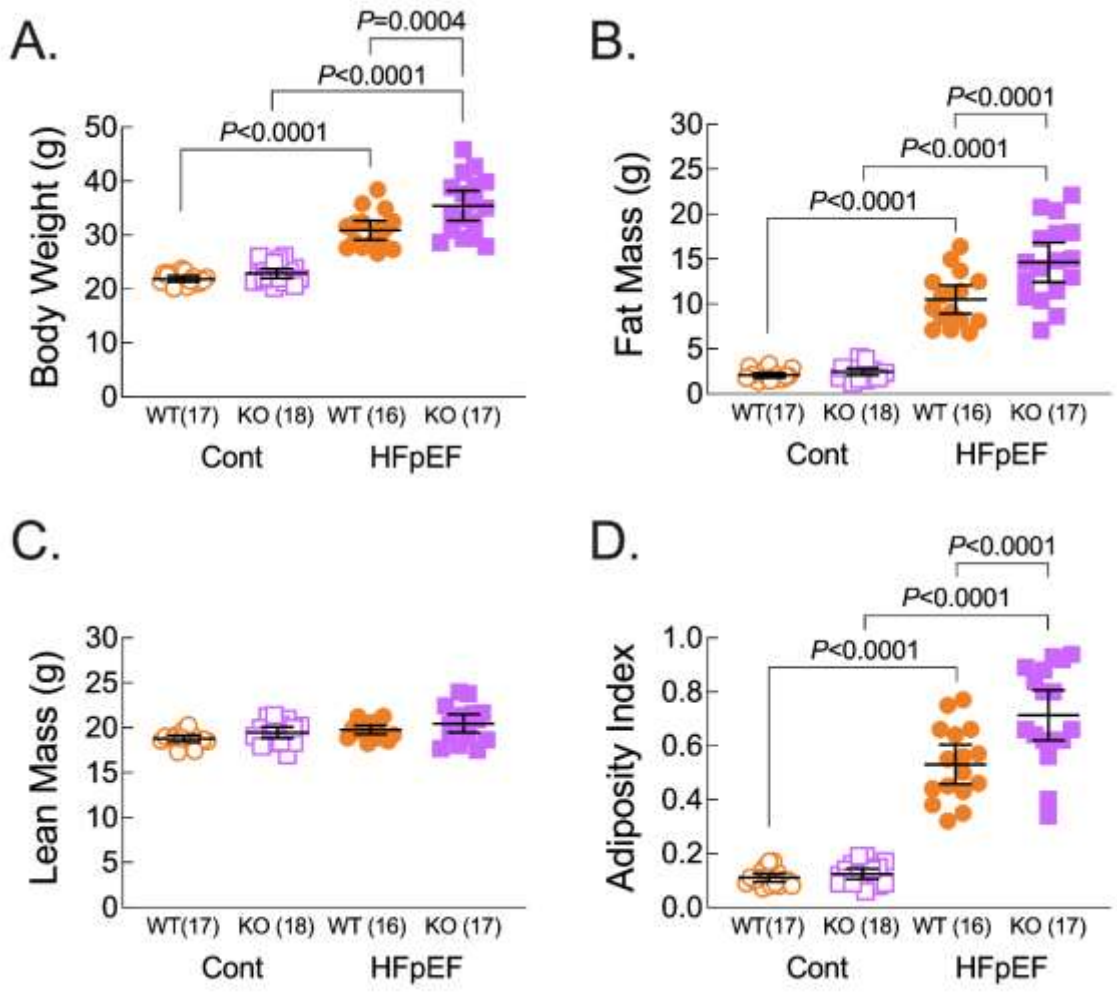

Figure 1. The HFpEF-MetS diet increased obesity in female FFAR4KO mice relative to female WT mice

Female wild-type (WT, orange) and FFAR4KO (KO, purple) mice were fed a control diet (Cont., open symbols) or the combination of a high-fat (42%)/high-sucrose (30%) diet and L-NAME (1 mg/ml) in the drinking water (HFpEF, closed symbols) for 20 wks. After 20 weeks, **A**. Body weight was recorded, and body composition, including: **B**. Fat Mass and **C**. Lean Mass were determined by EchoMRI; and **D**. Adiposity Index (fat mass/lean mass) was calculated. Data (**A-D**) are presented as Mean ± 95% CI and were analyzed by two-way ANOVA with Tukey's multiple comparison test.

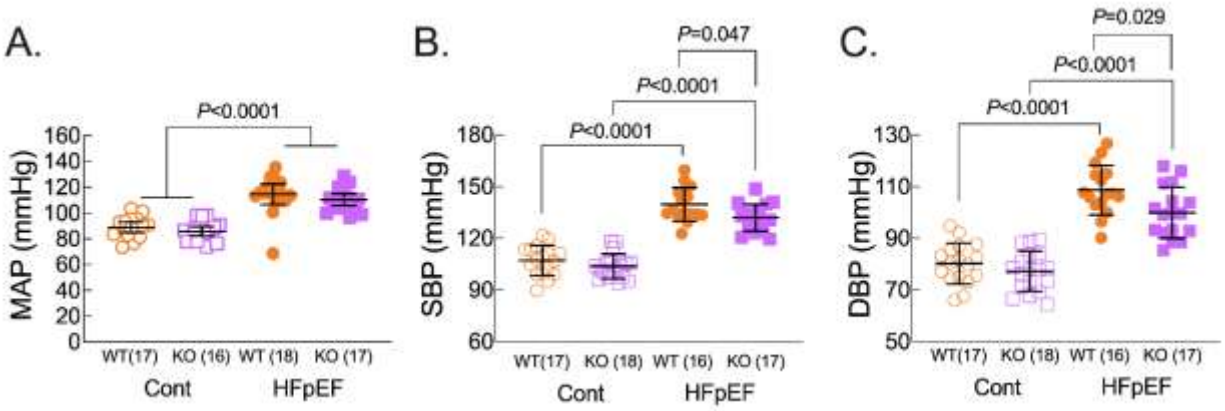

Figure 2. The HFpEF-MetS diet induced a similar level of mild hypertension in female WT and FFAR4KO mice.

Female wild-type (WT, orange) and FFAR4KO (KO, purple) mice were fed a control diet (Cont., open symbols) or the combination of a high-fat (42%)/high-sucrose (30%) diet and L-NAME (1 mg/ml) in the drinking water (HFpEF, closed symbols) for 20 wks. After 20 weeks, **A.** Mean Arterial Pressure (MAP), **B.** Systolic Blood Pressure (SBP), and **C.** Diastolic Blood Pressure (DBP) was measured by tail-cuff**.** Data (**A-C**) are presented as Mean ± 95% CI and were analyzed by two-way ANOVA with Tukey's multiple comparison test.

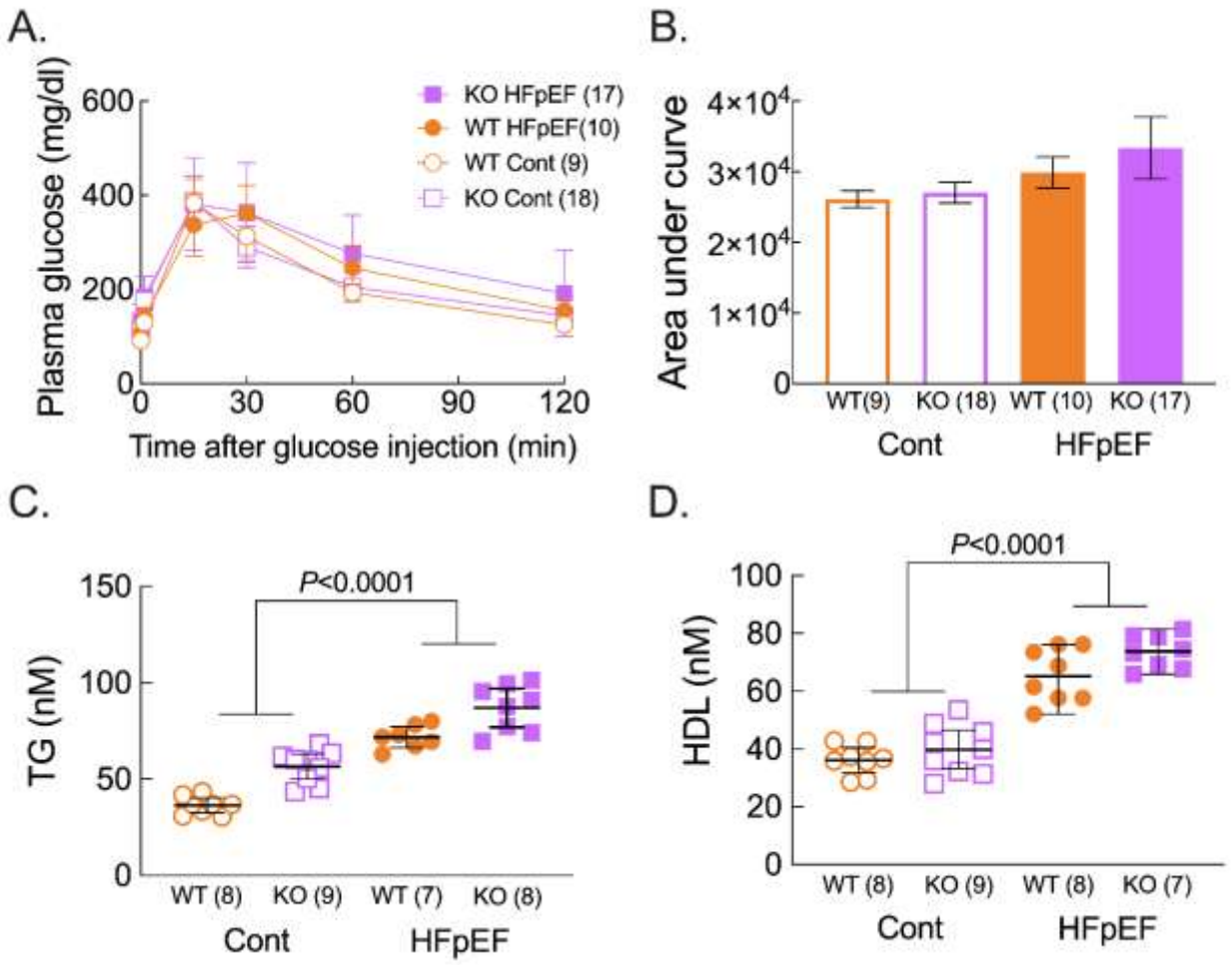

Figure 3. The HFpEF-MetS diet induced a trend towards glucose intolerance and a similar increase in TG and HDL levels in both genotypes.
Female wild-type (WT, orange) and FFAR4KO (KO, purple) mice were fed a control diet (Cont., open symbols) or the combination of a high-fat (42%)/high-sucrose (30%) diet and L-NAME (1 mg/ml) in the drinking water (HFpEF, closed symbols) for 20 wks. After 20 weeks,
A. Intraperitoneal glucose tolerance test (IPGTT). **B.** Area under the curve of the IPGTT. **C.** Triglyceride levels and **D.** High density lipoprotein levels were measured from plasma. Data (**A-D**) are presented as Mean ± 95% CI and were analyzed by two-way ANOVA with Tukey's multiple comparison test.

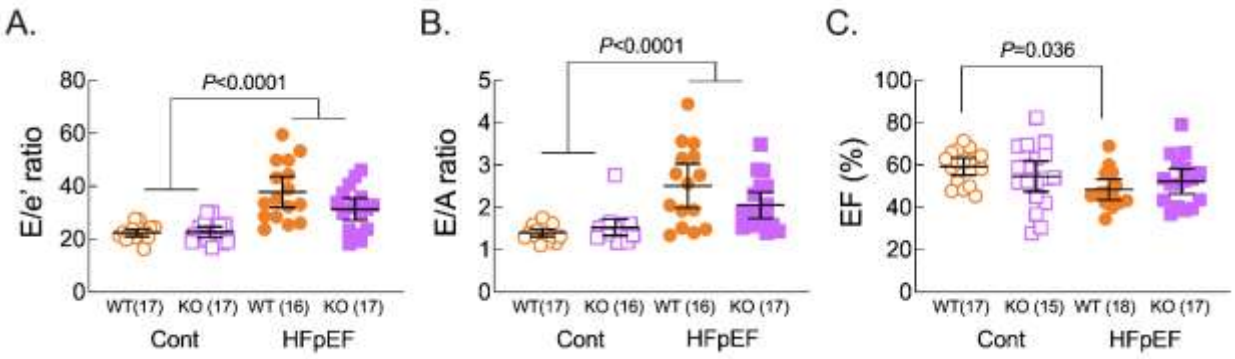

Figure 4. The HFpEF-MetS diet induced a similar level of diastolic dysfunction in female WT and FFAR4KO mice

Cardiac function was measured by echocardiography in female wild-type (WT, orange) and FFAR4KO (KO, purple) mice after 20 weeks on the control diet (Cont., open symbols) or the HFpEF-MetS diet (HFpEF, closed symbols).**A.** E/e' ratio. **B.** E/A ratio. **C.** Ejection fraction (EF,%). Data (**A-C**) are presented as Mean ± 95% CI and were analyzed by two-way ANOVA with Tukey's multiple comparison test.

Table 1: Metabolic parameters in female mice after 20 weeks on diet

Metabolic Parameter	**WT Cont (17)**	**KO Cont (18)**	**WT HFpEF (16)**	**KO HFpEF (17)**	**ANOVA** Primary	Diet	Genotype
BW (g)	21.9 (21.3, 22.4)	22.9 (22.0, 23.7)	30.9 (29.0, 32.7)	35.5 (32.7, 38.2)	0.0306	<0.0001	0.0010
Fat mass (g)	2.1 (1.8, 2.4)	2.4 (2.0, 2.8)	10.5 (8.9, 12.0)	14.6 (12.4, 16.8)	0.0043	<0.0001	0.0008
Lean mass (g)	18.8 (18.4, 19.2)	19.5 (18.9, 20.1)	19.8 (19.3, 20.3)	20.5 (19.5, 21.5)	0.9645	0.0020	0.0323
Adiposity index	0.1 (0.09,0.1)	0.1 (0.1,0.1)	0.5 (0.5, 0.6)	0.7 (0.6, 0.8)	0.0039	<0.0001	0.0008
Plasma TG (nM)	39.7 (34.8, 45.4)	53.6 (48.8, 58.3)	72.5 (67.4, 77.6)	86.4 (81.4, 91.4)	0.4144	<0.0001	<0.0001
Plasma HDL (nM)	35.8 (32.6, 39.0)	39.0 (35.1, 42.9)	55.3 (52.1, 58.6)	67.0 (62.9, 71.1)	0.2429	<0.0001	0.0167
SBP (mmHg)	107.0 (102.7, 111.6)	103.7 (100.1, 107.3)	139.7 (134.5, 144.9)	132.0 (128.0, 136.0)	0.2908	<0.0001	0.0076
DBP (mmHg)	80.2 (76.2, 84.3)	77.2 (73.4, 81.1)	108.7 (103.6, 113.8)	99.9 (94.9, 105.0)	0.1836	<0.0001	0.0077
MAP (mmHg)	88.9 (84.7, 93.0)	85.7 (82.1, 89.4)	114.6 (106.6, 122.5)	110.3 (105.7, 115.0)	0.8283	<0.0001	0.1408

Data are presented as Mean ± standard error for the number of mice indicated in parentheses. TG, triglyceride; HDL, high density lipoprotein; SBP, systolic blood pressure; DBP, diastolic blood pressure; MAP; mean arterial pressure. ANOVA denotes the results of the two-way ANOVA with the *P* values shown for the primary interaction as well as the effects of diet or genotype.

Table 2: Cardiac function in female mice after 20 weeks on diet.

Cardiac function	WT Cont (17)	KO Cont (18)	WT HFpEF(16)	KO HFpEF (17)	ANOVA primary	Diet
EF (%)	59.31 (55.2, 63.4)	54.6 (47.4, 61.8)	48.4 (43.6, 53.3) (15)	52.3 (46.4, 58.2)	0.1183	0.0183
SV (ul)	32.33 (30.0, 34.6)	31.0 (27.3, 34.6)	27.8 (25.0, 30.5) (15)	29.3 (25.8, 32.9)	0.3335	0.0438
FS (%)	31.04 (28.3, 33.8)	28.6 (23.8, 33.3)	24.1 (21.1, 27.2) (15)	26.8 (22.8, 30.7)	0.1553	0.0179
EDV (ul)	54.89 (51.5, 58.2)	58.0 (53.5, 62.4)	57.9 (53.6, 62.2) (15)	56.4 (51.5, 61.2)	0.2631	0.7355
ESV (ul)	22.57 (19.5, 25.6)	27.0 (21.2, 32.9)	30.1 (25.9, 34.3) (15)	27.0 (22.9, 31.2)	0.0831	0.0810
CO (ml/min)	14.4 (13.0, 15.9)	14.8 (13.0, 16.5)	11.9 (10.5, 13.3) (15)	13.5 (11.9, 15.1)	0.4240	0.0117
IVS; s (mm)	1.3 (1.2, 1.4)	1.3 (1.2, 1.4)	1.3 (1.2, 1.4) (15)	1.3 (1.2, 1.5)	0.7024	0.8485
IVS; d (mm)	0.9 (0.9, 1.0)	0.9 (0.9, 1.0)	1.0 (0.9, 1.1) (15)	1.0 (0.9, 1.1)	0.6444	0.1075
LVID; s (mm)	2.5 (2.4, 2.6)	2.6 (2.4, 2.9)	2.2 (2.6, 3.0) (15)	2.6 (2.5, 2.9)	0.0983	0.0645
LVID; d (mm)	3.6 (3.5, 3.7)	3.7 (3.6, 3.8)	3.7 (3.6, 3.8) (15)	3.6 (3.5, 3.8)	0.3370	0.8626
LVPW; s (mm)	1.1 (1.0, 1.2)	1.0 (0.8, 1.0)	1.0 (0.9, 1.1) (15)	0.9 (0.8, 1.0)	0.3758	0.4224
LVPW; d (mm)	0.8 (0.7, 0.8)	0.6 (0.6, 0.7)	0.8 (0.7, 0.8) (15)	0.7 (0.6, 0.8)	0.4449	0.2925
LV mass corrected (mg)	84.4 (78.6, 90.2)	80.6 (73.7, 87.5)	94.7 (83.6, 105.8) (15)	87.5 (76.7, 98.3)	0.6819	0.0415
LVRI	29.2 (27.3, 30.9)	27.5 (24.9, 30.0)	32.0 (28.9, 35.1) (15)	30.2 (26.3, 34.0)	0.9576	0.0484
E/A	1.4 (1.3, 1.5)	1.5 (1.3, 1.7) (16)	2.5 (2.0, 3.0) (15)	2.1 (1.7, 2.4)	0.0505	<0.0001
E (mm/s)	680.3 (619.0, 741.6)	672.5 (618.3, 726.7) (17)	754.0 (710.4, 797.7)	773.6 (717.9, 829.3)	0.5955	0.0011
A (mm/s)	488.4 (449.9, 527.0)	448.8 (407.0, 490.5)	336.0 (273.4, 398.6) (15)	397.1 (352.8, 441.3)	0.0256	<0.0001
E/e'	22.4 (21.0, 23.8)	22.6 (20.6, 24.7) (17)	37.8 (32.0, 43.7) (16)	31.3 (27.1, 35.5)	0.0806	<0.0001
HR (bpm)	445.0 (422.5, 467.4)	479.5 (453.7, 505.3)	428.3 (411.0, 445.6) (15)	459.0 (442.1, 478.9)	0.9082	0.0872

Data are presented as Mean ± standard error for the number of mice indicated in parentheses. HR, heart rate; SV, stroke volume; EF, ejection fraction; FS, fractional shortening; EDV, end diastolic volume; ESV, end systolic volume; CO, cardiac output; IVS;s, interventricular septal thickness at systole; IVS;d, interventricular septal thickness at diastole; LVID;s, left ventricular internal diameter systole; LVID;d, left ventricular internal diameter diastole; LVPW;s, left ventricular posterior wall systole; LVPW;d, left ventricular posterior wall diastole; LVRI, left ventricular remodeling index; E/A, early mitral valve filling velocity/ late mitral valve filling velocity; E, early mitral valve filling velocity ; E/E', early mitral valve filling velocity/early mitral annular tissue velocity; GLS, global longitudinal strain; RLPSR, reverse longitudinal peak strain rare; PAT, pulmonary artery acceleration time normalized to heart rate. ANOVA denotes the results of the two-way ANOVA with the *P* values shown for the primary interaction as well as the effects of diet or genotype.

CHAPTER 4:Loss of FFAR4 promoted systematic pro-inflammatory state by regulating oxylipin synthesis

Naixin Zhang[1], Katherine A. Murphy[1], Brian Harsch[2], Brandon M. Wagner[1], Jenna Mendelson[1], Chastity L. Healy[1], Gregory C. Shearer[2], and Timothy D. O'Connell[1]

[1]Department of Integrative Biology and Physiology, University of Minnesota, Minneapolis, MN 55455 USA

[2]Department of Nutritional Sciences, The Pennsylvania State University, University Park, PA 16801 USA

4.1 Summary

We previously demonstrated that FFAR4-mediated cardioprotection was dependent upon activation of cPLA2α and production of 18-HEPE [6]. Therefore, to define the mechanistic basis underlying the cardioprotective effects of FFAR4 in HEpEF-MetS, we evaluated oxylipin production in our mouse model of HFpEF. In male FFAR4KO mice, the HFpEF-MetS diet altered the balance of inflammatory oxylipins both systemically in HDL and in the heart, decreasing 18-HEPE levels, while increasing levels of the AA-derived, proinflammatory oxylipin 12-HETE. This increased 12-HETE/18-HEPE ratio reflected a more pro-inflammatory state systemically in the heart, and was associated with increased CD64$^+$ macrophages in the heart, which in turn correlated with worsened ventricular remodeling in male FFAR4KO hearts. Interestingly, the increase in the 12-HETE/18-HEPE ratio was only observed in males, which correlated with the worsened cardiac outcomes in male FFAR4KO mice relative to females. In a broader context, our data suggest that FFAR4 prevents the negative impact of MetS in the heart and suggests FFAR4 might

be a novel therapeutic target in cardiometabolic disease.

4.2 Introduction

We previously demonstrated that in the context of pressure-overload induced heart failure, FFAR4-mediated cardioprotection was dependent upon activation of cPLA2α and production the cardioprotective, EPA-derived oxylipin 18-HEPE [6]. In cardiac myocytes cultured from WT but not FFAR4KO mice, we found that the FFAR4 agonist TUG-891 directly and specifically increased production of 18-HEPE [6]. Furthermore, TUG-891 and 18-HEPE each attenuated cardiac myocyte death induced by oxidative stress in wild-type cardiac myocytes, and 18-HEPE rescued cell death in FFAR4KO cardiac myocytes [6].

In support of our findings, increased 18-HEPE levels in macrophages from fat-1 transgenic mice are cardioprotective in the context of pressure overload, but more importantly, direct injection of 18-HEPE is also cardioprotective [30]. In addition, EPA supplementation increased 18-HEPE levels and attenuated atherosclerosis in mice [31]. To date, no receptor has been identified for 18-HEPE that might explain these cardioprotective effects, however, 18-HEPE is the precursor for E-series resolvins (RvE), which signal through the GPR ChemR23 [32, 33]. RvE1 is a member of a family of specialized pro-resolving mediators (SPM), which are derived from ω3-PUFAs and as the name implies, mediate resolution of inflammation. Previous studies indicate that RvE1 attenuates ischemic injury both ex vivo [35] and in vivo [36]. In total, these studies suggest that both 18-HEPE and RvE1 are both cardioprotective.

Interestingly, ChemR23 is expressed in macrophages [37], but expression is restricted to naïve and M1-like macrophages, which respond to chemerin produced in inflamed tissue to recruit macrophages, while RvE1 promotes repolarization of M1-like macrophages towards a more resolving M2-like phenotype [42]. Further, the balance between the two ChemR23 ligands, chemerin and RvE1, might dictate functional outcomes [43].

Previous reports suggest that systemic, non-resolving inflammation is associated with MetS and might promote HFpEF [91, 92, 101]. Based on these findings, we hypothesized that loss of FFAR4 alters oxylipin balance with a reduction in 18-HEPE levels that promotes a pro-inflammatory state in the context of HFpEF-MetS.

4.3 Methods

Cardiac and HDL oxylipin content

Cardiac tissue oxylipins were taken from the apex of mouse hearts. Each tissue sample weight was measured (approximately 50 mg) and recorded and subjected to homogenization followed by oxylipin extraction. Plasma lipoproteins were separated by FPLC followed by measurement of esterified oxylipins in HDL as previously described [6]. HDL and homogenized cardiac tissue samples were spiked with BHT/EDTA (0.2 mg/mL), six deuterated octadecanoid and eicosanoid surrogates (20 µL of 1000 nM concentration with final concentration of 50 nM after reconstitution) and subjected to liquid-liquid extraction to isolate lipid content. Samples were then hydrolyzed in 0.1 M methanolic sodium hydroxide to release

ester-linked oxylipins and subjected to solid phase extraction using Chromabond HLB sorbent columns (Machery Nagel, Duren, Germany). Oxylipins were eluted with 0.5 mL of methanol with 0.1% acetic acid and 1 mL of ethyl acetate and dried under nitrogen stream and reconstituted in 200 mL methanol acetonitrile (1:1) with 100 nM of 1-cyclohexyluriedo-3-dodecanoic acid used as internal standard.

Samples were analyzed by liquid chromatography using a Waters Acquity UPLC coupled to Waters Xevo triple quadrupole mass spectrometer equipped with electrospray ionization source (Waters, Milford, MA). 5 mL of the extract was injected, and separation was performed using a CORTECS UPLC C18 2.1 x 100 mm with 1.6 µM particle size column. Flow rate was set at 500 mL/min and consisted of a gradient run using water with 0.1% acetic acid (Solvent A) and acetonitrile isopropanol, 90:10 (Solvent B) for 15 minutes (25% to 95% of Solvent B was set from 0 to 11 min and held at 100% Solvent B from 11 to 13 min. The system was then re-equilibrated and conditioned at 25% Solvent B from 13 to 15 min.). Electrospray ionization operated in negative ion mode with capillary set at 2.7 kV, desolvation temperature set at 600°C, and source temp set to 150°C. Optimal oxylipin MRM transitions were previously identified by direct injection of pure standards onto the mass spectrometer and using cone voltage and collision energy ramps to optimize detection and most prevalent daughter fragments. Calibration curves were generated prior to each run using standards for each oxylipin. Peak detection and integrations were achieved through Target Lynx (Waters, Milford, MA) and each peak inspected for accuracy and corrected when needed.

RNA isolation and qPCR

RNA was isolated from the apex of the heart using the RNeasy Fibrous Tissue Mini Kit (Qiagen, Germantown MD, USA #74704,) after 20 weeks. RNA concentration was determined by NanoDrop Spectrophotometer (Thermo Fisher, Waltham, MA, USA) and cDNA was synthesized by reverse transcription using the qScript cDNA SuperMix Kit (Quantabio, Beverly, MA, USA #95047-100). Target gene expression was quantified by qRT-PCR using the Bio-Rad (Hercules, CA, USA) iTaq Universal SYBR Green SuperMix (#1725120) and CFX96 Real-Time System.

Primer sequences:

FFAR4 fwd CGGCGGGGACCAGGAAAT

FFAR4 rvs GTCTTGTTGGGACACTCGGA

Gpr31 fwd CCACCAGTCTGCCATTCTTTG,

Gpr31 rvs ACTGTCGTCAGGAAGGCTACT

Cmklr1 fwd ATGGAGTACGACGCTTACAACG

Cmklr1 rvs GGTGGCGATGACAATCACCA

Macrophage staining

Cryosections were prepared as mentioned in the Chapter 2. Cryosections were stained with primary antibodies to detect CD64 (R&D Systems, Minneapolis, MN, USA #AF2074), and subsequently stained with secondary antibodies conjugated to either Alexa fluor 568 (donkey anti-goat, Fisher, Waltham, MA, USA #A11057). To quantify macrophage density, sections were imaged at 20X using a BZ-X800 fluorescent microscope. Using NIH FIJI software, image contrast was adjusted to better visualize the positive staining. Following conversion to 8-bit images, and application of the threshold function, images were further converted into bi-color

mode. Subsequently, 7-9 regions of interests (ROIs) with a total area be-tween 600000~2000000 mm2 near the endocardium were randomly selected to calculate the number of CD64+ macrophages using an automated quantification algorithm to count particles (positively stained cells). Using this algorithm, macrophage density of the total area was calculated from each heart and was averaged within each treatment group.

Statistical analysis

Where specified, principal components analysis (PCA) was used for dimension reduction of oxylipin matrices on log-transformed, standardized concentrations. Mixed models were used to account for within mouse differences in oxylipin concentrations. Statistical significance was set at 0.05; Tukey's test was used to test for specified post-hoc differences using JMP version 13.2.1.

4.4 Results

Sex, genotype, and diet (HFpEF status) can independently affect HDL oxylipin profiles in mice

Oxylipin content in circulating HDL was quantified as an index of systemic FFAR4-cPLA2α activity. 57 oxylipins were identified and analyzed using principal component analysis (PCA) across all groups. In WT mice, the HFpEF-MetS diet had a significant effect on HDL oxylipin profile, and shifted the oxylipin profile from male WT and female mice to the top left quadrant towards the right quadrant, which is defined by increased HDL levels of 18-HEPE, 12-HEPE and 4-HDoHE (Figure 1A, green symbols and orange symbols, Figure 1B). In FFAR4KO mice, HDL oxylipin

profiles from both males and females on the control diet were shifted to the in the bottom two quadrants, suggesting they do not share the same HDL oxylipin content as WT mice. Furthermore, the HFpEF-MetS diet shifted the oxylipin profile from male FFAR4KO mice towards a more pro-inflammatory state, and were clustered in the lower right quadrant which is defined by increased levels of 5-HETE, 12-HETE, 15-HETE, and 13-HODE (Figure 1A, blue symbols, Figure 1B). Female FFAR4KO mice shifted towards the left quadrant relative to FFAR4KO males, suggesting that FFAR4KO females were not as pro-inflammatory as FFAR4KO males (Figure 1A, purple symbols, Figure 1B).

Loss of FFAR4 increased the 12-HETE/18-HEPE ratio in HDL in response to MetS in males

To simplify further analysis we focused on two oxylipins: 18-HEPE, which helped define HDL oxylipin composition in WT mice, and 12-HETE, which helped define HDL oxylipin content in male FFAR4KO mice. Subsequently, we calculated the 12-HETE/18-HEPE ratio in HDL as an indicator of the systemic inflammatory state.

18-HEPE: In male WT mice, the HFpEF-MetS diet slightly increased 18-HEPE levels in HDL (Figure 2A, green symbols). In male FFAR4KO mice, 18-HEPE levels were lower in HDL from mice on the control diet (Figure 2A, open symbols), while the HFpEF-MetS diet further reduced 18-HEPE in HDL (Figure 2A, blue symbols). In total, loss of FFAR4 significantly reduced basal levels of 18-HEPE in HDL, and prevented any compensatory increase in 18-HEPE, resulting in significantly lower levels in 18-HEPE in response to the HFpEF-MetS diet (Figure 2A, closed symbols).

12-HETE: In male WT mice, the HFpEF-MetS diet increased 12-HETE levels in HDL (Figure 2B, green symbols). In male FFAR4KO mice, 12-HETE levels were elevated in HDL (Figure 2B, open symbols), and the HFpEF-MetS diet further increased 12-HETE levels in HDL(Figure 2B, blue symbols). In total, loss of FFAR4 significantly increased basal levels of 12-HETE in HDL from males (higher). While the HFpEF-MetS diet increased 12-HETE in HDL, this basal difference accounted for the higher levels of 12-HETE in FFAR4KO mice relative to WT from males (Figure 2B, closed symbols).

12-HETE/18-HEPE ratio: In male WT mice, the HFpEF-MetS diet slightly increased the 12-HETE/18-HEPE ratio in HDL (Figure 2C, green symbols). In male FFAR4KO mice, the basal 12-HETE/18-HEPE ratio in HDL was elevated, owing largely to elevated basal levels of 12-HETE. However, the loss of FFAR4 provoked a dramatic increase in the 12-HETE/18-HEPE ratio in HDL in the males in response to HFpEF-MetS diet (Figure 2C, blue closed symbols), largely due to the combination of decreased 18-HEPE levels and increased 12-HETE levels in FFAR4KO mice compared to WT mice.

Loss of FFAR4 did not have an effect on the 12-HETE/18-HEPE ratio in HDL in response to MetS in females

18-HEPE: In female WT mice, the HFpEF-MetS diet slightly increased 18-HEPE levels in HDL (Figure 3A, orange symbols). In female FFAR4KO mice, 18-HEPE levels were lower in HDL from mice on the control diet (Figure 3A, open symbols), and the HFpEF-MetS diet had little effect on 18-HEPE levels in HDL (Figure 3A, purple symbols). In total, loss of FFAR4 significantly reduced basal levels

of 18-HEPE in HDL, and prevented any compensatory increase in 18-HEPE, resulting in significantly lower levels in 18-HEPE in response to the HFpEF-MetS diet (Figure 3A, closed symbols).

12-HETE: In female WT mice, the HFpEF-MetS diet increased 12-HETE levels in HDL (Figure 3B, orange symbols). Conversely, in female FFAR4KO mice, 12-HETE levels were lower in HDL (Figure 3B, compare open symbols), and increased by the HFpEF-MetS diet (Figure 3B, purple symbols). In total, loss of FFAR4 decreased basal levels of 12-HETE in HDL from females, opposite of males. While the HFpEF-MetS diet increased 12-HETE in HDL, this basal difference accounted for the lower levels of 12-HETE in FFAR4KO female relative to WT (Figure 3B, closed symbols).

12-HETE/18-HEPE ratio: In female WT mice, the HFpEF-MetS diet slightly increased the 12-HETE/18-HEPE ratio (Figure 3C, orange symbols). In female FFAR4KO mice, the basal 12-HETE/18-HEPE ratio is minimally elevated relative to WT (Figure 3C, open symbols), and slightly increased by the HFpEF-MetS diet.

Loss of FFAR4 increased the basal 12-HETE/18-HEPE ratio in the heart and in response to MetS in males.

18-HEPE and 12-HETE levels were measured in both the esterified (membrane) and non-esterified (NEOx, free) fractions from male hearts to understand how the loss of FFAR4 in the context of HFpEF secondary to MetS affected FFAR4-cPLA2α activity in the male heart specifically.

18-HEPE: Similar to HDL, 18-HEPE levels were lower in the male FFAR4KO heart at baseline (Figure 4A, 4D, open symbols), and while the HFpEF-MetS diet

increased 18-HEPE in the male WT heart two-fold (Figure 4A, 4D, green symbols), 18-HEPE increased to a much smaller degree in the FFAR4KO heart (Figure 4A, 4D, blue symbols). In short, the loss of FFAR4 reduced basal levels of 18-HEPE in the heart, and attenuated the compensatory increase in 18-HEPE levels in response to MetS (Figure 4A, 4D, closed symbols).

12-HETE: 12-HETE levels in the heart mirrored changes observed in HDL. Basal 12-HETE levels were higher in the FFAR4KO (Figure 4B, 4E, open symbols), and the HFpEF-MetS diet induced similar increases in the 12-HETE in WT (Figure 4B, 4E, green symbols) and FFAR4KO hearts (Figure 4B, 4E, blue symbols). This resulted in high levels of 12-HETE in the FFAR4KO heart relative to WT in response to MetS (Figure 4B, 4E, closed symbols).

12-HETE/18-HEPE ratio: Interestingly, the 12-HETE/18-HEPE ratio was increased in FFAR4KO hearts both at baseline and in response to the HFpEF-MetS diet (Figure 4C, 4F).

Expression of FFAR4 and CMKLR1, a receptor for E-series Resolvins, was increased in male FFAR4KO hearts.

To determine if downstream signaling of 12-HETE and 18-HEPE are affected, expression level of corresponding receptors of these two oxylipins as well as FFAR4 were evaluated. In WT mice, the HFpEF-MetS diet significantly increased FFAR4 expression (Figure 5A). In FFAR4KO mice, the HFpEF-MetS diet significantly increased CMKLR1 expression relative to WT (Figure 5B), while GPR31 expression was elevated in the FFAR4KO heart regardless of diet (Figure 5C).

Loss of FFAR4 increased CD64^{+} macrophages in response to MetS in male

hearts, which correlated with worsened ventricular remodeling.

To determine the inflammatory status in the hearts, the number of $CD64^+$ macrophages was quantified in male WT and FFAR4KO hearts. In male WT hearts, the HFpEF-MetS diet increased the number of $CD64^+$ macrophages, indicating an increase in total macrophage number, while the HFpEF-MetS diet induced a further significant increase in $CD64^+$ macrophages in the male FFAR4KO hearts (Figure 6A, B). Furthermore, the number of $CD64^+$ macrophages was positively correlated with diastolic dysfunction (E/e', Figure 6C, E/A, Figure 6D) and inversely correlated with microvascular rarefaction (Figure 6E).

4.5 Discussion

Initially, we evaluated overall oxylipin in HDL to gain insights into how systemic FFAR4-cPLA2α-mediated oxylipin synthesis would change in response to the HFpEF-MetS diet and the loss of FFAR4. A principal component analysis revealed that WT and FFAR4KO mice shared distinct oxylipin profiles, and HFpEF-MetS diet shifted FFAR4KO male mice towards a more systemic inflammatory state.

We previously demonstrated that in cardiac myocytes, FFAR4-cPLA2α signaling specifically induced the production of the EPA-derived, pro-resolving oxylipin 18-HEPE, which protected cardiac myocytes from oxidative stress [6]. Interestingly, a recent report indicated that the arachadonic acid (AA)-derived, pro-inflammatory oxylipin 12-hydroxyeicosatetraenoic acid (12-HETE) exacerbates endothelial dysfunction, and that antagonizing 12-HETE improved outcomes in mouse model of HFpEF in Type 2 diabetic db/db mice [119]. Therefore, we

determined how loss of FFAR4 in the context of HFpEF secondary to MetS might impact 18-HEPE and 12-HETE levels. First, the loss of FFAR4 was correlated with decreased synthesis of 18-HEPE but increased synthesis of 12-HETE in males, but not females. Second, in WT mice, MetS was associated with increased 18-HEPE and 12-HETE synthesis, such that the overall balance between the pro-inflammatory 12-HETE and pro-resolving 18-HEPE was largely maintained. Finally, and most importantly, the loss of FFAR4 dramatically impaired the ability to increase 18-HEPE synthesis while further increasing 12-HETE synthesis in males. The net result being that in male FFAR4KO, the 12-HETE/18-HEPE ratio was significantly increased, suggesting a more pro-inflammatory state in the male FFAR4KO heart that correlated with the worsened cardiovascular outcomes. Furthermore, the relatively lower 12-HETE/18-HEPE ratio in female FFAR4KO mice, suggesting a less pro-inflammatory state in response to MetS, provided mechanistic insight into the sex-based differences observed in the FFAR4KO mice.

18-HEPE and 12-HETE were also measured in the male hearts to evaluate the effect of FFAR4 deficiency on oxylipin production in the heart specifically. The esterified (membrane) and non-esterified (NEOx, free) fractions shared the same pattern of oxylipin production. In short, 18-HEPE was reduced at basal level as well as in response to MetS in the FFAR4KO hearts, and 12-HETE was increased in response to MetS in the FFAR4KO hearts, which collectively resulted in the high levels of 12-HETE/18-HEPE in the FFAR4KO hearts both at baseline and in response to MetS, suggesting a pro-inflammatory state in the FFAR4KO heart even at baseline.

18-HEPE and 12-HETE are agonists that can lead to downstream activation of GPCR signaling, 18-HEPE through conversion to E-Series resolvins (RvE1) and activation of CMKLR1 (ChemR23) [32], and 12-HETE through activation of GPR31 [120] and BLT1 receptors [33]. Therefore, to define the relationship between the increased levels of 18-HEPE, decreased levels of 12-HETE in FFAR4KO mice, and expression of their cognate receptors in the heart, we measured whole heart FFAR4, CMKLR1, and GPR31 mRNA expression. We surprisingly found that FFAR4 was increased in response to HFpEF-MetS diet in WT mice given that we previously found that FFAR4 expression was decreased in human HF [6]. In addition, the increased levels of CMKLR1 and GPR31 in the male FFAR4KO heart, along with the changes in their respective ligands support the idea that the HFpEF-MetS diet might have induced a more pro-inflammatory state in the male FFAR4KO heart.

Recently, it has become clear that cardiac macrophages represent a diverse cell population that plays a critical role in cardiac homeostasis and the response to cardiac injury [121, 122]. Furthermore, systemic inflammation and recruitment of macrophages to the heart might promote HFpEF, and a few studies have suggested that macrophage numbers are increased in models of hypertension/chronic kidney disease or aging that resemble HFpEF [123-125], as well as human HFpEF patients [125]. To understand the effect of HFpEF-MetS diet on the immune cell number in the heart, we quantified the number of CD64+ macrophages in male WT and FFAR4KO hearts. As we expected, increased CD64+ macrophages were observed in WT hearts in response to MetS. More importantly, the further increase in this $CD64^{+}$ macrophage population in FFAR4KO hearts in response to MetS is consistent with

the increased 12-HETE/18-HEPE ratio in these mice. Interestingly, the tight correlation again supported the hypothesis that inflammation drives HFpEF remodeling.

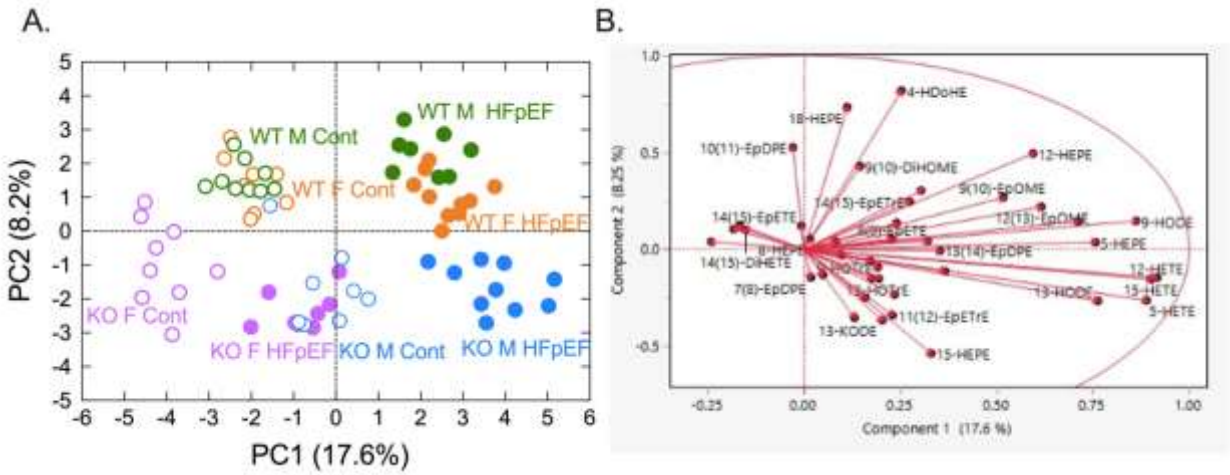

Figure 1. Sex, genotype, and diet (HFpEF status) can independently affect HDL oxylipin profiles in mice

After 20 weeks on diet (Cont., open symbols, HFpEF, closed symbols), plasma was collected from both male and female, WT and FFAR4KO mice (Male: WT, green; KO, blue, Female: WT, orange; KO, purple) and HDL oxylipin content was detected by liquid chromatography/mass spectrometry. Principle component analysis was performed to analyze oxylipin profiles across the groups **A.** Score plot of oxylipin profiles in both male and female, WT and FFAR4KO mice at basal levels or levels in response to MetS. **B.** Loading plot of oxylipin profiles.

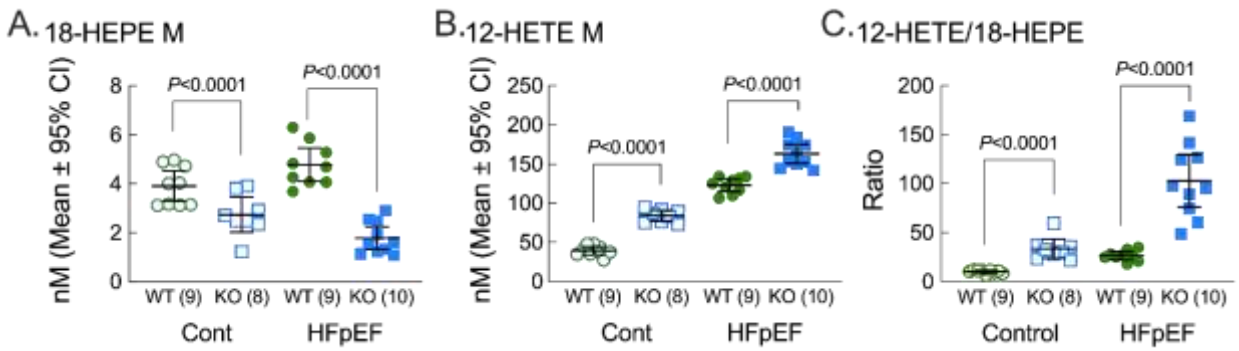

Figure 2. Loss of FFAR4 increased the 12-HETE/18-HEPE ratio in HDL in response to MetS in males

After 20 weeks on diet (Cont., open symbols, HFpEF, closed symbols), plasma was collected from male WT and FFAR4KO mice (WT, green; KO, blue) and HDL oxylipin content was detected by liquid chromatography/mass spectrometry. **A.** Levels of the 18-HEPE, an EPA-derived, pro-resolving oxylipin in HDL. **B.** Levels of the 12-HETE, an AA-derived, pro-inflammatory oxylipin in HDL. and **C.** 12-HETE/18-HEPE ratio in HDL. Data are presented as Mean ± 95% CI and were analyzed by two-way ANOVA with Tukey's multiple comparison test.

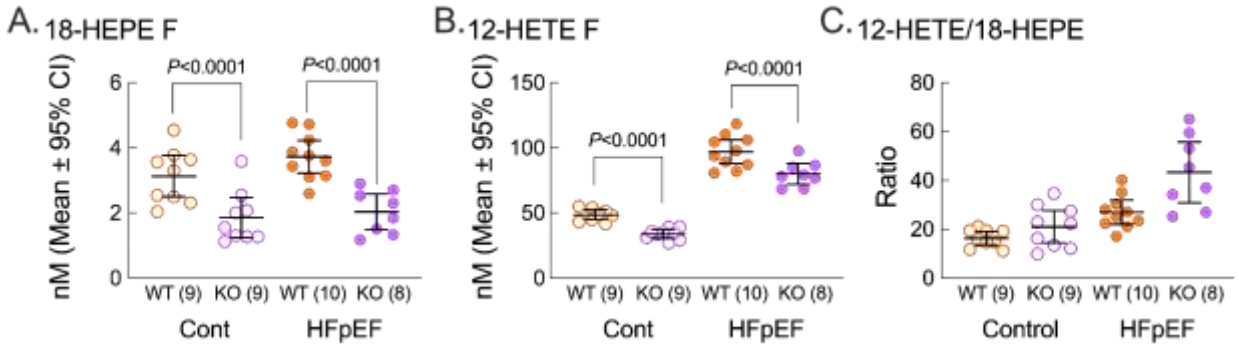

Figure 3. Loss of FFAR4 did not have an effect on the 12-HETE/18-HEPE ratio in HDL in response to MetS in females

After 20 weeks on diet (Cont., open symbols, HFpEF, closed symbols), plasma was collected from female, WT and FFAR4KO mice (WT, orange; KO, purple) and HDL oxylipin content was detected by liquid chromatography/mass spectrometry. **A.** Levels of the 18-HEPE, an EPA-derived, pro-resolving oxylipin in HDL. **B.** Levels of the 12-HETE, an AA-derived, pro-inflammatory oxylipin in HDL. and **C.** 12-HETE/18-HEPE ratio in HDL. Data are presented as Mean ± 95% CI and were analyzed by two-way ANOVA with Tukey's multiple comparison test.

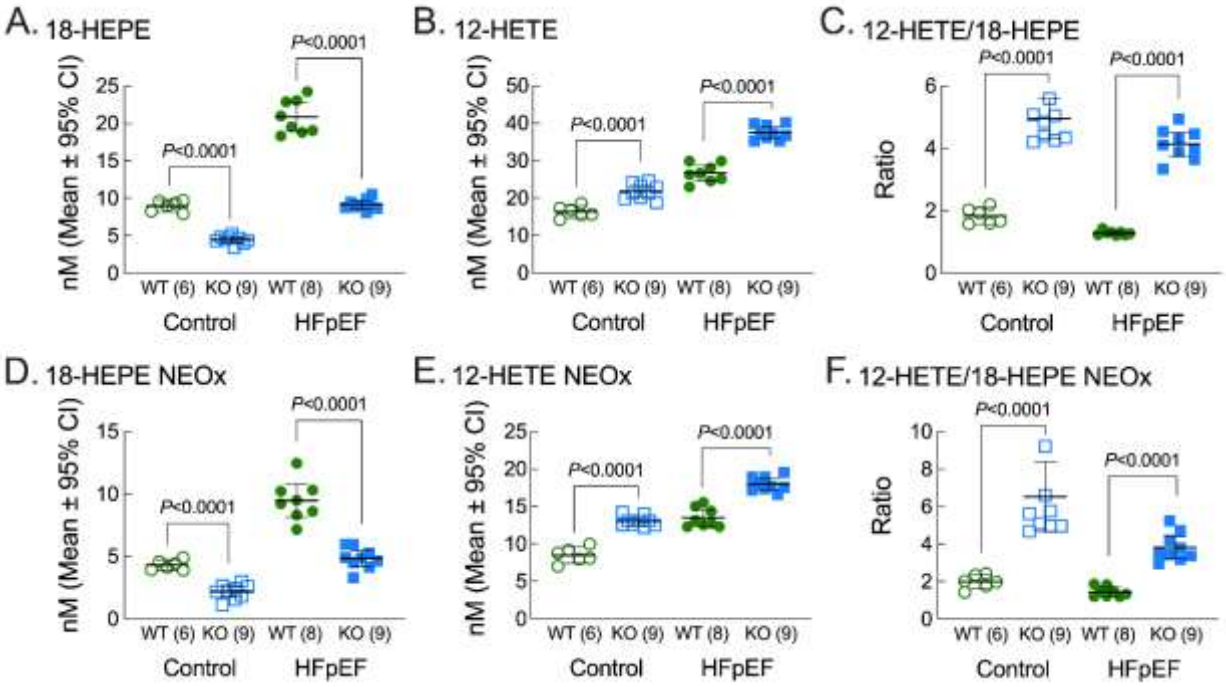

Figure 4. Loss of FFAR4 increased the basal 12-HETE/18-HEPE ratio in the heart and in response to MetS in males.
After 20 weeks on diet (Cont., open symbols, HFpEF, closed symbols), hearts were harvested from both male, WT (WT, green) and FFAR4KO (KO, blue) mice, and heart oxylipin content in the esterified and non-esterified (NEOx) fractions was detected by liquid chromatography/mass spectrometry. **A, D.** 18-HEPE, esterified, non-esterified; **B, E.** 12-HETE, esterified, non-esterified; and **C, F.** 12-HETE/18-HEPE ratio, esterified, non-esterified. Data are presented as Mean ± 95% CI and were analyzed by two-way ANOVA with Tukey's multiple comparison test.

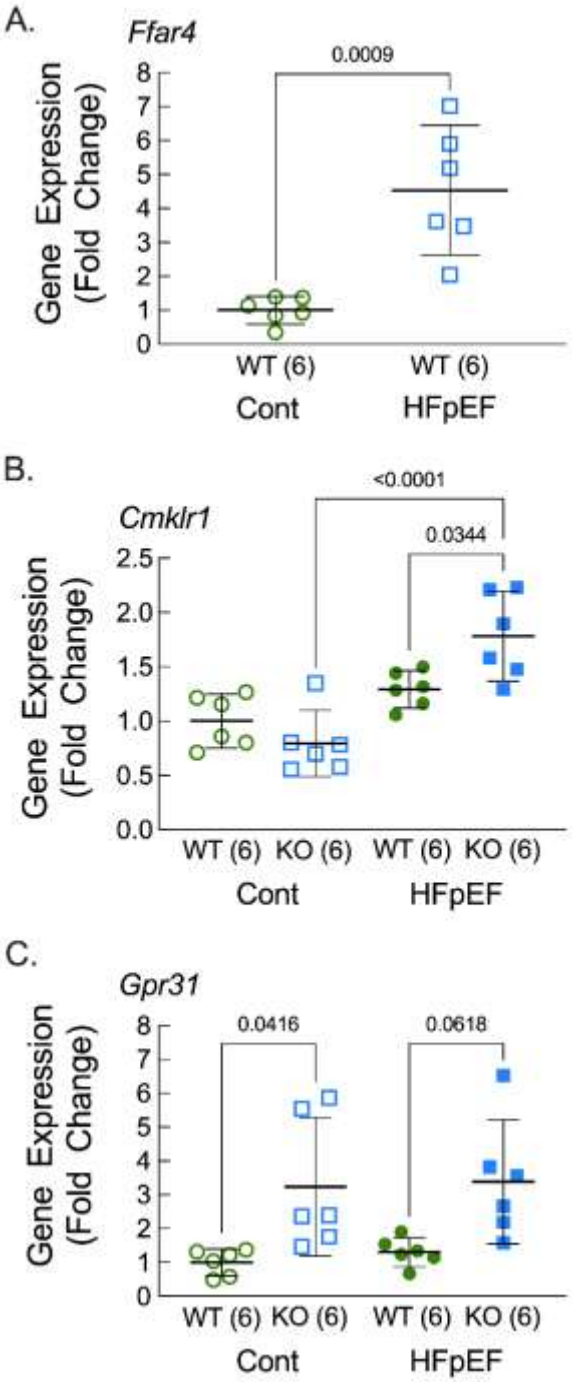

Figure 5. Expression of FFAR4 and CMKLR1, a receptor for E-series Resolvins, was increased in male FFAR4KO hearts.
After 20 weeks on diet (Cont., open symbols, HFpEF, closed symbols), RNA was isolated from male WT (WT, green) and FFAR4KO (KO, blue) hearts, and **A.** FFAR4, **B.** CMKLR1 and **C.** GPR31 mRNA levels were quantified by qRT-PCR. Data are presented as Mean ± 95% CI and were analyzed by two-way ANOVA with Tukey's multiple comparison test.

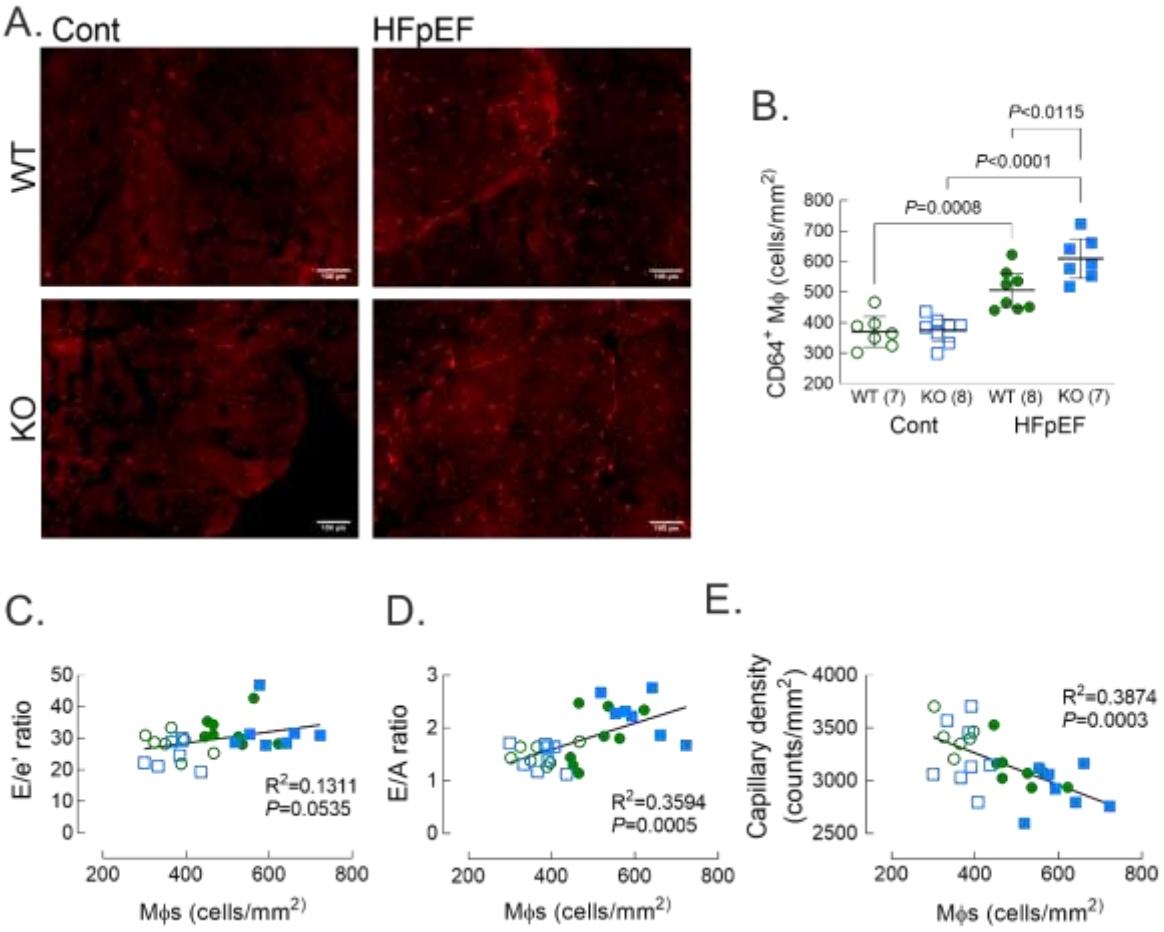

Figure 6. Loss of FFAR4 increased CD64+ macrophages in response to MetS in male hearts, which correlated with worsened ventricular remodeling.
A-B. After 20 weeks on diet (Cont., open symbols, HFpEF, closed symbols), ventricular sections from male WT (WT, green) and FFAR4KO (KO, blue) hearts were stained CD64 to detect the total macrophage population (**A**) and total CD64+ cells were counted (**B**). Data (**B**) are presented as Mean ± 95% CI and were analyzed by two-way ANOVA with Tukey's multiple comparison test. **C-E.** Total CD64+ macrophages were correlated with markers of HFpEF remodeling: **C.** E/e' ratio; **D.** E/A ratio; and **E.** Capillary density.

CHAPTER 5: Conclusions and future directions

5.1 Conclusions

Of the roughly 6 million total cases of HF in the US, the prevalence of HFpEF now exceeds 50% [86, 91],, and despite the recent success of sodium-glucose co-transporter inhibitors (SGLT2i) to reduces HF hospitalization (empagliflozin, EMPEROR-Preserved [87] and dapagliflozin, DELIVERY [88]), therapeutic options for HFpEF remain limited. Here, we have identified a novel cardioprotective role for FFAR4 in the context of HFpEF secondary to MetS, suggesting a potentially new therapeutic target for the management of cardiometabolic disease. In response to a dietary challenge designed to induce MetS, modified from the original 2-hit HFpEF model proposed by Schiattarella *et al.* [103], we found that systemic deletion of FFAR4 surprisingly did not affect development of MetS, but significantly worsened ventricular remodeling in male mice. Conversely, in female mice lacking FFAR4, this HFpEF-MetS diet induced greater weight gain, but no worsening of ventricular remodeling.

Mechanistically, loss of FFAR4 decreased levels of the EPA-derived, pro-resolving oxylipin 18-HEPE, while increasing the levels of the AA-derived, pro-inflammatory oxylipin 12-HETE in HDL and hearts from male mice to a far greater degree than from female mice fed the HFpEF-Mets diet. This resulted in a dramatic increase in the 12-HETE/18-HEPE ratio in male FFAR4KO mice fed the HFpEF-Mets diet, which suggests; 1. In males, loss of FFAR4 induced a more pro-inflammatory

state both systemically and in the heart in response to MetS that correlated with the worsened remodeling in males; and 2. In females, loss of FFAR4 did not increase the 12-HETE-/18-HEPE ratio in response to MetS, largely due to lower basal levels of 12-HETE in female FFAR4KO mice relative to males, providing a plausible mechanistic explanation for the observed sex-based difference.

18-HEPE is the sole precursor for E-series resolvins (RvE), which are ligands for the GPCR CMKLR1 (ChemR23) [32] , whereas 12-HETE is a ligand for GPR31 [120] and leukotriene B4 receptor BLT1 [33]. In male FFAR4KO mice, CMKLR1 expression was lower at baseline, but showed a much larger increase in response to the HFpEF-MetS diet, while GPR31 was elevated regardless of diet in the male FFAR4KO, suggesting a potential link between decreased 18-HEPE levels, increased 12-HETE levels, and macrophage function in male FFAR4KO mice on the HFpEF-MetS diet. As mentioned, HFpEF is proposed to be a disease of systemic inflammation [91], and in fact, we provide the first evidence in this 2-hit HFpEF-MetS model that $CD64^+$ macrophage numbers are increased in WT hearts. More importantly, we observed a further increase in $CD64^+$ macrophages in male FFAR4KO hearts, correlating with the heightened pro-inflammatory state in these mice. Briefly, the data suggest that FFAR4 controls the pro/anti-inflammatory oxylipin balance in the heart to modulate macrophage function and attenuate HFpEF remodeling.

Inflammation secondary to comorbidities associated with HFpEF, including MetS and chronic kidney disease, are proposed to drive HFpEF remodeling [91, 92, 101]. In support of this hypothesis, inflammation associated with hypertension,

obesity, and diabetes predicted incident HFpEF, but not HFrEF in the Health, Aging, and Body Composition study (Health ABC) [126]. Plasma markers of inflammation including soluble IL-1 receptor like 1 (IL1RL1), C-reactive protein (CRP), growth and differentiation factor 15 (GDF15) are high in HFpEF patients [127, 128]. Furthermore, CRP is correlated with LV end-diastolic pressure, and CRP is associated with asymptomatic diastolic dysfunction in MetS [129]. In patients with HFpEF, LV biopsies showed evidence of increased VCAM expression, increased $CD3^+$, $CD11^+$ and $CD45^+$ leukocytes, and increased TGFβ1 expression, suggesting a link between myocardial inflammation and HFpEF [130]. In the heart, inflammation can induce endothelial cell death and dysfunction leading to microvascular rarefaction and disruption of endothelial-myocyte communication with decreased NO resulting in stiff, hypertrophied cardiac myocytes [131], as well as recruitment of inflammatory monocytes and macrophages that can induce interstitial fibrosis [130, 131]. Here, we found an increased number of $CD64^+$ macrophages in male WT hearts on the HFpEF-MetS diet, with a further increase in $CD64^+$ macrophages in male FFAR4KO hearts, supporting the assertion that inflammation drives HFpEF. However, it remains to be determined if the increased number of $CD64^+$ macrophages observed in WT hearts and the even greater increase observed in FFAR4KO hearts were causative to the observed worsened ventricular remodeling in response to MetS.

Here, we also report the first data demonstrating that loss of FFAR4 reduced cardiac 18-HEPE levels *in vivo*, supporting our prior *in vitro* data from cardiac myocytes indicating that activation of FFAR4 increased 18-HEPE levels [6]. Furthermore, loss of FFAR4 increased 12-HETE levels, increasing the 12-HETE/18-

HEPE ratio, and suggesting a more pro-inflammatory state in the male FFAR4KO heart both at baseline and in response to the HFpEF-MetS diet. In the heart, prior studies indicate that 12-HETE worsens ischemic injury, induces maladaptive hypertrophy, and worsens HF [132], and a recent study indicated that 12-HETE specifically worsens HFpEF remodeling [119]. Ultimately, the increased 12-HETE/18-HEPE ratio in male FFAR4KO hearts was associated with an altered immune response, with increased $CD64^+$ macrophage numbers, which correlated with worsened HFpEF remodeling. This suggests a novel paradigm in which one GPCR, FFAR4, functions in a feed-forward mechanism to regulate downstream GPCR agonists (18-HEPE, CMKLR1; 12-HETE, GPR31) to attenuate the cardiac inflammatory response to cardiometabolic disease.

Recently, we demonstrated that in adult cardiac myocytes, FFAR4-cPLA2α signaling directly and uniquely increased synthesis of 18-HEPE [6], which helps to explain the reduced levels of 18-HEPE in HDL and hearts of FFAR4KO mice both at baseline and in response to the HFpEF-MetS diet. Increased levels of 18-HEPE, secondary to EPA-supplementation or in fat-1-transgenic mice that convert ω6- to ω3-PUFAs, are associated with prevention of atherosclerosis and pathologic ventricular remodeling post-TAC [30, 31]. Furthermore, 18-HEPE directly inhibits cardiac myocyte death [6], and exogenous, unesterified 18-HEPE prevents post-TAC remodeling [31]. Collectively, these findings suggest that 18-HEPE is cardioprotective, but its mechanism of action remains unclear. To date, no receptor has been identified for 18-HEPE, however, 18-HEPE is the precursor for E-series resolvins (RvE), which signal through CMKLR1 (ChemR23). CMKLR1 is expressed in

macrophages [37], smooth muscle cells [30], endothelial cells [38], and adipocytes [39], and based on direct effects of 18-HEPE to prevent CM cell death [6], and RvE1 infusion to attenuate post-infarction remodeling [40], we speculate that CMKLR1 might also be expressed in cardiac myocytes. Interestingly, CMKLR1 binds to two entirely different ligands; the peptide chemerin, a macrophage chemoattractant [41], and E-series resolvins that are derived from EPA/18-HEPE [32]. In macrophages, CMKLR1 expression is restricted to naïve and more proinflammatory macrophages, which respond to chemerin produced in inflamed tissue to recruit macrophages, while RvE1 promotes a shift in proinflammatory macrophages towards a more pro-resolving phenotype [42]. In a mouse atherosclerosis model, EPA supplementation increased 18-HEPE levels and prevented atherosclerosis progression [30]. However, systemic deletion of CMKLR1 in this context also increased macrophage uptake of oxidized LDL, reduced phagocytosis, and increased plaque size [31]. However, a separate study seemed to reach the opposite conclusion [43], which might reflect differences in the balance of the two CMKLR1 ligands. In total, the reduced levels of 18-HEPE in male FFAR4KO mice suggests the potential for more pro-inflammatory signaling through macrophage CMKLR1.

Positive results with icosapent ethyl (EPA) in the Reduction of Cardiovascular Events with EPA-Intervention Trial (REDUCE-IT) [133] and the Effect of Vascepa in Improving Coronary Atherosclerosis in People with High Triglycerides Taking Statin Therapy Trial (EVAPORATE) [134] to improve cardiovascular outcomes have renewed interest in the mechanistic basis for EPA-mediated cardioprotection. Following the original identification of FFAR4 (GPR120) as a receptor for long-chain

fatty acids [20], there has been considerable interest in the idea that FFAR4 mediates these protective effects. However, detailed *in vitro* studies of FFAR4 pharmacology suggest that in general, PUFAs, including ω3-PUFAs (EPA) and ω6-PUFAs (AA), have relatively similar efficacy and potency, and are not biased agonists [13]. Assuming this is correct, it presents a conundrum in explaining the beneficial effects of ω3-PUFAs versus ω6-PUFAs in terms of FFAR4 ligand binding or activation of immediate downstream signaling pathways. Adding to this complexity is the idea that ω3-PUFAs and EPA in particular have several proposed mechanisms of action including receptor mediated signaling through FFAR1/4 and Peroxisome Proliferator-Activated Receptors (PPARs), but also production of oxylipins (e.g. 18-HEPE), and direct effects on membrane structure [135]. Our current results and previous work [6] indicate that FFAR4-cPLA2α signaling in cardiac myocytes shows surprising specificity to induce the production of 18-HEPE. Given that cPLA2α does not have a reading function and will cleave whichever PUFA is found in the sn-2 position of membrane phospholipids, it is logical to suggest that altering ω3/ω6 levels in membrane phospholipids through dietary supplementation could alter production of their cognate oxylipins. This concept is also consistent with our assertion that the mechanism by which FFAR4 prevents HFpEF remodeling is by controlling pro/anti-inflammatory oxylipin balance to attenuate inflammation.

In female FFAR4KO mice, the HFpEF-Mets diet induced a greater accumulation of fat, but surprisingly, this did not translate to worsened cardiac outcomes. If anything, female FFAR4KO hearts showed a trend towards less

diastolic dysfunction. Although there is some controversy, more studies seem to suggest that loss of FFAR4 worsens metabolic outcomes with little effect on weight gain in mice challenged with HFD [8, 10, 53, 54]. Interestingly, none of these prior studies examined females. Furthermore, we specifically assessed cardiometabolic disease, by including a hypertensive challenge with the HFD, while none of these prior studies measured cardiac outcomes. Nonetheless, our results indicate that loss of FFAR4 induced 15% more weight gain over 20 weeks in female mice, suggesting that FFAR4 attenuates obesity in females. This finding might inform previous studies in which the examination of the FFAR4R270H polymorphism and obesity in humans has produced conflicting results HFD [8, 10, 53, 54]. Additionally, in the context of human disease, HFpEF patients tend to be older and female [86], a population in which all HF is more prevalent [83]. In our HFpEF-MetS model, female WT mice developed slightly less diastolic dysfunction, similar to previous reports suggesting female mice are protected from HFpEF [117], a seeming discrepancy with humans. Further, despite the increased weight gain, female FFAR4KO mice showed no worsening of diastolic dysfunction relative to female WT mice. One possible explanation for the sex-based difference between humans and mice is that this might simply reflect a higher survival rate of human females with cardiovascular disease who become more susceptible to HFpEF with age.

In conclusion, we demonstrate for the first time that FFAR4 attenuates cardiometabolic disease, and present novel mechanistic insight into how FFAR4 modulates oxylipin levels to attenuate inflammation and prevent HFpEF remodeling. Furthermore, we suggest a plausible mechanism through FFAR4-cPLA2α mediated

EPA-derived oxylipin synthesis that sheds new light on the basis of EPA-mediated cardioprotection. Finally, based on the experimental success of synthetic FFAR4 agonist to attenuate metabolic disease [7, 19, 57], we suggest that FFAR4 might be a novel therapeutic target in cardiometabolic disease.

5.2 Future directions

5.2.1 The relationship between inflammation and HFpEF

In my thesis project, I have shown that the loss of FFAR4 promoted a more systemic pro-inflammatory state in a mouse model of HFpEF-MetS in males, verified by oxylipin analysis as well as an increase in total macrophages in FFAR4KO hearts. In addition, the increase in total macrophages is nicely correlated with worsening of cardiac remodeling in response to MetS, suggesting inflammation has a strong association with development of HFpEF. However, whether increased macrophages/ inflammation is causative to the worsened outcome in FFAR4KO mice remains to be determined. Based on the high levels of inflammatory markers in HFpEF patients and the fact that inflammation can induce endothelial cell death and interstitial fibrosis which may contribute to the development of HFpEF [91], we hypothesize that inflammation drives progression of HFpEF. To test this hypothesis, we would like to measure 1) plasma cytokines and cardiac macrophage phenotypes at earlier time points, 5, 10 weeks to determine if increased inflammation precedes worsening to the HFpEF-like phenotype we observed in WT and if these inflammatory readouts are further worsened in FFARKO mice. This experiment is designed based on our pilot

finding that at 8 weeks of dietary intervention, no significant cardiac remodeling was observed in mice in response to HFpEF-MetS, although MetS was already established. If our hypothesis is correct, we would expect to see that increased levels of pro-inflammatory cytokines would be detected in the plasma and increased numbers of total and pro-inflammatory macrophages would be found in the heart at earlier time points, suggesting inflammation occurs before the onset of HFpEF-MetS.

5.2.2 Activation of FFAR4 as a therapeutic strategy

Data in my thesis using a loss of function model, suggests that FFAR4 is required to attenuate pathologic remodeling in response to HFpEF-MetS. However, whether direct activation of FFAR4, either with dietary supplementation with cardioprotective ω3-PUFAs, an FFAR synthetic ligand, or cardiac-specific transgenic overexpression of FFAR4 will promote cardioprotection is yet to be determined. In adipose tissue, activation of FFAR4 with the ω3-PUFA or the synthetic ligands such as TUG-891, cpdA, or compound 34, can attenuate metabolic disease [7, 8, 19, 57]. In addition, my data showed that while loss of FFAR4 did not have an effect on development of MetS in male mice, loss of FFAR4 worsened cardiac outcomes, suggesting FFAR4 has a direct cardioprotective effect. These data provide a strong rationale for the hypothesis that activation of FFAR4 in cardiac myocytes attenuates HFpEF-MetS. To test this hypothesis, we can employ our recently develop FFAR4 CRE-sensitive FFAR4 Tg mouse crossed with a cardiac-specific CRE-driver mouse to determine if cardiac myocytes specific overexpression of FFAR4 will attenuates HFpEF-MetS. Although not necessarily cardiac-specific, but of potential clinical

relevance, we can test if a synthetic FFAR ligand, such as TUG-891, or dietary supplementation with cardioprotective ω3-PUFAs can attenuate HFpEF-MetS.

5.2.3 FFAR4 cardioprotective signaling mechanisms

My work suggests that MetS increased $CD64^+$ macrophages in the heart in WT mice. More importantly, MetS induced a further increase in $CD64^+$ macrophages in FFAR4KO hearts. The increase in macrophage numbers induced by MetS were also supported by preliminary studies from our lab analyzing immune cell populations in WT hearts by cytometry by time of flight (CyTOF). In WT mice, HFpEF-MetS increased total macrophages abundance in the heart, mainly due to the increase of recruited macrophages ($CCR2^+TimD4^-$).

Interestingly, we have also found that in Raw264.7 macrophages, the FFAR4 synthetic ligand TUG-891 increased production of 18-HEPE simultaneous to a depression of 5-lipoxygenase activity, normally considered a pro-inflammatory pathway. Therefore, we hypothesize that activation of FFAR4 induces an anti-inflammatory/pro-resolving phenotype in macrophages that might attenuate pathologic remodeling in HFpEF-MetS. I suggest that additional experiments to test this hypothesis would include defining the effect of loss of FFA4 in the context of HFpEF-MetS on 1) macrophages phenotype and number by flow cytometry 2) cardiac macrophage oxylipin synthesis 3) systemic inflammation, which would be measured systematic cytokine/chemokine production.

In addition to inflammation, oxidative stress is also associated with MetS and HF. Recently, in a model of HFpEF, increased IL-1β and IL-18 levels leading to

cardiac myocyte NLRP3 inflammasome activation, down regulation of Sirt3 and mitochondrial protein acetylation were associated with oxidative stress and mitochondrial dysfunction [107]. Furthermore, a recent paper in our lab demonstrated that FFAR4 protects from oxidative stress through increased production of the EPA-derived, pro-resolving oxylipin 18-HEPE, and upregulation of several antioxidant genes including aldehyde dehydrogenase 1 (Aldh1), heme-oxygenase 1 (Hmox1), and cyclooxygenase 2 (Ptgs2) [6]. Therefore, I hypothesize that activation of FFAR4 attenuates oxidative stress to attenuate pathologic remodeling in HFpEF-MetS. Strategies to address this hypothesis in our HFpEF model would include: 1) measuring oxidative damage and NLRP3 inflammasome activation, as well as ox/redox genes; 2) measuring mitochondrial function including mitochondrial oxygen consumption rate and ROS production.

BIBLIOGRAPHY

1. Kimura, I., et al., *Free Fatty Acid Receptors in Health and Disease.* Physiol Rev, 2020. **100**(1): p. 171-210.
2. Milligan, G., et al., *Complex Pharmacology of Free Fatty Acid Receptors.* Chem Rev, 2017. **117**(1): p. 67-110.
3. Alvarez-Curto, E. and G. Milligan, *Metabolism meets immunity: The role of free fatty acid receptors in the immune system.* Biochem Pharmacol, 2016. **114**: p. 3-13.
4. Ichimura, A., et al., *Free fatty acid receptors as therapeutic targets for the treatment of diabetes.* Front Pharmacol, 2014. **5**: p. 236.
5. Eclov, J.A., et al., *EPA, not DHA, prevents fibrosis in pressure overload induced heart failure; potential role of free fatty acid receptor 4.* J Lipid Res, 2015. **56**: p. 2297-2308.
6. Murphy, K.A., et al., *Free fatty acid receptor 4 responds to endogenous fatty acids to protect the heart from pressure overload.* Cardiovasc Res, 2022. **118**(4): p. 1061-1073.
7. Oh da, Y., et al., *A Gpr120-selective agonist improves insulin resistance and chronic inflammation in obese mice.* Nat Med, 2014. **20**(8): p. 942-7.
8. Oh, D.Y., et al., *GPR120 is an omega-3 fatty acid receptor mediating potent anti-inflammatory and insulin-sensitizing effects.* Cell, 2010. **142**(5): p. 687-98.
9. Gotoh, C., et al., *The regulation of adipogenesis through GPR120.* Biochem Biophys Res Commun, 2007. **354**(2): p. 591-7.
10. Ichimura, A., et al., *Dysfunction of lipid sensor GPR120 leads to obesity in both mouse and human.* Nature, 2012. **483**(7389): p. 350-4.
11. Quesada-Lopez, T., et al., *The lipid sensor GPR120 promotes brown fat activation and FGF21 release from adipocytes.* Nat Commun, 2016. **7**: p. 13479.
12. Burns, R.N. and N.H. Moniri, *Agonism with the omega-3 fatty acids alpha-linolenic acid and docosahexaenoic acid mediates phosphorylation of both the short and long isoforms of the human GPR120 receptor.* Biochem Biophys Res Commun, 2010. **396**(4): p. 1030-5.
13. Christiansen, E., et al., *Activity of dietary fatty acids on FFA1 and FFA4 and characterisation of pinolenic acid as a dual FFA1/FFA4 agonist with potential effect against metabolic diseases.* Br J Nutr, 2015. **113**(11): p. 1677-88.
14. Watson, S.J., A.J. Brown, and N.D. Holliday, *Differential signaling by splice variants of the human free fatty acid receptor GPR120.* Mol Pharmacol, 2012. **81**(5): p. 631-42.
15. O'Connell, T.D., et al., *omega3-Polyunsaturated fatty acids for heart failure: Effects of dose on efficacy and novel signaling through free fatty acid receptor 4.* J Mol Cell Cardiol, 2017. **103**: p. 74-92.
16. Galindo, M.M., et al., *G protein-coupled receptors in human fat taste perception.* Chem Senses, 2012. **37**(2): p. 123-39.
17. Roh, J., et al., *Heart Failure With Preserved Ejection Fraction: Heterogeneous Syndrome, Diverse Preclinical Models.* Circ Res, 2022. **130**(12): p. 1906-1925.
18. Hudson, B.D., et al., *The pharmacology of TUG-891, a potent and selective agonist of the free fatty acid receptor 4 (FFA4/GPR120), demonstrates both potential opportunity and possible challenges to therapeutic agonism.* Mol Pharmacol, 2013. **84**(5): p. 710-25.

19. Azevedo, C.M., et al., *Non-Acidic Free Fatty Acid Receptor 4 Agonists with Antidiabetic Activity.* J Med Chem, 2016. **59**(19): p. 8868-8878.
20. Hirasawa, A., et al., *Free fatty acids regulate gut incretin glucagon-like peptide-1 secretion through GPR120.* Nat Med, 2005. **11**(1): p. 90-4.
21. Croze, M.L., et al., *Free fatty acid receptor 4 inhibitory signaling in delta cells regulates islet hormone secretion in mice.* Mol Metab, 2021. **45**: p. 101166.
22. Cordeaux, Y. and S.J. Hill, *Mechanisms of cross-talk between G-protein-coupled receptors.* Neurosignals, 2002. **11**(1): p. 45-57.
23. Li, X., et al., *Endogenously generated omega-3 fatty acids attenuate vascular inflammation and neointimal hyperplasia by interaction with free fatty acid receptor 4 in mice.* J Am Heart Assoc, 2015. **4**(4).
24. Leslie, C.C., *Cytosolic phospholipase A(2): physiological function and role in disease.* J Lipid Res, 2015. **56**(8): p. 1386-402.
25. Dennis, M.K., et al., *Identification of a GPER/GPR30 antagonist with improved estrogen receptor counterselectivity.* J Steroid Biochem Mol Biol, 2011. **127**(3-5): p. 358-66.
26. Shearer, G.C. and R.E. Walker, *An overview of the biologic effects of omega-6 oxylipins in humans.* Prostaglandins Leukot Essent Fatty Acids, 2018. **137**: p. 26-38.
27. Cheshmehkani, A., et al., *Free-fatty acid receptor-4 (FFA4) modulates ROS generation and COX-2 expression via the C-terminal beta-arrestin phosphosensor in Raw 264.7 macrophages.* Biochem Pharmacol, 2017. **146**: p. 139-150.
28. Liu, Y., et al., *The fish oil ingredient, docosahexaenoic acid, activates cytosolic phospholipase A(2) via GPR120 receptor to produce prostaglandin E(2) and plays an anti-inflammatory role in macrophages.* Immunology, 2014. **143**(1): p. 81-95.
29. Li, X., Y. Yu, and C.D. Funk, *Cyclooxygenase-2 induction in macrophages is modulated by docosahexaenoic acid via interactions with free fatty acid receptor 4 (FFA4).* FASEB J, 2013. **27**(12): p. 4987-97.
30. Endo, J., et al., *18-HEPE, an n-3 fatty acid metabolite released by macrophages, prevents pressure overload-induced maladaptive cardiac remodeling.* J Exp Med, 2014. **211**(8): p. 1673-87.
31. Laguna-Fernandez, A., et al., *ERV1/ChemR23 Signaling Protects Against Atherosclerosis by Modifying Oxidized Low-Density Lipoprotein Uptake and Phagocytosis in Macrophages.* Circulation, 2018. **138**(16): p. 1693-1705.
32. Arita, M., et al., *Stereochemical assignment, antiinflammatory properties, and receptor for the omega-3 lipid mediator resolvin E1.* J Exp Med, 2005. **201**(5): p. 713-22.
33. Arita, M., et al., *Resolvin E1 selectively interacts with leukotriene B4 receptor BLT1 and ChemR23 to regulate inflammation.* J Immunol, 2007. **178**(6): p. 3912-7.
34. Serhan, C.N. and B.D. Levy, *Resolvins in inflammation: emergence of the pro-resolving superfamily of mediators.* J Clin Invest, 2018. **128**(7): p. 2657-2669.
35. Keyes, K.T., et al., *Resolvin E1 protects the rat heart against reperfusion injury.* Am J Physiol Heart Circ Physiol, 2010. **299**(1): p. H153-64.
36. Zhang, J., et al., *The Anti-inflammatory Mediator Resolvin E1 Protects Mice Against Lipopolysaccharide-Induced Heart Injury.* Front Pharmacol, 2020. **11**: p. 203.
37. Samson, M., et al., *ChemR23, a putative chemoattractant receptor, is expressed in monocyte-derived dendritic cells and macrophages and is a coreceptor for SIV and some primary HIV-1 strains.* Eur J Immunol, 1998. **28**(5): p. 1689-700.
38. Kaur, J., et al., *Identification of chemerin receptor (ChemR23) in human endothelial cells: chemerin-induced endothelial angiogenesis.* Biochem Biophys Res Commun,

2010. **391**(4): p. 1762-8.
39. Goralski, K.B., et al., *Chemerin, a novel adipokine that regulates adipogenesis and adipocyte metabolism.* J Biol Chem, 2007. **282**(38): p. 28175-88.
40. Liu, G., et al., *Early treatment with Resolvin E1 facilitates myocardial recovery from ischaemia in mice.* Br J Pharmacol, 2018. **175**(8): p. 1205-1216.
41. Wittamer, V., et al., *Specific recruitment of antigen-presenting cells by chemerin, a novel processed ligand from human inflammatory fluids.* J Exp Med, 2003. **198**(7): p. 977-85.
42. Herova, M., et al., *ChemR23, the receptor for chemerin and resolvin E1, is expressed and functional on M1 but not on M2 macrophages.* J Immunol, 2015. **194**(5): p. 2330-7.
43. van der Vorst, E.P.C., et al., *Hematopoietic ChemR23 (Chemerin Receptor 23) Fuels Atherosclerosis by Sustaining an M1 Macrophage-Phenotype and Guidance of Plasmacytoid Dendritic Cells to Murine Lesions-Brief Report.* Arterioscler Thromb Vasc Biol, 2019. **39**(4): p. 685-693.
44. Tanaka, T., et al., *Cloning and characterization of the rat free fatty acid receptor GPR120: in vivo effect of the natural ligand on GLP-1 secretion and proliferation of pancreatic beta cells.* Naunyn Schmiedebergs Arch Pharmacol, 2008. **377**(4-6): p. 515-22.
45. Iwasaki, K., et al., *Free fatty acid receptor GPR120 is highly expressed in enteroendocrine K cells of the upper small intestine and has a critical role in GIP secretion after fat ingestion.* Endocrinology, 2015. **156**(3): p. 837-46.
46. Suckow, A.T., et al., *Alteration of the glucagon axis in GPR120 (FFAR4) knockout mice: a role for GPR120 in glucagon secretion.* J Biol Chem, 2014. **289**(22): p. 15751-63.
47. Sparks, S.M., et al., *Identification of diarylsulfonamides as agonists of the free fatty acid receptor 4 (FFA4/GPR120).* Bioorg Med Chem Lett, 2014. **24**(14): p. 3100-3.
48. Zhang, D., et al., *Insulinotropic effects of GPR120 agonists are altered in obese diabetic and obese non-diabetic states.* Clin Sci (Lond), 2017. **131**(3): p. 247-260.
49. Moran, B.M., et al., *Evaluation of the insulin-releasing and glucose-lowering effects of GPR120 activation in pancreatic beta-cells.* Diabetes Obes Metab, 2014. **16**(11): p. 1128-39.
50. Wang, Y., et al., *GPR120 protects lipotoxicity-induced pancreatic beta-cell dysfunction through regulation of PDX1 expression and inhibition of islet inflammation.* Clin Sci (Lond), 2019. **133**(1): p. 101-116.
51. Stone, V.M., et al., *GPR120 (FFAR4) is preferentially expressed in pancreatic delta cells and regulates somatostatin secretion from murine islets of Langerhans.* Diabetologia, 2014. **57**(6): p. 1182-91.
52. Zhao, Y.F., et al., *GPR120 Regulates Pancreatic Polypeptide Secretion From Male Mouse Islets via PLC-Mediated Calcium Mobilization.* Endocrinology, 2020. **161**(10).
53. Cho, H.J., et al., *Free Fatty Acid Receptor 4 Mediates the Beneficial Effects of n-3 Fatty Acids on Body Composition in Mice.* Calcif Tissue Int, 2017. **101**(6): p. 654-662.
54. Nakamoto, K., et al., *DHA supplementation prevent the progression of NASH via GPR120 signaling.* Eur J Pharmacol, 2018. **820**: p. 31-38.
55. Vestmar, M.A., et al., *Functional and genetic epidemiological characterisation of the FFAR4 (GPR120) p.R270H variant in the Danish population.* J Med Genet, 2016. **53**(9): p. 616-23.
56. Kim, K.W., et al., *Homegrown Macrophages.* Immunity, 2016. **45**(3): p. 468-470.
57. Schilperoort, M., et al., *The GPR120 agonist TUG-891 promotes metabolic health by*

stimulating mitochondrial respiration in brown fat. EMBO Mol Med, 2018. **10**(3).
58. Gozal, D., et al., *Treatment with TUG891, a free fatty acid receptor 4 agonist, restores adipose tissue metabolic dysfunction following chronic sleep fragmentation in mice.* Int J Obes (Lond), 2016. **40**(7): p. 1143-9.
59. Hilgendorf, K.I., et al., *Omega-3 Fatty Acids Activate Ciliary FFAR4 to Control Adipogenesis.* Cell, 2019. **179**(6): p. 1289-1305 e21.
60. Moniri, N.H., *Free-fatty acid receptor-4 (GPR120): Cellular and molecular function and its role in metabolic disorders.* Biochem Pharmacol, 2016. **110-111**: p. 1-15.
61. Talukdar, S., J.M. Olefsky, and O. Osborn, *Targeting GPR120 and other fatty acid-sensing GPCRs ameliorates insulin resistance and inflammatory diseases.* Trends Pharmacol Sci, 2011. **32**(9): p. 543-50.
62. Liu, K.L., et al., *Docosahexaenoic acid inhibits inflammation via free fatty acid receptor FFA4, disruption of TAB2 interaction with TAK1/TAB1 and downregulation of ERK-dependent Egr-1 expression in EA.hy926 cells.* Mol Nutr Food Res, 2016. **60**(2): p. 430-43.
63. Yan, Y., et al., *Omega-3 fatty acids prevent inflammation and metabolic disorder through inhibition of NLRP3 inflammasome activation.* Immunity, 2013. **38**(6): p. 1154-63.
64. Trayhurn, P. and G. Denyer, *Mining microarray datasets in nutrition: expression of the GPR120 (n-3 fatty acid receptor/sensor) gene is down-regulated in human adipocytes by macrophage secretions.* J Nutr Sci, 2012. **1**: p. e3.
65. Raptis, D.A., et al., *GPR120 on Kupffer cells mediates hepatoprotective effects of omega3-fatty acids.* J Hepatol, 2014. **60**(3): p. 625-32.
66. Codoner-Alejos, A., J. Carrasco-Luna, and P. Codoner-Franch, *The rs11187533 C>T Variant of the FFAR4 Gene Is Associated with Lower Levels of Fasting Glucose and Decreases in Markers of Liver Injury in Children with Obesity.* Ann Nutr Metab, 2020. **76**(2): p. 122-128.
67. Miyauchi, S., et al., *Distribution and regulation of protein expression of the free fatty acid receptor GPR120.* Naunyn Schmiedebergs Arch Pharmacol, 2009. **379**(4): p. 427-34.
68. Lee, K.P., et al., *omega-3 Polyunsaturated fatty acids accelerate airway repair by activating FFA4 in club cells.* Am J Physiol Lung Cell Mol Physiol, 2017. **312**(6): p. L835-L844.
69. Prihandoko, R., et al., *Pathophysiological regulation of lung function by the free fatty acid receptor FFA4.* Sci Transl Med, 2020. **12**(557).
70. Lotfi, R., et al., *Imbalanced serum levels of resolvin E1 (RvE1) and leukotriene B4 (LTB4) in patients with allergic rhinitis.* Mol Biol Rep, 2020. **47**(10): p. 7745-7754.
71. Wu, Q., et al., *Identification of G-protein-coupled receptor 120 as a tumor-promoting receptor that induces angiogenesis and migration in human colorectal carcinoma.* Oncogene, 2013. **32**(49): p. 5541-50.
72. Houthuijzen, J.M., *For Better or Worse: FFAR1 and FFAR4 Signaling in Cancer and Diabetes.* Mol Pharmacol, 2016. **90**(6): p. 738-743.
73. Liu, Z., et al., *Omega-3 fatty acids and other FFA4 agonists inhibit growth factor signaling in human prostate cancer cells.* J Pharmacol Exp Ther, 2015. **352**(2): p. 380-94.
74. Hopkins, M.M., et al., *Eicosopentaneoic Acid and Other Free Fatty Acid Receptor Agonists Inhibit Lysophosphatidic Acid- and Epidermal Growth Factor-Induced Proliferation of Human Breast Cancer Cells.* J Clin Med, 2016. **5**(2).
75. Chung, H., et al., *Omega-3 fatty acids reduce obesity-induced tumor progression*

independent of GPR120 in a mouse model of postmenopausal breast cancer. Oncogene, 2015. **34**(27): p. 3504-13.
76. Kiepura, A., et al., *The Anti-Atherosclerotic Action of FFAR4 Agonist TUG-891 in ApoE-Knockout Mice Is Associated with Increased Macrophage Polarization towards M2 Phenotype.* Int J Mol Sci, 2021. **22**(18).
77. Jiang, T., et al., *Agonism of GPR120 prevents ox-LDL-induced attachment of monocytes to endothelial cells.* Chem Biol Interact, 2020. **316**: p. 108916.
78. Kamata, R., et al., *EPA Prevents the Development of Abdominal Aortic Aneurysms through Gpr-120/Ffar-4.* PLoS One, 2016. **11**(10): p. e0165132.
79. Heidenreich, P.A., et al., *2022 AHA/ACC/HFSA Guideline for the Management of Heart Failure: Executive Summary: A Report of the American College of Cardiology/American Heart Association Joint Committee on Clinical Practice Guidelines.* Circulation, 2022. **145**(18): p. e876-e894.
80. McDonagh, T.A., et al., *2021 ESC Guidelines for the diagnosis and treatment of acute and chronic heart failure: Developed by the Task Force for the diagnosis and treatment of acute and chronic heart failure of the European Society of Cardiology (ESC) With the special contribution of the Heart Failure Association (HFA) of the ESC.* Rev Esp Cardiol (Engl Ed), 2022. **75**(6): p. 523.
81. Ponikowski, P., et al., *Heart failure: preventing disease and death worldwide.* ESC Heart Fail, 2014. **1**(1): p. 4-25.
82. Virani, S.S., et al., *Heart Disease and Stroke Statistics-2020 Update: A Report From the American Heart Association.* Circulation, 2020. **141**(9): p. e139-e596.
83. Tsao, C.W., et al., *Heart Disease and Stroke Statistics-2022 Update: A Report From the American Heart Association.* Circulation, 2022. **145**(8): p. e153-e639.
84. Tsao, C.W., et al., *Temporal Trends in the Incidence of and Mortality Associated With Heart Failure With Preserved and Reduced Ejection Fraction.* JACC Heart Fail, 2018. **6**(8): p. 678-685.
85. Gayat, E., et al., *Heart failure oral therapies at discharge are associated with better outcome in acute heart failure: a propensity-score matched study.* Eur J Heart Fail, 2018. **20**(2): p. 345-354.
86. Dunlay, S.M., V.L. Roger, and M.M. Redfield, *Epidemiology of heart failure with preserved ejection fraction.* Nat Rev Cardiol, 2017. **14**(10): p. 591-602.
87. Anker, S.D., et al., *Empagliflozin in Heart Failure with a Preserved Ejection Fraction.* N Engl J Med, 2021. **385**(16): p. 1451-1461.
88. Solomon, S.D., et al., *Dapagliflozin in Heart Failure with Mildly Reduced or Preserved Ejection Fraction.* N Engl J Med, 2022. **387**(12): p. 1089-1098.
89. Borlaug, B.A., *Evaluation and management of heart failure with preserved ejection fraction.* Nat Rev Cardiol, 2020. **17**(9): p. 559-573.
90. Shah, S.J., et al., *Phenomapping for novel classification of heart failure with preserved ejection fraction.* Circulation, 2015. **131**(3): p. 269-79.
91. Shah, S.J., et al., *Phenotype-specific treatment of heart failure with preserved ejection fraction: A multiorgan roadmap.* Circulation, 2016. **134**(1): p. 73-90.
92. Paulus, W.J. and C. Tschope, *A novel paradigm for heart failure with preserved ejection fraction: comorbidities drive myocardial dysfunction and remodeling through coronary microvascular endothelial inflammation.* J Am Coll Cardiol, 2013. **62**(4): p. 263-71.
93. Mohammed, S.F., et al., *Coronary microvascular rarefaction and myocardial fibrosis in heart failure with preserved ejection fraction.* Circulation, 2015. **131**(6): p. 550-9.
94. Borlaug, B.A., et al., *Effects of sildenafil on ventricular and vascular function in heart*

failure with preserved ejection fraction. Circ Heart Fail, 2015. **8**(3): p. 533-41.
95. Packer, M. and D.W. Kitzman, *Obesity-Related Heart Failure With a Preserved Ejection Fraction: The Mechanistic Rationale for Combining Inhibitors of Aldosterone, Neprilysin, and Sodium-Glucose Cotransporter-2.* JACC Heart Fail, 2018. **6**(8): p. 633-639.
96. Altara, R., et al., *Targeting Obesity and Diabetes to Treat Heart Failure with Preserved Ejection Fraction.* Front Endocrinol (Lausanne), 2017. **8**: p. 160.
97. Kristensen, S.L., et al., *Clinical and Echocardiographic Characteristics and Cardiovascular Outcomes According to Diabetes Status in Patients With Heart Failure and Preserved Ejection Fraction: A Report From the I-Preserve Trial (Irbesartan in Heart Failure With Preserved Ejection Fraction).* Circulation, 2017. **135**(8): p. 724-735.
98. Bhatia, R.S., et al., *Outcome of heart failure with preserved ejection fraction in a population-based study.* N Engl J Med, 2006. **355**(3): p. 260-9.
99. Lam, C.S., et al., *Epidemiology and clinical course of heart failure with preserved ejection fraction.* Eur J Heart Fail, 2011. **13**(1): p. 18-28.
100. Zakeri, R., et al., *Temporal relationship and prognostic significance of atrial fibrillation in heart failure patients with preserved ejection fraction: a community-based study.* Circulation, 2013. **128**(10): p. 1085-93.
101. Lam, C.S.P., et al., *Heart failure with preserved ejection fraction: from mechanisms to therapies.* Eur Heart J, 2018. **39**(30): p. 2780-2792.
102. Cornall, L.M., et al., *Diet-induced obesity up-regulates the abundance of GPR43 and GPR120 in a tissue specific manner.* Cell Physiol Biochem, 2011. **28**(5): p. 949-58.
103. Schiattarella, G.G., et al., *Nitrosative stress drives heart failure with preserved ejection fraction.* Nature, 2019. **568**(7752): p. 351-356.
104. de Lucia, C., et al., *Echocardiographic Strain Analysis for the Early Detection of Left Ventricular Systolic/Diastolic Dysfunction and Dyssynchrony in a Mouse Model of Physiological Aging.* J Gerontol A Biol Sci Med Sci, 2019. **74**(4): p. 455-461.
105. Kraker, K., et al., *Effects of empagliflozin and target-organ damage in a novel rodent model of heart failure induced by combined hypertension and diabetes.* Sci Rep, 2020. **10**(1): p. 14061.
106. Schnelle, M., et al., *Echocardiographic evaluation of diastolic function in mouse models of heart disease.* J Mol Cell Cardiol, 2018. **114**: p. 20-28.
107. Deng, Y., et al., *Targeting Mitochondria-Inflammation Circuit by beta-Hydroxybutyrate Mitigates HFpEF.* Circ Res, 2021. **128**(2): p. 232-245.
108. Mallery, J.A., et al., *Effects of heart rate and pulmonary artery pressure on Doppler pulmonary artery acceleration time in experimental acute pulmonary hypertension.* Chest, 1991. **100**(2): p. 470-3.
109. Stokke, T.M., et al., *Geometry as a Confounder When Assessing Ventricular Systolic Function: Comparison Between Ejection Fraction and Strain.* J Am Coll Cardiol, 2017. **70**(8): p. 942-954.
110. Barbier, P., et al., *Reliability and feasibility of longitudinal AFI global and segmental strain compared with 2D left ventricular volumes and ejection fraction: intra- and inter-operator, test-retest, and inter-cycle reproducibility.* Eur Heart J Cardiovasc Imaging, 2015. **16**(6): p. 642-52.
111. Scantlebury, D.C. and B.A. Borlaug, *Why are women more likely than men to develop heart failure with preserved ejection fraction?* Curr Opin Cardiol, 2011. **26**(6): p. 562-8.
112. Steinberg, B.A., et al., *Trends in patients hospitalized with heart failure and preserved*

left ventricular ejection fraction: prevalence, therapies, and outcomes. Circulation, 2012. **126**(1): p. 65-75.
113. Borlaug, B.A. and W.J. Paulus, *Heart failure with preserved ejection fraction: pathophysiology, diagnosis, and treatment.* Eur Heart J, 2011. **32**(6): p. 670-9.
114. Lee, D.S., et al., *Relation of disease pathogenesis and risk factors to heart failure with preserved or reduced ejection fraction: insights from the framingham heart study of the national heart, lung, and blood institute.* Circulation, 2009. **119**(24): p. 3070-7.
115. Regitz-Zagrosek, V., E. Lehmkuhl, and M.O. Weickert, *Gender differences in the metabolic syndrome and their role for cardiovascular disease.* Clin Res Cardiol, 2006. **95**(3): p. 136-47.
116. Eaton, D.M., et al., *Sex-specific responses to slow progressive pressure overload in a large animal model of HFpEF.* Am J Physiol Heart Circ Physiol, 2022. **323**(4): p. H797-H817.
117. Tong, D., et al., *Female Sex Is Protective in a Preclinical Model of Heart Failure With Preserved Ejection Fraction.* Circulation, 2019. **140**(21): p. 1769-1771.
118. Cao, Y., et al., *Sex differences in heart mitochondria regulate diastolic dysfunction.* Nat Commun, 2022. **13**(1): p. 3850.
119. Otto, M., et al., *Development of heart failure with preserved ejection fraction in type 2 diabetic mice is ameliorated by preserving vascular function.* Life Sci, 2021. **284**: p. 119925.
120. Guo, Y., et al., *Identification of the orphan G protein-coupled receptor GPR31 as a receptor for 12-(S)-hydroxyeicosatetraenoic acid.* J Biol Chem, 2011. **286**(39): p. 33832-40.
121. Lavine, K.J., et al., *The Macrophage in Cardiac Homeostasis and Disease: JACC Macrophage in CVD Series (Part 4).* J Am Coll Cardiol, 2018. **72**(18): p. 2213-2230.
122. Zaman, R., H. Hamidzada, and S. Epelman, *Exploring cardiac macrophage heterogeneity in the healthy and diseased myocardium.* Curr Opin Immunol, 2021. **68**: p. 54-63.
123. Loredo-Mendoza, M.L., et al., *The role of inflammation in driving left ventricular remodeling in a pre-HFpEF model.* Exp Biol Med (Maywood), 2020. **245**(8): p. 748-757.
124. Wilck, N., et al., *Nitric oxide-sensitive guanylyl cyclase stimulation improves experimental heart failure with preserved ejection fraction.* JCI Insight, 2018. **3**(4).
125. Hulsmans, M., et al., *Cardiac macrophages promote diastolic dysfunction.* J Exp Med, 2018. **215**(2): p. 423-440.
126. Kalogeropoulos, A., et al., *Inflammatory markers and incident heart failure risk in older adults: the Health ABC (Health, Aging, and Body Composition) study.* J Am Coll Cardiol, 2010. **55**(19): p. 2129-37.
127. Sanders-van Wijk, S., et al., *Circulating biomarkers of distinct pathophysiological pathways in heart failure with preserved vs. reduced left ventricular ejection fraction.* Eur J Heart Fail, 2015. **17**(10): p. 1006-14.
128. Santhanakrishnan, R., et al., *Growth differentiation factor 15, ST2, high-sensitivity troponin T, and N-terminal pro brain natriuretic peptide in heart failure with preserved vs. reduced ejection fraction.* Eur J Heart Fail, 2012. **14**(12): p. 1338-47.
129. Shah, S.J., et al., *High-sensitivity C-reactive protein and parameters of left ventricular dysfunction.* J Card Fail, 2006. **12**(1): p. 61-5.
130. Westermann, D., et al., *Cardiac inflammation contributes to changes in the extracellular matrix in patients with heart failure and normal ejection fraction.* Circ Heart Fail, 2011. **4**(1): p. 44-52.

131. Franssen, C., et al., *Myocardial microvascular inflammatory endothelial activation in heart failure with preserved ejection fraction.* JACC Heart Fail, 2016. **4**(4): p. 312-24.
132. Pascale, J.V., P.A. Lucchesi, and V. Garcia, *Unraveling the Role of 12- and 20- HETE in Cardiac Pathophysiology: G-Protein-Coupled Receptors, Pharmacological Inhibitors, and Transgenic Approaches.* J Cardiovasc Pharmacol, 2021. **77**(6): p. 707-717.
133. Bhatt, D.L., et al., *Cardiovascular Risk Reduction with Icosapent Ethyl for Hypertriglyceridemia.* N Engl J Med, 2019. **380**(1): p. 11-22.
134. Budoff, M., et al., *Effect of Vascepa (icosapent ethyl) on progression of coronary atherosclerosis in patients with elevated triglycerides (200-499 mg/dL) on statin therapy: Rationale and design of the EVAPORATE study.* Clin Cardiol, 2018. **41**(1): p. 13-19.
135. O'Connell, T.D., et al., *Mechanistic insights into cardiovascular protection for omega-3 fatty acids and their bioactive lipid metabolites.* Eur Heart J Suppl, 2020. **22**(Suppl J): p. J3-J20.